International Scientific-Technical and Production Journal

The Paton WELDING JOURNAL

November
2004
11

English translation of the monthly «Avtomaticheskaya Svarka» (Automatic Welding) journal published in Russian since 1948

Founders: *E.O. Paton Electric Welding Institute of the NAS of Ukraine*
International Association «Welding»
Publisher: *International Association «Welding»*

Address:
E.O. Paton Electric Welding Institute,
International Association «Welding»,
11, Bozhenko str., 03680, Kyiv, Ukraine
Tel.: (38044) 227 67 57
Fax: (38044) 268 04 86
E-mail: journal@paton.kiev.ua
http://www.nas.gov.ua/pwj

State Registration Certificate
KV 4790 of 09.01.2001

Subscriptions:
$460, 12 issues per year,
postage and packaging included.
Back issues available.

CONTENTS

FLASH-BUTT WELDING OF DISPERSION-HARDENED COPPER ALLOY OF Cu–Al_2O_3 SYSTEM

V.S. KUCHUK-YATSENKO, V.I. SHVETS, P.N. CHVERTKO, G.N. GORDAN, A.G. SAKHATSKY and **I.P. REMENYAK**
E.O. Paton Electric Welding Institute, NASU, Kiev, Ukraine

Technological process of flash-butt welding of dispersion-hardened copper alloy AL-25 (C 15725) with a forced joint formation is considered. Data of metallographic and X-ray spectral microanalysis of microstructure and results of mechanical tests of welded joints are given.

Keywords: *flash-butt welding, upsetting force, time of welding, dispersion-hardened copper alloy, recrystallization, flash, microstructure*

One of the important requirements specified for advanced structural materials is preserving of their performance at temperatures close to the melting temperature.

Hardening of alloys using thermomechanical treatment is realized at temperatures not exceeding $(0.3–0.4)T_m$. Opportunities of a complex alloying in combination with heat treatment are wider. In some cases it is possible to increase the operating temperatures of alloys up to $(0.7–0.8)T_m$.

Composite alloys, in particular the dispersion-hardened alloys (DHA) possess heat resistance of the higher level. Hardening of these alloys is attained by adding of stable dispersed (1–20 nm) refractory compounds (oxides, carbides, nitrides and others) into matrix, which do not interact with matrix up to temperature of melting. Hardening particles influence actively the formation of substructure of alloys and its stabilization under the service conditions. DHA preserve a long-time serviceability at temperatures of $(0.90–0.95)T_m$.

Increase in heat resistance of copper alloys by the dispersion hardening, unlike the alloying, does not almost deteriorate the electric and heat conductivity, i.e. main characteristics that define the field of their application [1]. This is very important for material of windings of rotors of electric engines, tubular heat exchangers, parts of electric vacuum devices, electric contactors and others, operating at increased temperatures.

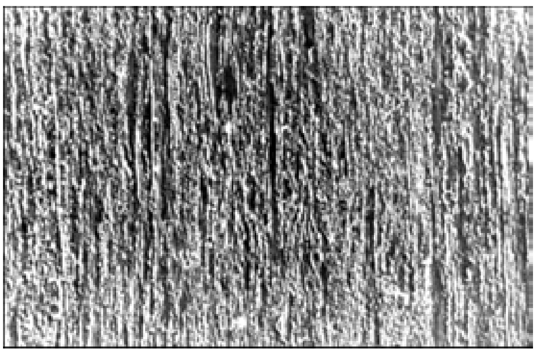

Figure 1. Microstructure of as-delivered alloy AL-25 (C 15725) (×500)

Dispersion-hardened copper is used widely in welding industry in manufacture of electrodes for spot and seam welding, nozzles for automatic and semi-automatic shielded-gas welding machines. Service life of these products is 5–10 times increased as compared with traditional copper products.

The main problem in DHA joining by different methods of fusion welding is the fact that when the parent metal is transferred into molten state the ordered distribution of hardening particles is violated. The resulting microheterogeneities decrease greatly the strength characteristics of the joints [2, 3].

Flash-butt welding with a forced joint formation is one of many methods allowing joining of almost all the known metals and alloys, guaranteeing high stability and quality of the joints [4].

We have studied the feasibility of use of the resistance butt welding for producing joints of copper, dispersion hardened by aluminium oxide (Al_2O_3). In experiments, the alloy AL-25 (C 15725) of the following composition (according to ASTM / AWS) was used, wt.%: 99.39–99.50Cu, 0.45–0.55Al_2O_3, up to 0.01Fe, up to 0.01Pb, up to 0.4[O]. Rods of 16 mm diameter were joined. Microstructure (Figures 1 and 4), chemical inhomogeneity, distribution of microhardness and strength characteristics of welded joints produced were examined.

Metallographic examinations and X-ray spectral microanalysis were performed using the optical microscope «Neophot 32», scanning electron microscope JSM-840, microscope-microanalyzer T-200 and Cameca microprobe MS-50. Microhardness was measured in the LECO hardness meter. Replicas were made at 0.1 N load and 15 s holding time. Distance between replicas was 10 μm. Before examinations the samples were subjected to mechanical polishing and ion-vacuum etching. Experimental samples were welded in laboratory flash-butt welding machine of 100 kV·A capacity. The use of the traditional technological diagram of resistance butt welding did not allow us to produce welded joints of the required quality.

The positive result was attained in use of the technological diagram of welding with a forced weld formation and an increased «heat» insulator, developed at the E.O. Paton Electric Welding Institute [5–7]. The given technological diagram (Figure 2) envisages

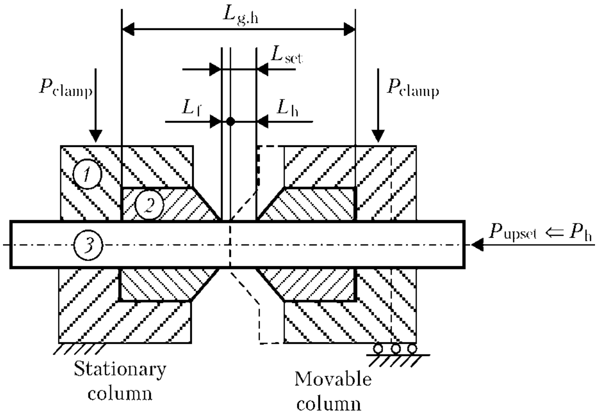

Figure 2. Scheme of flash-butt welding with a forced joint formation: *1* — clamps; *2* — forming device; *3* — workpieces being welded; – – – — final position of a movable column (see the rest designations in the text)

the application of a special technological equipment, furnished with a special technological rigging, equipped with heat-resistant electro- and heat-insulating forming elements. In initial position the samples to be welded are set at some initial distance L_{set}, including tolerances for welding and clamped at a clamping force $P_{clamp} = (2.5–3.0)P_{upset}$ (clamping force in upsetting). Then the samples being joined are clamped at a small force P_h and welding current is switched on.

The passing current heats the areas of general heating $L_{g.h}$, which is 6–10 times higher than L_{set}. The highest heat generation is occurred in the zone of contact of surfaces being joined. Here, the areas under the forming elements play the role of thermal barriers, thus providing a rapid and uniform heating of samples. In the process of heating the metal is deformed under the action of heating force P_h and the movable clamp is displaced for value L_h, and then the higher upsetting force is applied P_{upset} under the action of which the intensive plastic deformation of samples welded is occurred up to position L_f. The remnants of overheated metal are extruded into a flash, which is removed by knives of the forming device just after the welding current disconnection. Welding parameters are as follows: P_h = 9–14 MPa; P_{upset} = 1100–1800 MPa; secondary open-circuit voltage $U_{o.-c}$ = 4–7 V; τ_w = 5–10 s.

Metallographic examinations showed that formation of welded joints is accompanied by a significant plastic deformation (width of deformation zone is about 10 mm) and almost complete removal of a liquid phase from the joint (Figure 3). A fibrous structure is preserved in the deformation zone. As is seen from the microstructure analysis, the processes of recrystallization are proceeding in a narrow layer at the contact boundary. The width of this layer within the joint limits is not stable and reaches 200 μm (Figure 4). The band of elongated coarse grains across the upsetting direction is observed at the butt line. With removal from the butt the size of grains is decreased and they acquire an equiaxial shape. It should be noted that the presence of single pores is observed

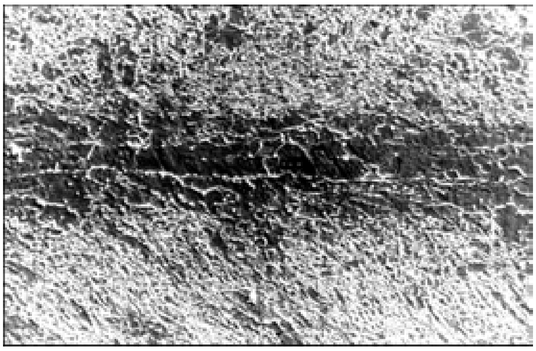

Figure 4. Microstructure of joint of alloy AL-25 (C 15725) (×350)

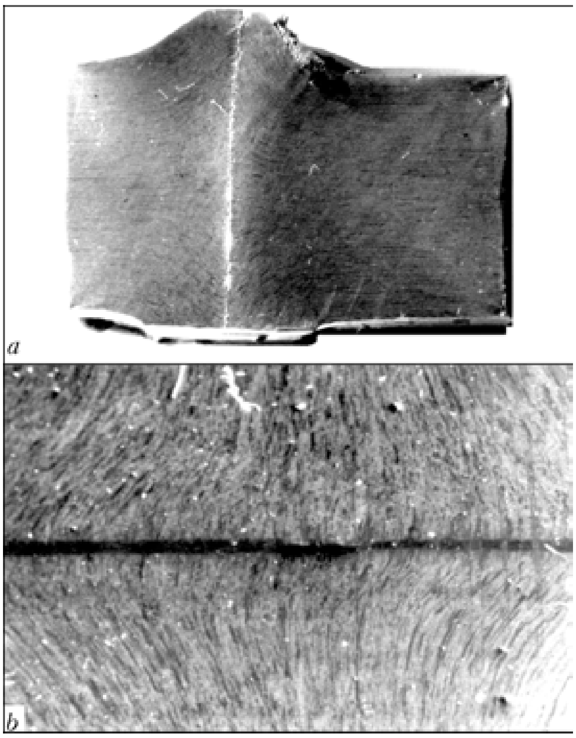

Figure 3. General view (*a*) and macrostructure of welded joint (*b*) of alloy AL-25 (C 15725) (×20)

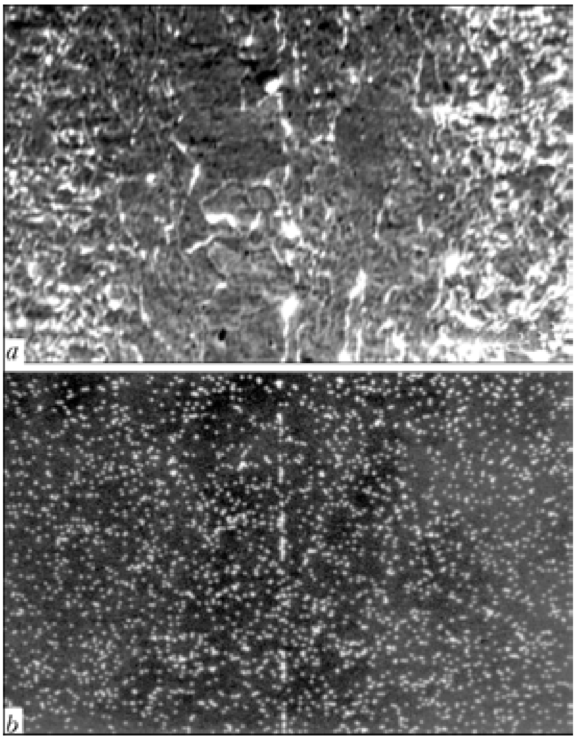

Figure 5. Distribution of aluminium in transverse section of welded joint of alloy AL-25 (C 15725): *a* — microstructure (×400); *b* — scanning pattern of region examined

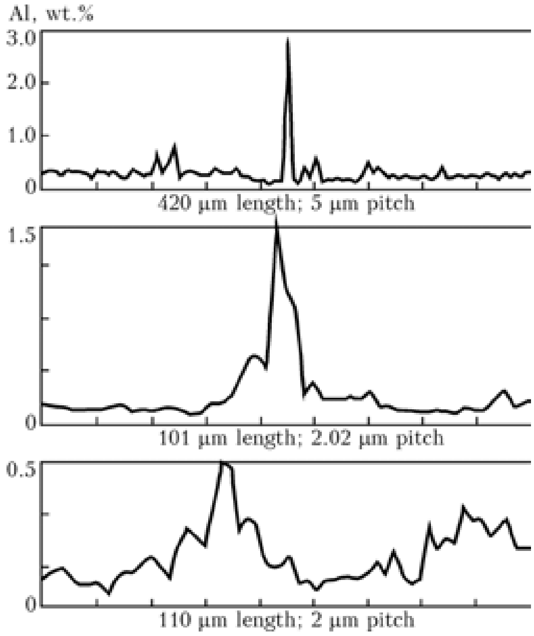

Figure 6. Profilograms of aluminium distribution in transverse section in line of contact of AL-25 (C 15725) welded joint

at the contact boundary in parallel with the formation of common grains.

Study of distribution of microhardness in the joint showed that the coarse grains at the contact boundary are characterized by minimum values *HV* 0.1-828–880. Microhardness is increased in adjacent grains of a smaller size and reaches the values of microhardness of the parent metal *HV* 0.1-1290 in the region of non-coarse grains. Width of the joint zone with a decreased hardness is 50–80 μm.

Study of distribution of particles Al_2O_3 in the joint was made from the results of X-ray microanalysis of aluminium distribution. This is admissible, as the aluminium oxide in copper is characterized by the high stability.

In accordance with a scanning pattern (Figure 5, *b*) allowing recording the change in concentrations of 2–3 wt.%, distribution of particles Al_2O_3 in the joint is uniform and does not differ from that in the parent metal. Areas of a local increase in concentration of aluminium are observed at the contact boundary. At a linear scanning through these areas at a sensitivity of not less than 0.5 wt.%, the peaks in intersection of thickened boundaries of grains in the butt zone are observed on the curves of aluminium distribution (Figure 6). Aluminium concentration is increased up to 1.5–3.0 wt.%. Violation of uniformity of distribution of Al_2O_3 particles is negligible and due to a partial extrusion of a liquid phase during upsetting.

The rupture strength of joints was 0.75–0.80 of the parent metal strength. Fracture of specimens occurs in weld at a negligible plastic deformation. The fracture surface is fine crystalline.

Electron fractographic examinations showed that pitting relief, typical of a tough fracture, is dominated in microstructure of fracture surface at the presence of elements of a quasi-cleavage (Figure 7). This is explained by the fact that the fracture is occurred along the narrow layer of the recrystallized metal.

Distribution of aluminium in elements of structure of fracture surface is almost uniform. At some regions

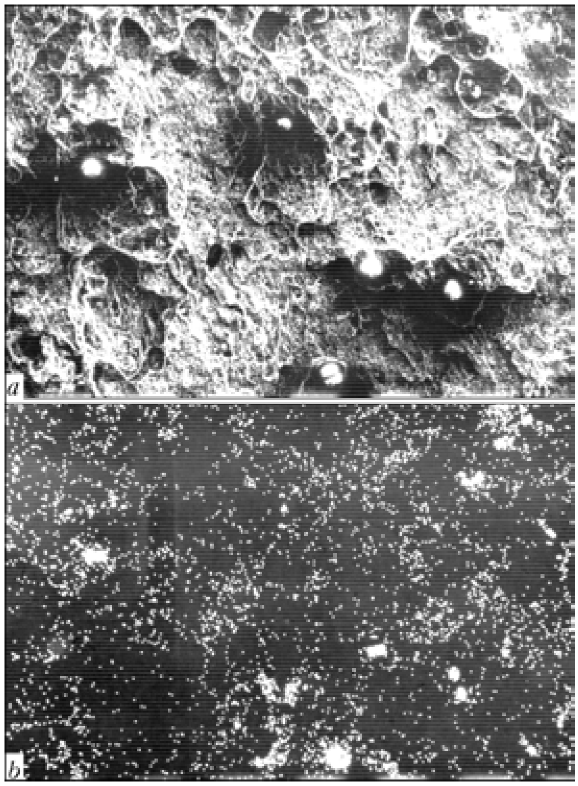

Figure 7. Distribution of aluminium on the fracture surface of joint of alloy AL-25 (C 15725): *a* — fractographic pattern of region examined; *b* — scanning pattern (×100)

the inclusions of up to 20 μm size are observed in microcavities, enriched with aluminium, which cannot be initiators of fractures.

CONCLUSIONS

1. Agglomeration of particles of aluminium oxide in the AL-25 (C 15725) joints produced by flash-butt welding, is negligible and has a local nature.

2. Strength of welded joints at static rupture was 0.75–0.80 of the parent metal strength. Strength characteristics of the joint are defined by the properties of the recrystallized metal zone.

3. The further investigations as to the preparation for welding and postweld heat treatment of parts will be able to guarantee the improvement of mechanical properties of the joints.

4. Successful use of flash-butt welding for producing quality joints from dispersion-hardened copper alloys requires development of a specialized welding equipment.

1. Portnoj, K.I., Babich, B.N. (1974) *Dispersion-hardened materials*. Moscow: Metallurgiya.
2. McFayden, A.A., Kapoor, R.R., Eagar, T.W. (1990) Effect of second particles on direct brazing of alumina dispersion hardened copper. *Welding Res. Suppl.*, **11**, 399.
3. Ambroziak, A., Lison, R. (1992) Welding and brazing material. *Welding and Cutting*, **7**, 124–126.
4. Kuchuk-Yatsenko, S.I. (1992) *Flash-butt welding*. Kiev: Naukova Dumka.
5. Sakhatsky, G.P., Lebedev, V.K., Shirokovsky, R.M. et al. *Resistance butt welding method*. USSR author's cert. 495174. Int. Cl. 1323 K 11 / 04. Publ. 15.12.75.
6. Sakhatsky, G.P., Butnik, A.P. (1970) Resistance butt welding of high purity copper. *Avtomatich. Svarka*, **12**, 24–27.
7. Sakhatsky, G.P., Litvinchuk, M.D., Shelest, N.A. (1968) Technology and machine for butt welding of copper coils. *Ibid*., **6**, 58–60.

PECULIARITIES OF FORMATION OF STRUCTURE OF STEEL TO ALUMINIUM JOINTS IN FLASH-BUTT WELDING

L.I. MARKASHOVA, P.N. CHVERTKO, I.P. REMENYAK, E.V. POLOVETSKY and **T.A. ALEKSEENKO**
E.O. Paton Electric Welding Institute, NASU, Kiev, Ukraine

Considered are principles of formation of structure and phase composition of steel to aluminium joints made by flash-butt welding. It is shown that phase composition affects performance and mechanical properties of the joints.

Keywords: *flash-butt welding, phase formation, steel-aluminium joint, fracture character, stoichiometric composition, intermetallic compound, electrical resistance, microhardness*

Wide engineering application of welded joints in dissimilar materials is attributable in many respects to unique possibilities of combining advantages of each of the joined materials in finished parts. For example, joints of aluminium and its alloys to different grades of steels combine light weight and corrosion resistance of aluminium and strength of steel. This explains extensive utilisation of the combined steel-aluminium structures and assemblies in aircraft, space and nuclear power engineering, as well as in automotive, ship building, chemical and other industries.

However, production of sound joints involves problems associated with substantial differences in thermal-physical properties of the materials joined (melting point, linear thermal expansion coefficients, thermal conductivity and heat capacity), which causes formation of considerable stresses within the welding zone [1, 2].

Another important cause of instability of mechanical and service properties of the joints of metals differing in limited mutual solubility (steel and aluminium being among them) is susceptibility to formation of brittle intermetallic phases within the zone of their contact interaction [3, 4].

To solve the set of the above problems, technologists and researchers have to address the general task — comprehensively study principles of structure and phase formation within the welding zone at different process parameters in order to identify causes of decrease in mechanical characteristics and other properties of welded joints between steel and aluminium. Some of the results obtained are given in this article.

The article considers peculiarities of formation of structure and character of phase formation within the welding zone in steel-aluminium joints (steel St3 + aluminium alloy AK4) made under different conditions of continuous flash-butt welding (FBW). Billets to be welded had a cross section area of about 110–112 mm^2.

Experiments were conducted using the laboratory flash-butt welding machine with a power of 190 kV·A and upsetting force of up to 130 kN, the speed of a movable column ranging from 0.1 to 32 mm / s and the upsetting speed amounting to 250 mm / s. Two batches of samples were welded. The welding time was 4 (mode I) and 8 s (mode II).

Investigations were conducted by optical and analytical scanning electron microscopy, which made it possible to generate information on the effect of process parameters on concentration, structure and transformations of phases within the welding zone, as well as on the character of fracture of the resulting joints and their electrical characteristics.

Figures 1 and 2 show a general view of structure and fragments of the welding zone in St3 + AK4 welded joints made in modes I and II. Figures 3 and 4 show variations in the content of chemical elements with transition from one of the metals welded (aluminium alloy AK4) through the interface in its different regions differing in structure and phase precipitates (PP) to the other metal (steel St3).

Figure 5 shows distribution of volume fraction V and size of PP along the welding zone using different process conditions. The character of fracture of the joints made in the modes under consideration is shown in Figure 6, and experimental data characterising dependence of local values of electrical resistance R of the joints upon the size of intermetallic phases formed within the welding zone are shown in Figure 7.

As proved by examinations, the joints between monolithic samples of steel St3 and aluminium alloy AK4, made in mode I, can be characterised as follows. The most dramatic change in the content of iron towards aluminium (from 12 to 2 wt.%) takes place at depth $\delta \cong 5$ μm from the interface. At depth $\delta \cong 50$–100 μm the iron content decreases to 0.3 wt.%. The main changes in the content of aluminium towards iron occur mostly at a depth of 5 μm (see Figure 3, *a*).

It should be noted that in the case of welded joints made in mode I a large portion (about 30 %) of the contact surface area is almost free from PP. Metal in these zones is characterised by an insignificant change in the content of chemical elements, i.e. corresponding

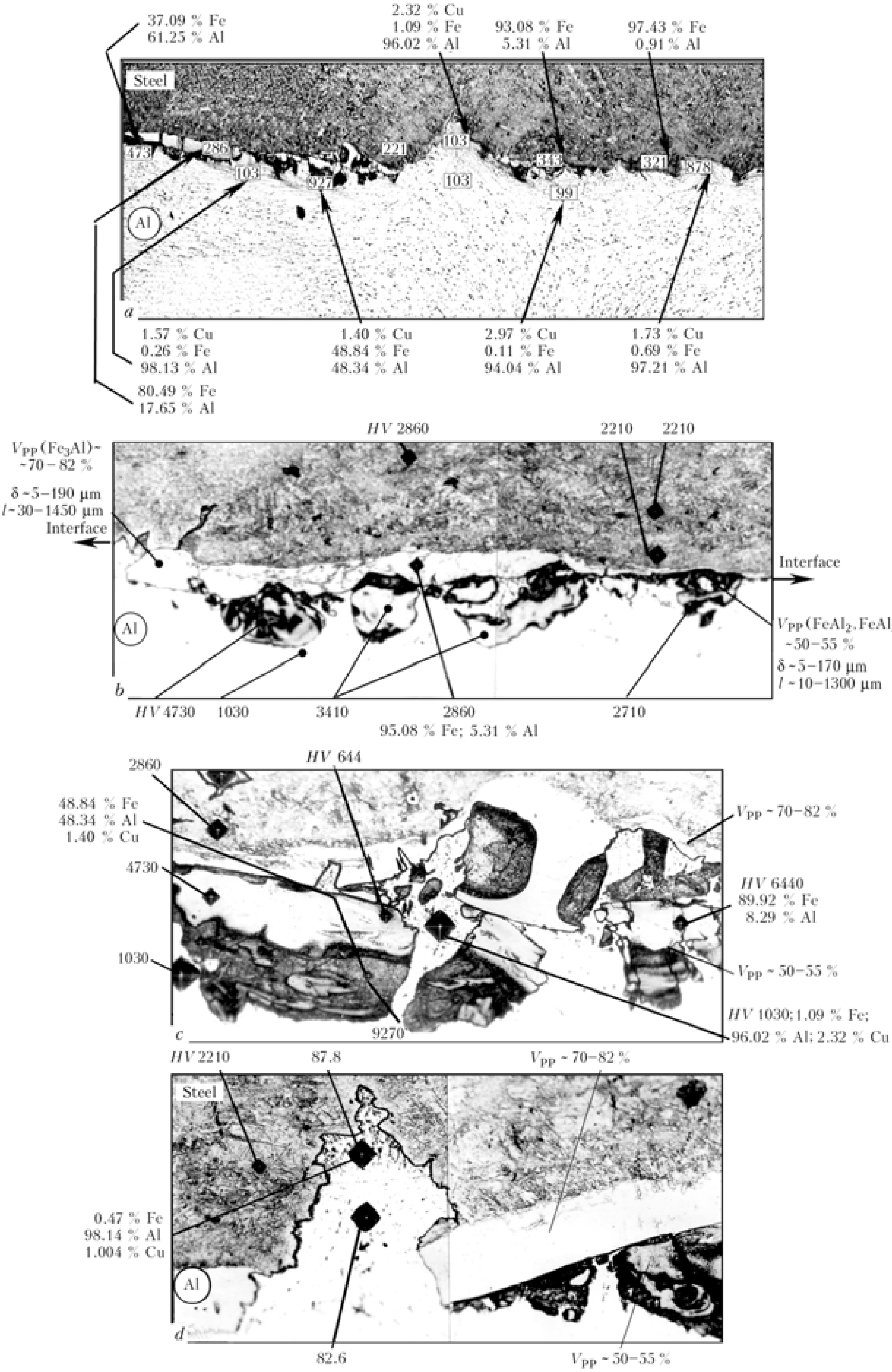

Figure 1. Microstructure of welding zone in the St3 + AK4 joint made by continuous FBW in mode I: *a* ---- general view (×50); *b–d* ---- individual regions with phase precipitates (×300). Here and in Figure 2 the elemental composition of phases is given in weight percent, the PP composition is given in volume percent, and Brinell microhardness is given in megapascals

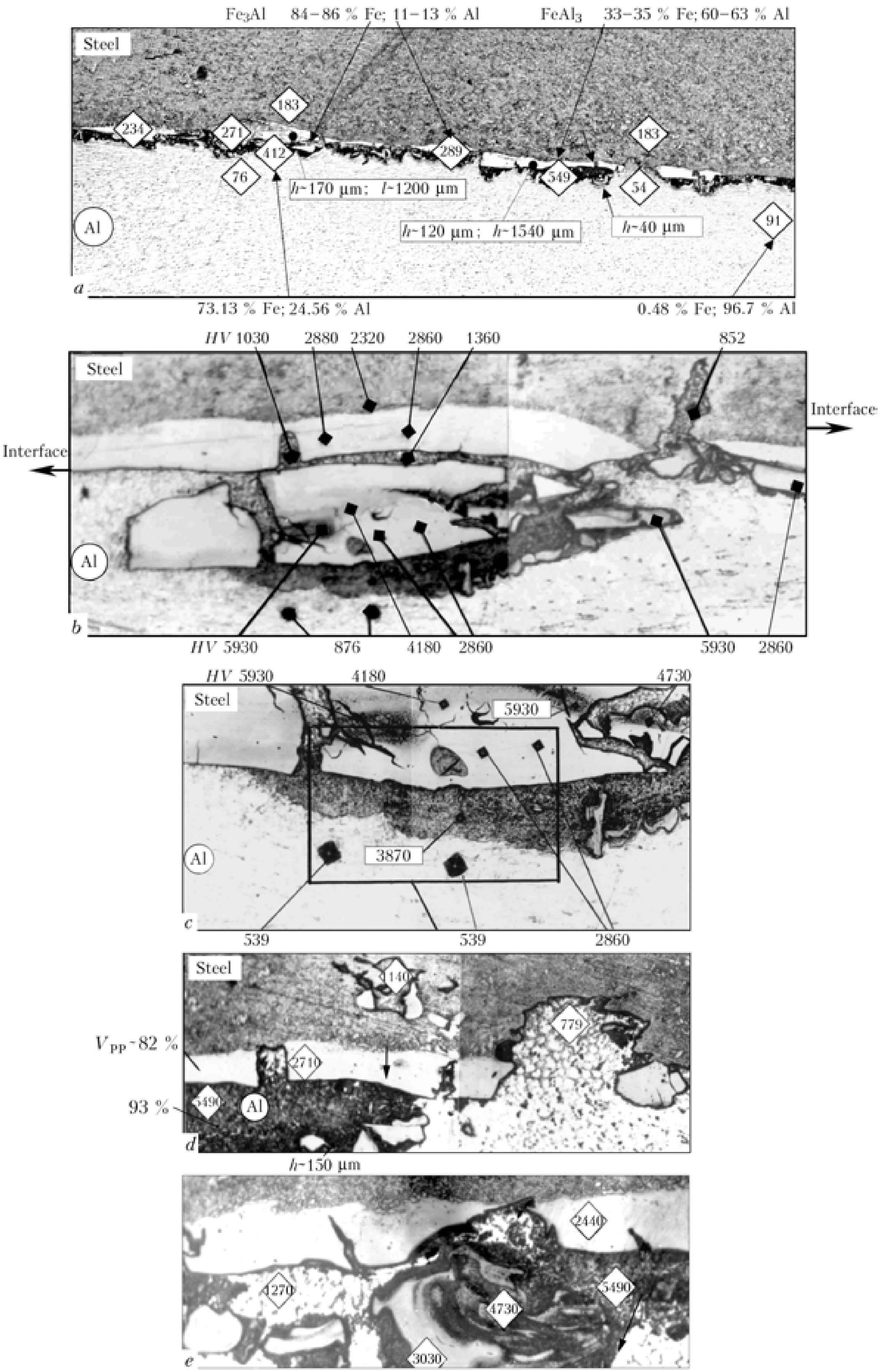

Figure 2. Microstructure of welding zone in the St3 + AK4 joint made by continuous FBW in mode II: *a* ---- general view (×50); *b*–*d* ---- individual regions with phase precipitates (*b* ---- ×156; *c* ---- ×150; *d*, *e* — ×300)

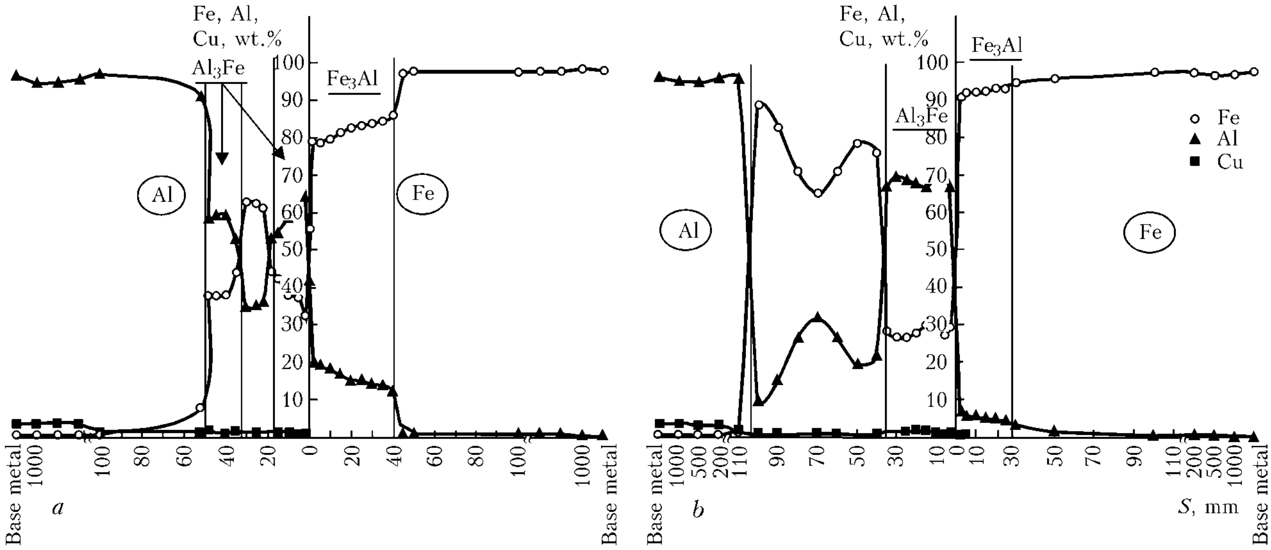

Figure 3. Variations in content of main chemical elements in the St3 + AK4 joint made by continuous FBW in modes I (*a*) and II (*b*): *S* — distance from interface

to the state of solid solution, and by a somewhat increased microhardness. Thus, on the aluminium alloy side the values of microhardness are approximately equal to *HV* 90–100 MPa (microhardness of base metal being approximately *HV* 760 MPa), whereas on the steel side they decrease to about *HV* 1150 MPa (microhardness of base metal being approximately *HV* 1680–1700 MPa).

Phase precipitates formed in the welding zone are mostly of an elongated shape and have the following characteristic sizes: thickness $h = 5$–170 μm and length l = 10–1300 μm. Quantitative estimation of size distribution of the phases shows that PP of a medium length ($l \cong$ 500–900 μm) constitute the highest amount (about 27 vol.% on the aluminium alloy side and up to 37 vol.% on the steel side), while the content of finer ($l \cong$ 10–300 μm) and coarser ($l \cong$ 1000–1300 μm) PP is 10–15 and 20–32 vol.% of the total amount of PP, respectively. The total content of PP on the aluminium alloy side is ≈ 50–55 vol.% and on the steel side — ≈ 70–82 vol.%.

Characteristically, the formed phases have a complex «composite» structure. This can be well seen in some enlarged images of structure and fragments of the phases (see Figure 1, *c*, *d*). Accordingly, the formed phases and components of the growing phases have a substantially differing microhardness. Thus, in local regions of the «composite» phases and in the individual phases it varies from *HV* 2400–2800 to *HV* 6400–9300 MPa. Specific composition of the forming phases was determined on the basis of a num-

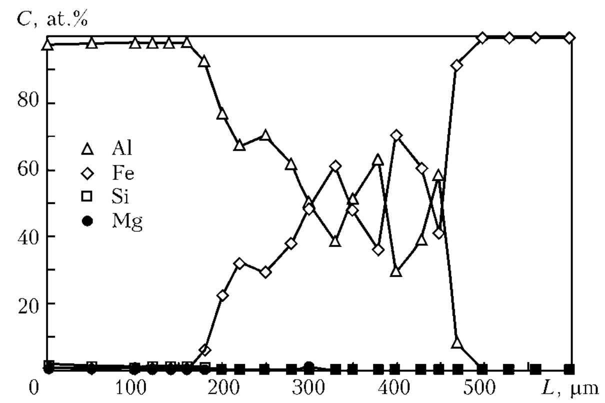

Figure 4. Variations in content of main chemical elements, *C*, in the St3 + AK4 joint made by continuous FBW in mode I: *L* — length of examined region

Variations in content of chemical elements (wt.%) in St3 + AK4 welded joint

L, μm	*Al*	*Fe*	*Si*	*Mg*
0	97.7	0	1.6	0.7
50	98.0	0	1.4	0.6
100	98.3	0	1.0	0.6
120	98.1	0	1.3	0.6
140	98.1	0	1.3	0.6
160	98.4	0	1.2	0.3
180	92.8	6.1	0.9	0.2
200	77.1	22.7	0.2	0
220	67.2	32.7	0.1	0
250	70.5	29.4	0.1	0
280	61.8	38.2	0	0
300	50.5	48.6	0	0.9
330	38.6	61.4	0	0
350	51.5	48.5	0	0
380	63.5	36.5	0	0
400	29.4	70.6	0	0
430	39.3	60.7	0	0
450	58.9	41.1	0	0
470	8.1	91.9	0	0
500	0	100.0	0	0
530	0	100	0	0
560	0	100	0	0
600	0	100	0	0

Note. Carbon and oxygen are absent.

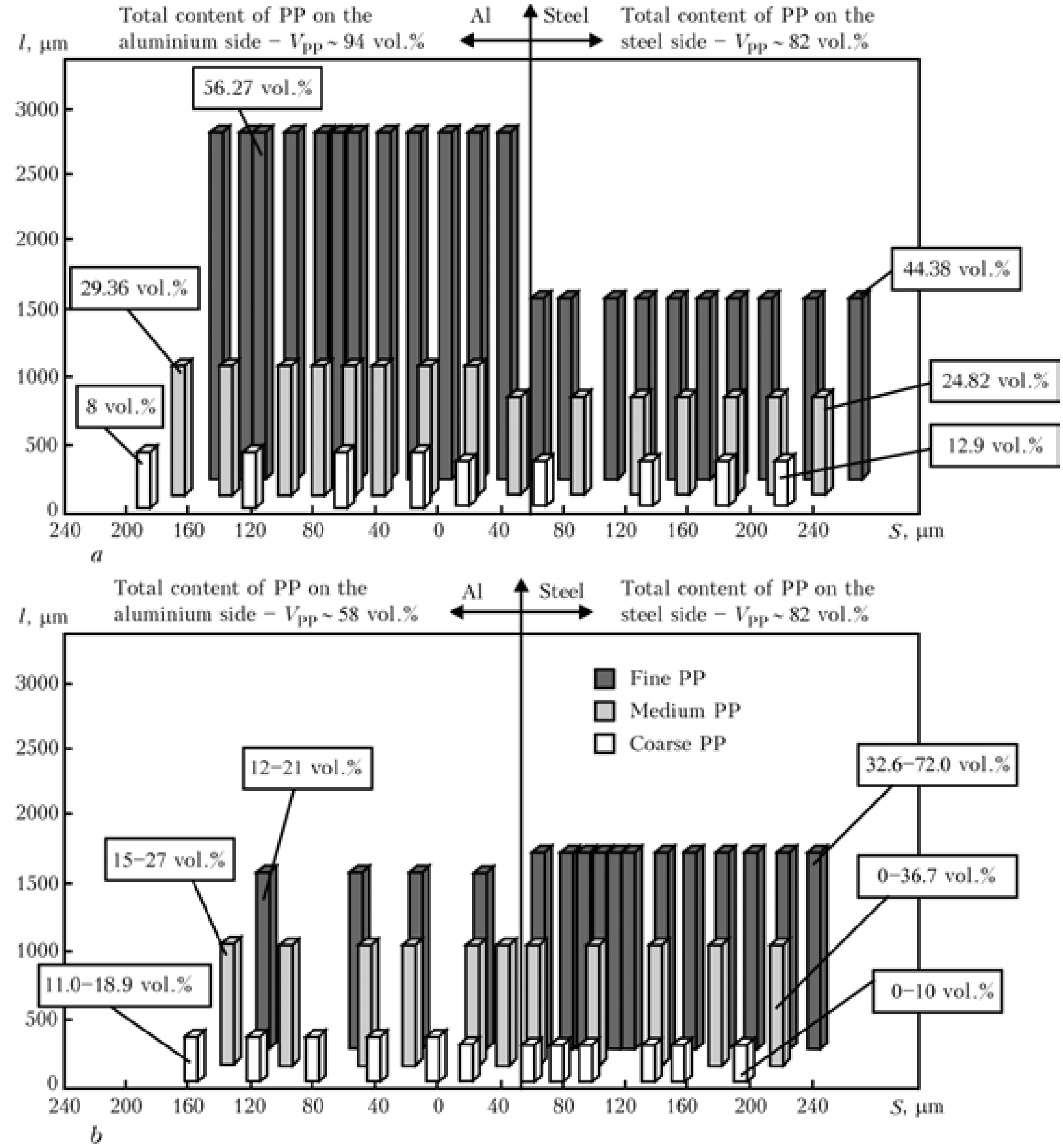

Figure 5. Volume fraction of PP in the St3 + AK4 joint made by continuous FBW in modes I (*a*) and II (*b*)

ber of local measurements of the content of chemical elements in each of the examined phases and their different fragments over the entire welding zone at different distances from the interface between the metals joined.

It can be seen in Figure 3, *a*, that stoichiometric composition of the phases formed in a certain region of the welding zone corresponds in the main to phases of the Al_3Fe and Fe_3Al types, whereas phases of the $FeAl_2$ type were revealed in other regions of a welded joint.

Examinations were also conducted to check the presence of oxide films in regions of the concentration of PP (see Figure 4). Detailed analysis of the content of chemical elements, including oxygen (Table), showed the absence of oxides in the considered regions containing intermetallic phases.

In the joints made under the longer time conditions of FBW (mode II), the most dramatic change in the content of iron towards aluminium from 20 (near the interface) to 7 wt.% is seen at a distance of about 5 μm from the interface. Then it gradually decreases to 0.37 wt.% (at a distance of up to 100 μm). Basic changes in the aluminium content (more dramatically from 2.0 to 0.8 wt.%, then with attenuation to 0.4 wt.%) take place at depths $\delta \cong 5$, 20 and 100 μm from the interface, respectively (see Figure 3, *b*). Increase in the welding time, compared with mode I, leads also to a substantial increase in volume fraction and size of PP in the welding zone (see Figure 5). The content of PP is ≈ 93–94 vol.% on the aluminium alloy side and 80–82 vol.% on the steel side.

In this case thickness of PP amounts to about 10–200 μm, their length being 20–2500 μm, and microhardness of PP is *HV* 2900, 4700 and 5900 MPa. However, on the steel side these precipitates are of a more dispersed character ($h \cong$ 5–220 μm, $l \cong$ 90–1340 μm), and their microhardness is lower, i.e. about *HV* 2400–2860 MPa. Stoichiometric composition of PP is mainly of the Fe_3Al type (on the steel side) and of the Al_3Fe and FeAl type (on the aluminium alloy side). It should be emphasised that composition of

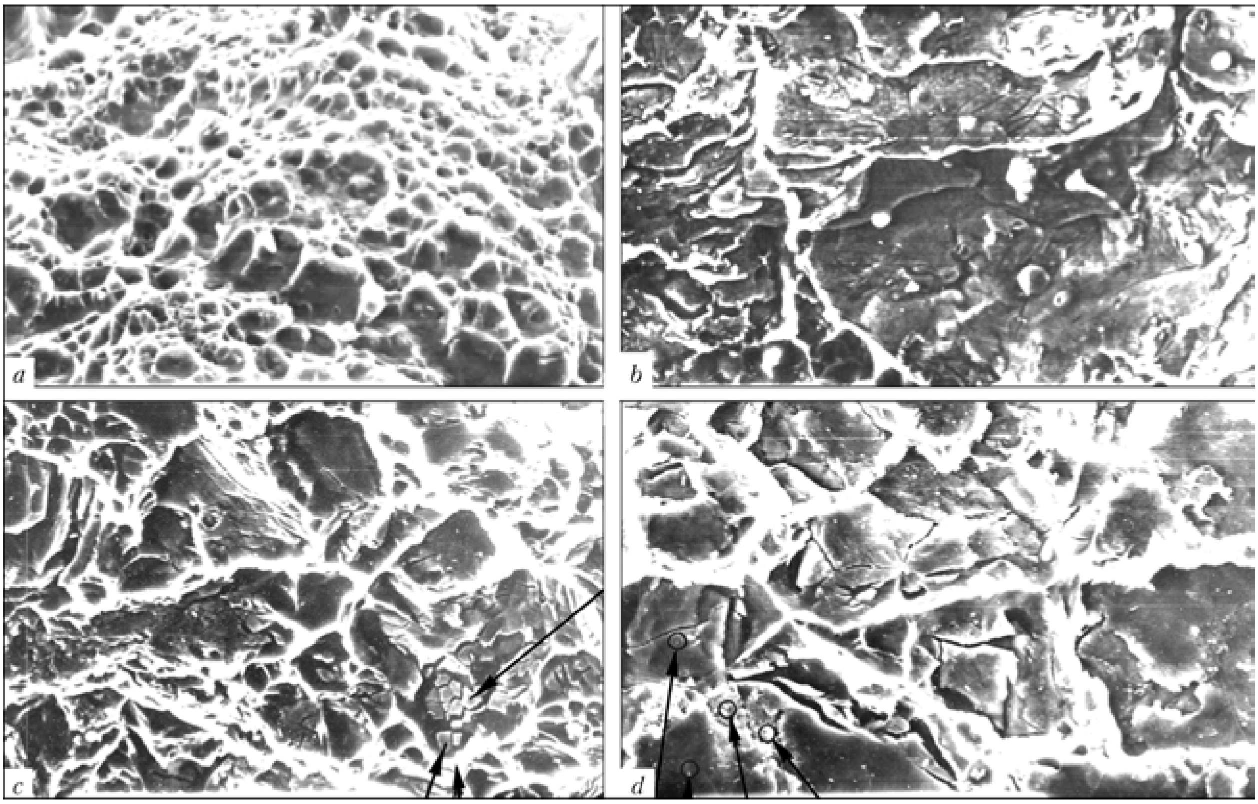

Figure 6. Microstructure of fracture on the aluminium alloy side in the St3 + AK4 joint made by continuous FBW in mode I (*a*, *c* — ×680) and II (*b* — ×300; *d* — ×680)

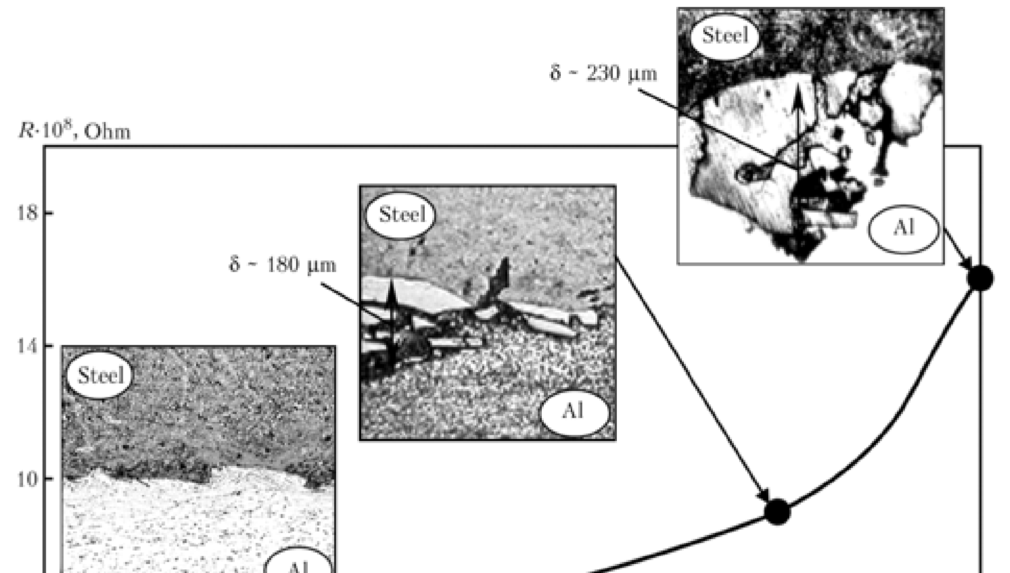

Figure 7. Dependence of local electrical resistance of the transition zone in the St3 + AK4 joint made by continuous FBW upon size *D* and volume fraction of PP

intermetallic compounds in this case remains almost similar to that of the phases formed in mode I. However, in addition to the formation of intermetallic phases of the Al_3Fe, Fe_3Al and $FeAl_2$ type taking place under the shorter time conditions, here we revealed also the phases with a more diverse composition, such as FeAl and Fe_2Al_5, as well as predominance of the phases with a more complicated morphological (composite) structure, which can be well seen in enlarged images of these phases (see Figure 2, *b–d*). Also seen is increase in volume fraction of intermetallics characterised by increased values of microhardness (*HRC* 400, 500, 600), which is revealed as a rule on the aluminium alloy side.

Structures of the formed phases of this type (intermetallics of the $FeAl_3$ type) with microhardness of approximately *HV* 600 MPa (see Figure 2, *c*) exhibit clearly defined networks of internal microcracks. Pronounced also are changes in structure and microhardness of base materials in the near-contact zone (see Figure 2, *c*, *d*), caused by formation of layers characterised by microheterogeneities: segregation clusters, fragmentation of structure and high gradients of microhardness that changes in a jump-like manner from *HV* 800 to *HV* 4000–6000 MPa.

As seen from the given results, under the longer time conditions (mode II) of FBW of solid billets the amount of the formed phases along the fusion line in steel to aluminium joints almost doubles, compared with that in the case of mode I with a shorter welding time. Besides, the coarser intermetallic phases dominate in this case (see Figure 5), which is caused by increase in time of the welding process leading to more intensive initiation and growth of the intermetallic phases. It should be noted that phases formed in this case have a more equilibrium (stable) stoichiometric composition, as well as much higher hardness and brittleness.

Fractography of the character of fracture of welded joints (see Figure 6) shows that in mode I the fracture surface is characterised by a tougher geometry (see Figure 6, *a*): typical cells are formed, the height of the walls of which is indicative of a substantial flow of metal prior to fracture. The tough character of fracture is revealed as a rule in the welding zones, where metal is in the form of solid solution with no phase formations, or where a substantial decrease in the iron content (approximately to 0.5–5.0 wt.%) is fixed in the solid solution, e.g. of aluminium with iron. The quasi-brittle character of fracture is related primarily to formation of finely dispersed intermetallic phases or phases of the Fe_3Al type having minimal microhardness (approximately *HV* 2400–2700 MPa). Formation of the brittle cleavage regions is induced primarily by brittle hard intermetallics of the $FeAl_3$, $FeAl_2$ and FeAl type (approximately with *HV* 4000–6000 and more than 9000 MPa) present in the welding zone, which is confirmed by X-ray microanalysis of fracture components.

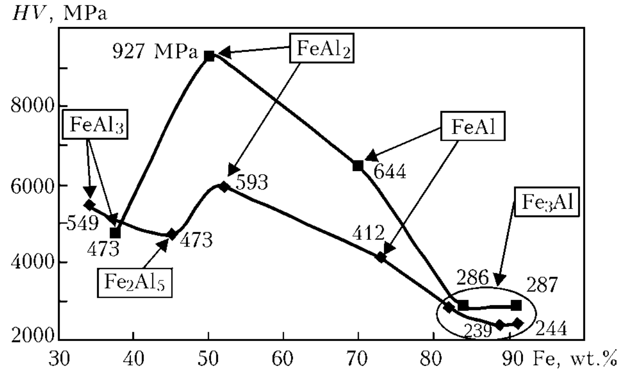

Figure 8. Dependence of microhardness of intermetallics upon their stoichiometric composition: ■, ◆ — modes I and II, respectively

Figure 8 shows relationship of the effect of composition of intermetallic phases with their microhardness. Wide spread of the microhardness values for the phases, e.g. *HV* 9270 and 5930 MPa (for $FeAl_2$) and *HV* 5490 and 4730 MPa (for $FeAl_3$), is related as a rule to the formation of a composite chemistry of the formed intermetallic phases, the components of which can change microhardness of phases of a simpler chemistry.

Mode I of continuous FBW is characterised mostly by a tough fracture with a tear of metal in aluminium, which proves the concentrational composition of metal in the cellular structure zone of fracture.

Comparative analysis of the types of fracture in steel-aluminium joints made by continuous FBW in modes I and II shows that mechanical properties of the joints are lower in the last case. Elements of a brittle cleavage and river pattern, indicating directions of formation and propagation of cracks, dominate in fracture surfaces. Analysis of chemical composition of individual fragments of the fracture pattern indicates that the cleavage facets are related as a rule to intermetallic phases Fe + Al, such as FeAl, $FeAl_3$, Fe_3Al, $FeAl_2$ and Fe_2Al_5, present in this region. The tough fracture components correspond to the zones with obvious predominance of aluminium or aluminium with a substantially decreased iron content (0.5–5.0 wt.%).

The tensile tests show that strength of the welded joints made in mode II is at a level of 280–300 MPa, while strength of the joints made in mode I is 300–322 MPa.

Measurements of electrical resistance *R* in local regions along the welding zone in steel-aluminium joints made under different conditions of FBW showed the following. Variations in the electrical resistance values directly within the contact zone have a clearly defined relationship with the presence of the formed phases and their size in this zone. Thus, electrical resistance along the fusion line free from the formed phases is $R \cong 3\cdot10^{-8}$ Ohm, while in the presence of the phases its value grows approximately by a factor of 3 to 5 ($R \cong (9–16)\cdot10^{-8}$ Ohm). Besides, if in the case of phases about 180 μm in size (thickness) $R \cong 9\cdot10^{-8}$ Ohm, then with increase in size of the phases it grows to $16\cdot10^{-8}$ Ohm (see Figure 7).

As seen from the above examination results, the amount and size of intermetallic phases formed within the welding zone of the FB welded steel-aluminium joints grow with increase in the welding time. The formed phases have a complex structure and heterogeneous composition, and in some cases they are the formations of a composite type, consisting of layers with a differing stoichiometric composition. Phases of a certain composition are characterised by different (sometimes substantially different) microhardness values. The highest microhardness is exhibited by phases of the type of $FeAl_2$ (up to *HV* 9000 MPa) and $FeAl_3$ (up to *HV* 5500 MPa), and the lowest microhardness is exhibited by phases of the type of Fe_3Al (up to *HV* 2800 MPa) and Fe_2Al_5 (up to *HV* 4800 MPa), the formation temperatures of which are 1140, 655, 555 and 1153 °C, respectively [5--9].

Given that the highest embrittlement effect on the character of fracture can be exerted by the intermetallic phases having a higher microhardness, in selection of temperature-time welding parameters it seems appropriate to avoid utilisation of welding temperatures close to temperatures of initiation of the most brittle and hard phases, or use the high heating and cooling rates that limit growth of such phases.

CONCLUSIONS

1. Using the shorter time conditions (welding time is 4 s) of continuous FBW of solid billets leads to formation along the welding zone of phases of the FeAl, Fe_3Al and $FeAl_2$ types, the content of which is about 50 vol.% (on the aluminium alloy side) and about 70 vol.% (on the steel side), as well as the region of solid solution, the content of which is about 30–40 vol.%. Fracture of the welded joints is mostly of a quasi-brittle and tough character, and strength is 300–322 MPa.

2. Under the longer time conditions (welding time is 8 s) the content of the formed phases along the fusion line almost doubles, the coarser intermetallic phases with a more equilibrium stoichiometric composition (mostly Al_3Fe), much higher microhardness (up to *HV* 4000–6000 MPa) and, accordingly, brittleness being dominant. Mechanical properties of the joints decrease, and their strength is 280–300 MPa.

3. While selecting temperature-time welding parameters, it is necessary to avoid utilisation of welding temperatures close to temperatures of initiation of the most brittle and hard phases, or use the high heating and cooling rates that limit growth of such phases.

4. Increase in volume fraction, density and depth of the phase formation region within the welding zone leads to growth of local values of electrical resistance: the values of electrical resistance change from $16\cdot10^{-8}$ to $9\cdot10^{-8}$ and $3\cdot10^{-8}$ Ohm in the zone of concentration of coarser phases, as well as in the zone of formation of finely-dispersed phases and solid solution.

5. It is shown that formation of intermetallic phases within the welding zone cannot be fully avoided under the considered conditions of FBW.

1. Kuchuk-Yatsenko, S.I. (1992) *Flash-butt welding.* Kiev: Naukova Dumka.
2. Gelman, A.S. (1970) *Principles of pressure joining*. Moscow: Mashinostroenie.
3. Tikhonov, L.V., Kononenko, V.A. (1985) *Mechanical properties of metals and alloys*. Refer. Book. Kiev: Naukova Dumka.
4. Ryabov, V.R. (1983) *Welding of aluminium and its alloys to other metals.* Kiev: Naukova Dumka.
5. Vol, A.E. (1962) *Structure and properties of binary metallic systems*. Vol. 2. Moscow: Fizmatgiz.
6. Kachanov, N.N., Mirkin, L.I. (1960) *X-ray structure analysis*. Moscow: Mashinostroenie.
7. Hansen, M. (1941) *Structures of binary alloys*. Vol. 1 / 2. Moscow: Mashinostroenie.
8. Vol, A.E. (1958) *Structure and properties of binary metallic systems*. Vol. 1. Moscow: Fizmatgiz.
9. Shank, F.A. (1973) *Structures of binary alloys*. Moscow: Metallurgiya.

CALCULATION OF MODES OF MAGNETIC-PULSE WELDING

A.S. PISMENNY, I.V. PENTEGOV, E.P. STEMKOVSKY, D.A. SHEJKOVSKY and **V.M. KISLITSYN**
E.O. Paton Electric Welding Institute, NASU, Kiev, Ukraine

A method is proposed to calculate the modes of magnetic-pulse welding, which combines the analytical method of calculation and numerical methods, using a PC. Application of this method allows calculation of magnetic-pulse welding parameters and selecting the optimum welding modes with an accuracy sufficient for practical purposes.

Keywords: *magnetic-pulse welding, calculation method, optimum welding modes*

Magnetic-pulse welding (MPW) is based on conversion of part of electric energy of the capacitor bank charge into mechanical energy, the pressure pulse being applied to the parts at the impact of magnetic field without any intervening medium. Welded joint formation in MPW is characterized by an intensive running of explosion-type processes.

During MPW a discharge of the capacitor bank to the inductor, generation of a strong electromagnetic field and formation of induced fields of eddy currents in the impelled part, interaction of these fields and motion of the impelled part towards the stationary pipe, collision and welding of the surfaces being joined proceed in a short time interval. In view of the diversity of the processes proceeding at MPW, it is rather difficult to calculate the optimum welding modes for specific parts because of the complexity of mathematical description of the problems with many parameters and solving non-linear equations.

In view of improvement of PC and availability of the necessary software, it is now expedient to apply analytical methods of process analysis in combination with the numerical methods of calculation in such complex cases.

The purpose of this study is applying the advantages of such a procedure to the case of calculation of the processes proceeding at MPW of pipes.

Let us consider the most widely used case of electric current flowing through a massive circular inductor, when a pre-charged capacitor bank is discharged to the latter [1], which is currently applied in all the known power sources for MPW. The power source (Figure 1) has capacitor bank C, where the capacity values are constant for a specific welding machine. In welding, capacitor bank C is charged up to rated voltage U_{C_r}, which is followed by its discharging to the inductor through end cell switch K. The U_{C_r} value can be varied in a broad range.

MPW uses an oscillatory mode of capacitor bank discharge. The law of discharge current variation in this case can be conveniently expressed in the form of a function of dimensionless parameter γ, as is given in [2]:

$$i(t) = \frac{2U_{C_r}}{\gamma R} e^{-\delta t} \sin \omega t; \quad \gamma = \sqrt{\frac{4L}{CR^2} - 1};$$

$$\omega = \sqrt{\frac{1}{LC} - \frac{R^2}{4L^2}} = \delta\gamma; \quad \delta = \frac{R}{2L}.$$

Parameters of the discharge contour of the machine C, R and L are taken to be constant in time and unchanged during the welding process. For parameter L this condition is satisfied in welding small diameter pipes, when the total inductance of the discharge contour varies only slightly during the time of flight t_f of the impelled pipe. We also assume that the start of motion of the part (pipe) practically coincides with the start of current pulse (moment of time $t = 0$).

Maximum discharge current is found from the following formula:

$$I_{max} = U_{C_r} \sqrt{\frac{C}{L}} e^{-\delta t_{max}}; \quad t_{max} = \frac{\operatorname{arctg} \gamma}{\omega},$$

where t_{max} is the time of reaching maximum current.

It should be further noted that the maximum rate of current rise is observed at the start of capacitor bank discharge, when $(di / dt)_{max} = U_{C_r} / L$ [3].

Figure 2 gives the schematic of MPW process, when applying the impact to the deformed part of the pipe.

Inductor-concentrator with the width of working section b_c usually has a conicity of the same angle α. Taking into account expression $\alpha = (b_p / 2)\sin \alpha$, the

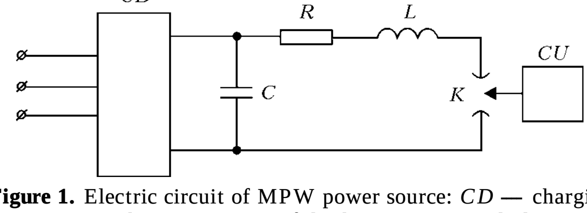

Figure 1. Electric circuit of MPW power source: CD — charging device; R — ohmic resistance of discharge circuit including resistance of the propelled pipe; L — inductance of discharge contour including inductance of magnetically-coupled inductor and welded parts; CU — control unit (for other designations see the text)

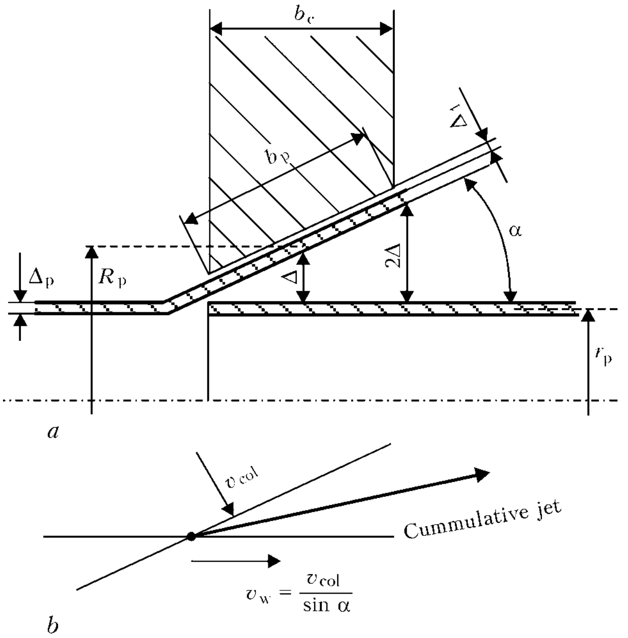

Figure 2. Schematics of MPW implementation at propelling the deformed section of the pipe (*a*) and forming of a cumulative jet (*b*): r_p — average radius of initial pipe-billet; R_p — average radius of expanded section of the impelled pipe in the welding zone; Δ_p — wall thickness of impelled pipe; Δ — average value of the gap between the pipes being joined; Δ_1 — average value of the gap between the inductor-concentrator and pipe; α — angle of pipe expansion; b_p — width of overlap (for other designations see the text)

mean radius of the pipe after expansion rolling is found from the following formula:

$$R_p = r_p + \Delta + \Delta_p = r_p + (b_p / 2)\sin\alpha + \Delta_p. \qquad (1)$$

From expression (1) we derive coefficient k_p, allowing for the change of the radius of the impelled pipe after expansion rolling:

$$k_\eth = (R_\eth / r_\eth) = 1 + [(\Delta + \Delta_\eth) / r_\eth].$$

In practical calculation of welding modes, used as the set values are the recommended ranges of some parameter values, which are obtained experimentally for various metals: this is the frontal collision velocity v_{col}, velocity of collision wave motion (points of convergence) v_w, and angle of collision α of the pipe [1]. A stable reproduction of the welding process can be guaranteed, if achievement of these parameters is ensured for this joint by variation of electric parameters of the power circuit of MPW machine. Let us consider the processes proceeding at discharge of the capacitor bank to electromagnetic inductor in MPW. The weight of the impelled expanded part of the pipe is

$$m = 2\pi r_\eth \Delta_\eth \gamma_\eth b_c,$$

where γ_p is the specific weight of the impelled pipe material.

Surface area S of magnetic field impact on the impelled pipe can be written as

$$S = 2\pi R_\eth b_\eth,$$

here and further on $b_p = b_c / \cos\alpha$ (Figure 2).

Force applied to the working section of the impelled pipe in the time interval up to the moment of magnetic field penetration through the pipe wall, is found from the following formula:

$$F = SB^2 / \mu_0,$$

where B is the average value of magnetic field induction in the gap between the inductor and impelled pipe; μ_0 is the magnetic constant.

In this case acceleration of the impelled part in its median part is equal to

$$a = F / m = B^2 / (\mu_0 \Delta_\eth \gamma_\eth) =$$
$$= [\mu_0 w^2 K_R^2 / \Delta_\eth \gamma_\eth b_\eth^2]\,(k_\eth / \cos\alpha) i(t)^2.$$

By the law of net current

$$B b_\eth / (\mu_0 K_R) = iw,$$

where $K_R = 1 - \Delta_1 / \pi b_p (1 - \exp[-\pi(b_p) / \Delta_1]$ is the Rogowsky factor; i is the current flowing through the inductor; w is the number of inductor turns (in our case $w = 1$).

Hence, the induction in the working zone is given by

$$B(t) = (\mu_0 w K_R / b_\eth) i(t).$$

Current velocity of the impelled pipe in its median part is found from the following formula:

$$v(t) = \int_0^t a(t)\,dt,$$

and the velocity of the impelled pipe in its median part at the moment of collision is

$$v_{col} = \int_0^{t_f} a(t)\,dt = \frac{w^2 \mu_0 K_R^2}{b_\eth^2 \Delta_\eth \gamma_\eth} \frac{k_\eth}{\cos\alpha} \int_0^{t_f} i(t)^2\,dt.$$

At this moment the collision velocity should be such that it satisfies the value of this parameter obtained experimentally for this material of the impelled pipe [1].

Average time of flight t_f is found from the following equation under the condition that the path covered by median part of the impelled pipe is equal to average value of gap Δ between colliding pipes (Figure 2):

$$\Delta = \int_0^{t_f} v\,dt = \frac{w^2 \mu_0 K_R^2}{b_\eth^2 \Delta_\eth \gamma_\eth} \frac{k_\eth}{\cos\alpha} \int_0^{t_f} \left(\int_0^t i(t)^2\,dt \right) dt. \qquad (2)$$

If Δ value is known, then we can find t_f by solving equation (2).

For the considered case, equation (2) cannot be solved for t_f analytically. However, for a specific task a numerical method using a PC program, for instance MathCAD, is applied to find average time of flight t_f of the impelled pipe from the following equation:

$$t_f = \text{root}\left[\Delta - \frac{\mu_0 K_R^2}{b_ð^2 \Delta_ð \gamma_ð} \frac{k_ð}{\cos\alpha} \int_0^x \left(\int_0^t i(t)^2 dt \right) dt,\ x\right].$$

With known values of t_f, the necessary design parameters of the welding mode can be found for a specific problem.

Conditional kinetic energy W_k (conditionality consists in that the different sections of the impelled pipe collide with a stationary pipe at different velocities and at different time) for impelled weight m is equal to

$$W_k = (m v_{col}^2)/2. \quad (3)$$

Values of conditional efficiency of the welding circuit in welding of one part are determined from the following expression:

$$\eta = 2 W_k / C U_{C_r}^2. \quad (4)$$

Sound velocity in liquid (in hydrodynamic shock wave) for the blank metal is equal to

$$v_s = (E_y / \gamma_ð)^{1/2},$$

where E, is the modulus of elasticity of the metal being welded.

Collision wave velocity v_w — cross-points, when the pipe is impelled at angle α (see Figure 2) should be below v_s to produce sound welding. It is found from the following formula:

$$v_w = (v_{col} / \sin\alpha).$$

As shown by practice, in order to produce sound welded joints by MPW, it is necessary to maintain certain values of v_{col} and v_w given in Table 1 [1].

Proceeding from the current concepts [1], the lower limit of collision velocity v_{col} is given by the conditions of formation of a cumulative jet (see Figure 2), and at v_{col} value below its lower limit value no welded joint forms, and just compression of the parts takes place. At values of velocities of collision v_{col} and collision wave v_w, exceeding the upper limit (Table 1), the welded joint develops defects. This is due to the following factors: first, development of tears and cracks in the welded metal under the impact of powerful sound waves on the weld at the velocity of the collision wave exceeding that of sound; secondly, presence of oxide films and other impurities in the welded joint metal due to the fact that the latter do not have enough time to leave the welding zone together with the cumulative jet due to «collapse» of the gap between the pipe surfaces being joined. Average value of collision velocity determines average time of flight t_f of impelled pipe. When the latter is impelled at angle α in the section of width b_c a certain time interval will be observed at which values of v_{col} satisfy the conditions of producing a sound welded joint, thus determining the width of the weld made by MPW process.

Table 1. Velocities of collision and collision waves for different materials

Metal/alloy	v_{col}, *m/s*	v_w, *km/s*
Aluminium	240–380	1.90–2.58
Copper	450–480	1.59–1.97
Bronze	About 400	2.12–3.24
Brass	460–520	1.77–3.14

In order to ensure a high quality of welding, it is also necessary to maintain a certain value of magnetic field pressure at the moment of part collision (upsetting). Instantaneous value of this pressure in welding is found from the following expression:

$$P(t) = B(t)^2 / \mu_0.$$

Magnetic field pressure at the moment of part collision corresponds to t_f

$$P_{col} = P(t_f).$$

Given below are calculations for two specific modes of aluminium pipe welding. Let us assume that the following geometrical parameters of the impelled pipe and welding zone are assigned: welding zone width; average gap between the inner pipe and impelled pipe billet Δ; gap between the inductor and impelled billet Δ_1; thickness and radius of impelled pipe r_p up to expansion; angle of pipe collision α.

Certain physical parameters characteristic for the processes proceeding at MPW are assumed to be known, namely absolute permeability of vacuum $\mu_0 = 4\pi \cdot 10^{-7}$ H / m, Rogowsky factor K_R [4], density γ_p and specific electric resistance of pipe metal ρ, modulus of elasticity E [5].

Variables are electric parameters of the process, namely total ohmic resistance of discharge contour R, total inductance of discharge contour L (taken to be a constant in calculations for the case, when the

Table 2. Calculated MPW parameters

Pipe diameter, mm	W_{in}, *kJ*	$L \cdot 10^5$, *mH*	*R, mOhm*	*Ñ*, μF	U_{C_r}, *kV*	$\rho_{Al} \cdot 10^8$, *Îhm·m*	$E_{Al} \cdot 10^{-9}$, *Pa*	γ_{Al}, kg/m^3	*di/dt, kA/m*
12	1.30	3.0	2.60	100	5.1	3.4	65	2700	170
20	1.57	3.3	2.74	100	5.6	3.4	65	2700	170

Table 2 (cont.)

Pipe diameter, mm	I_{max}, *kA*	$Â_{max}$, *Ò*	$Ð_{col}$, *Pa*	v_s, *km/s*	v_{col}, *m/s*	v_w, *km/s*	t_m, μs	t_f, μs	η, *%*
12	263	16.1	$6.0 \cdot 10^7$	4.91	243	2.32	59.875	9.5	5.50
20	275	16.9	$1.3 \cdot 10^8$	4.91	255	2.44	59.875	9.0	8.83

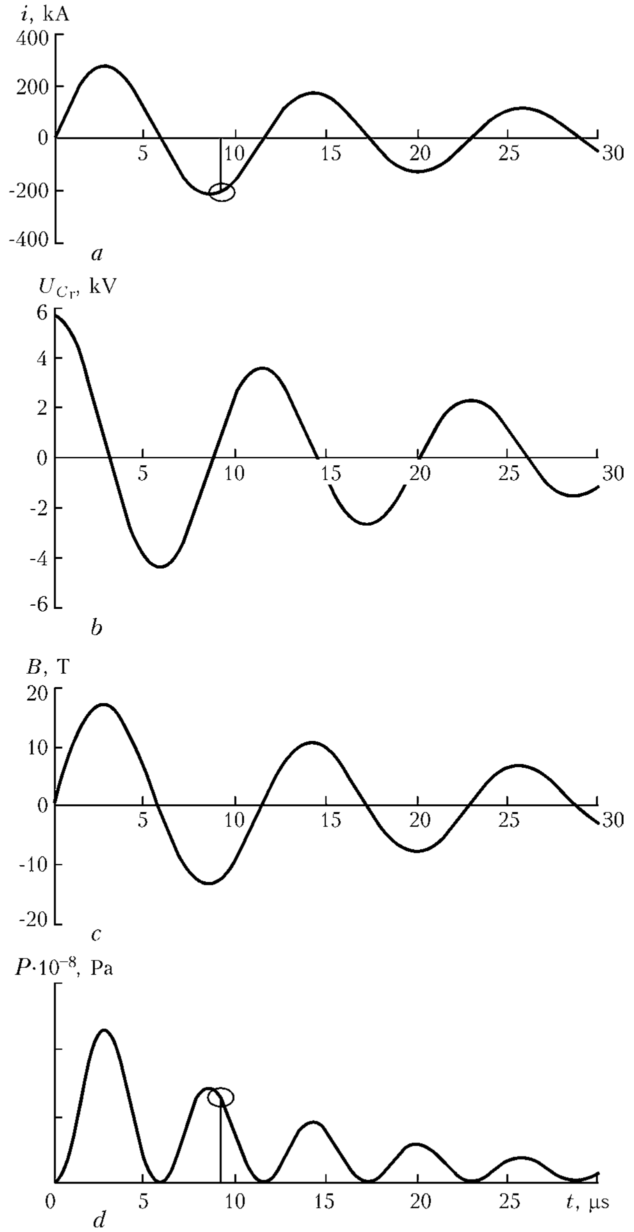

Figure 3. Calculated instant values of MPW parameters: *a* — discharge current $i(t)$; *b* — voltage of capacitor bank $U_{C_r}(t)$; *c* — magnetic induction in the working gap $B(t)$; *d* — magnetic pressure $P(t)$ (circles mark the moment of pipe collision and end of welding)

inductance of the impelled billet zone is equal to a small faction of L), integrator charge voltage U_{C_r}, integrator energy W_{in}, rate of current rise at the start of the discharge di / dt. MPW parameters were also calculated for the case, when a single-turn inductor-concentrator was used.

For this purpose satisfying inequality

$$t_m = (\mu_0 \Delta_\delta \Delta) / \rho > t_f,$$

where t_m is the time of magnetic field penetration through the impelled pipe, was checked, as well as maintaining the required ranges of collision velocities of the parts being welded, given in Table 1 [1].

The above calculations were used to determine the velocity of the collision wave, energy modes being calculated so that at normal running of MPW process the velocity were below that of sound in liquid, i.e. inequality $v_w < v_s$ should be satisfied. Range of these velocities is also given in Table 1 [1].

Since values C, L, R are constant, in order to stay within the limits of the above conditions, U_{C_r} values should be selected.

For a final estimate, the velocities of collision of parts v_{col} and collision wave v_w were calculated as the criterial parameters, the recommended values of which should be maintained to produce a sound welded joint [1]. In addition, average time of flight of the impelled part t_f and of magnetic field penetration through the impelled part t_m was calculated, so that inequality $t_m > t_f$ were satisfied. If achievement of these criterial parameters is ensured for the given joint, a stable reproduction of the welding process can be guaranteed.

Calculations were performed for aluminium pipes with the following geometrical parameters: thickness of impelled pipe of 1.35 mm; initial average gap between the inner and impelled pipe of 1.2 mm; initial gap between the inductor and impelled pipe of 1.5 mm.

Values of the main calculated parameters for the two variants of welding pipes with diameters of impelled pipes of 12 and 20 mm are given in Table 2. In all the cases $\alpha = 6°$ was assumed, and the conditional efficiency was calculated by formulas (3) and (4).

Figure 3 gives the calculated instantaneous values of MPW parameters in the case of an impelled pipe of 20 mm diameter. Curves in Figure 3 by the nature of parameter variation are similar to those produced for impelled pipe of 12 mm diameter.

Analyzing the calculation results given in Table 2, note the following aspects: in MPW of 12 mm diameter pipe the time of flight is $t_f = 9.5$ μs (1.75 current half-wave), and for a pipe of 20 mm diameter $t_f = 9$ μs (1.5 current half-wave), the time of the magnetic field penetration through the impelled part being the same in both the cases and equal to 60 μs; in welding of a large pipe of 20 mm diameter the conditional efficiency is greater ($\eta = 8.83$ %) than in welding of a pipe of 12 mm ($\eta = 5.50$ %).

In the case of welding large diameter pipes the charging voltage of the capacitor bank should be higher than in welding smaller diameter pipes so that the velocity of collision of the propelled parts and that of the wave were in the admissible range. In this case, the inductance and ohmic resistance of the welding machine discharge contour are increased, leading to lower frequency of oscillating discharge of the capacitor bank.

Thus, the proposed calculation procedure allows calculating the MPW parameters and selecting the optimum welding modes with an accuracy sufficient for practical purposes.

1. Dudin, D.A. (1979) *Magnetic-pulse welding of metals*. Moscow: Metallurgiya.
2. Pentegov, I.V., Stemkovsky, E.P., Shejkovsky, D.A. (1971) Parametric stabilisation of capacity discharge resistance welding conditions. *Avtomatich. Svarka*, **10**, 13–15.
3. Paton, B.E., Lebedev, V.K. (1969) *Electric equipment for resistance welding*. Moscow: Mashinostroenie.
4. Vasyutinsky, S.B. (1970) *Problems of theory and calculation of transformers*. Leningrad: Energiya.
5. Key, D., Lebi, T. (1962) *Tables of physical and chemical constants*. Moscow: Fizmatgiz.

ANTI-FRICTION PROPERTIES AND CORROSION RESISTANCE OF AL_2O_3 DETONATION COATINGS USED IN MARINE ENGINEERING

E.A. ASTAKHOV
E.O. Paton Electric Welding Institute, NASU, Kiev, Ukraine

The paper gives results of anti-friction and corrosion tests of the detonation coatings of Al_2O_3 in similar combination and in pair with high-tin bronze in water, including with an addition of grease lubricant, as well as results of long-time comparative tests of the above coatings in pair with caprolon. A satisfactory performance of samples simulating operation of bearings of the support assembly of rudder spindle is proved.

Keywords: *detonation coating, aluminium oxide, corrosion properties, friction pairs, specific pressure, friction coefficient, anti-friction properties*

Parts of a rudder and propeller complex of ships, i.e. rudder, stern and propeller shafts and screws, are vitally important devices, ensuring reliable and safe sailing of ships [1]. In this connection, selection of a material of coating to replace bronze covering of drive shafting to provide extension of life of a bearing assembly and, therefore, reduction of costs of repair because of corrosion and wear of bronze is a topical area in current research.

Research results given in studies [2, 3] indicate that the Al_2O_3 detonation coatings are characterised by a high level of adhesion strength (30–35 MPa) and microhardness (*HV* 11,500–12,500 MPa).

This study considers anti-friction properties and corrosion resistance of similar (Al_2O_3–Al_2O_3) and dissimilar (Al_2O_3–high-tin bronze Br.OF-10-1) friction pairs. The detonation coatings were applied to samples of steel 45, stainless steel 08Kh18N10T and titanium alloy 3M.

Anti-friction properties were studied using the heel friction machine of the LPI design [4]. The machine is intended for simulation and investigation of basic principles of the friction wear process for different combinations of pairs of materials. The studies were conducted on pairs of samples consisting of rings 8 mm high with outside and inside diameters of 52 and 32 mm, respectively, and three columns 5 mm in diameter and 14 mm wide fixed in a special washer. Wear resistance, friction coefficient and state of the working surface were used as the criteria of performance in friction. The total friction path during the tests was 5 km. Wear resistance was estimated from the relative wear criterion [5].

In a similar friction pair, aluminium oxide under a specific pressure of 5 MPa provided performance of the wear surfaces over a path of 5 km without damage, wear of a ring being 0.8 μm, that of columns being 8.9 μm and friction coefficient amounting to 0.346–0.585.

In a dissimilar friction pair, the column samples were made from bronze Br.OF-10-1. Transfer (spreading on) of the latter to the aluminium oxide coating surface took place in friction in water under a specific pressure of 10 MPa, which led to increase in the friction coefficient (μ) to 0.812. Wear of bronze also increased, as this was the case of friction of similar materials. Intensive spreading of bronze on the coating surface was accompanied as a rule by fatigue spalling and cracking of the coating. Wear of bronze amounted to 745 μm. Given that bronze Br.OF-10-1 has low performance in water (in friction on the aluminium oxide surface), it was subjected to extra friction tests by adding a disposable grease lubricant to water after each kilometre of the friction path. The use of a marine grease lubricant of the AMS-1 grade (Figure 1) dramatically changed the friction conditions, i.e. spreading of bronze and friction coefficient substantially decreased. Wear of bronze in this case was reduced more than 30 times. As shown by estimation of wear of the bronze washer and Al_2O_3 sprayed layer on the rudder spindle, wear of the Br.OF-10-1 rudder spindle bearing support during two years of operation may amount to 500 μm, and that of the sprayed layer — to 25 μm (in case of using a grease lubricant in water). The use of this friction pair without a lubricant is not permitted.

Depending upon the sailing region and type of a ship, stern bearings of drive shafting are made from rubber, caprolon or guaiac resin. The caprolon bearings have become most common lately. The second element of the friction pair is a bronze jacket, which is put on the main shaft by shrinkage or hydraulic press fit.

Specific pressure in a bearing is normally no more than 0.3 MPa, and friction rate is 6 m / s [6]. Investigations of performance of the Al_2O_3 coating for shafting bearing operation conditions were conducted using the SMTs-2 friction machine at a friction rate of 2 m / s and specific pressure of 0.5 MPa.

The tests were conducted on samples simulating the shaft–bearing system. A caprolon bushing 40 mm in diameter and 25 mm wide pressed into a special

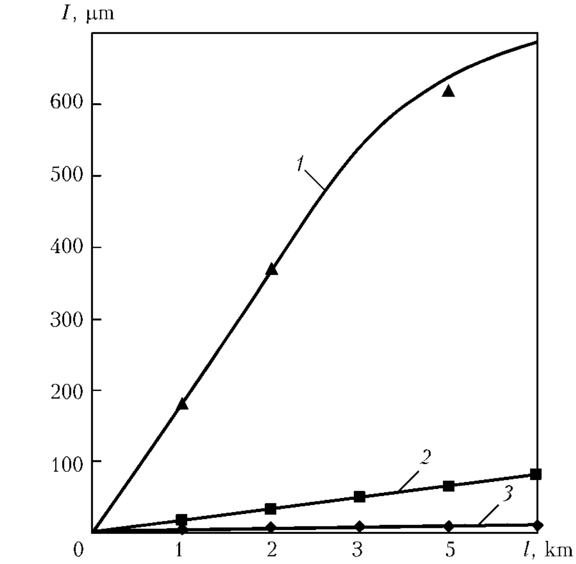

Figure 1. Dependence of wear I of friction pair upon friction path l at friction rate v = 0.25 m / s and specific pressure q = 5 (*1*), 10 (*2*) and 20 (*3*) MPa: *1* — Al_2O_3–Al_2O_3 in water (μ = 0.346–0.486); *2* — Br.OF-10-1–Al_2O_3 in water + AMS-1 (μ = 0.092–0.162); *3* — Br.OF-10-1–Al_2O_3 in water (μ = 0.380–0.812)

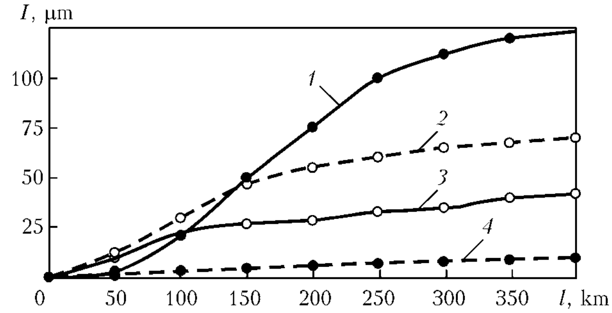

Figure 2. Dependence of wear of caprolon–Al_2O_3 (*1, 4*) (μ = 0.05–0.16) and caprolon–bronze (*2, 3*) (μ = 0.05–0.20) friction pairs at v = 2 m / s and q = 0.5 MPa: *1, 3* — wear of caprolon; *2, 4* — wear of bronze and Al_2O_3 coating, respectively

washer served as the bearing. The washer was mounted on the testing machine. The coating was deposited on the outside surface of the shaft and polished. The samples were placed in an air-tight testing chamber filled with running water. The samples in the form of rollers were measured using a vertical comparator of the IZV-2 model with a scaling division value of 0.1 μm, and the samples in the form of bushings — using an internal measuring device with a scale division value of 0.01 mm. Prior to the tests, the measurements were made before and after running in, as well as each 50 km of the friction path. The pair studied was run in by gradually increasing specific pressure from 0.1 to 0.5 MPa. The tests were conducted on coatings of Al_2O_3 in pair with caprolon. To obtain comparative data, the tests were conducted also on a pair of Br.OF-10-1–caprolon, which is widely applied in ship building.

As shown by results of long-time comparative tests (Figure 2), wear of caprolon in both friction pairs depends upon the friction path. It decreases and stabilises with increase in the friction path. In friction of caprolon on a high-tin bronze, its wear is lower than in friction on the Al_2O_3 coating. However, the wear of bronze is much higher than that of the coating. The wear surfaces of the coated samples exhibited no visible damages, but their gradual polishing took place. In friction of caprolon on bronze, the bronze wear particles penetrated into caprolon to form a solid bronze layer on its surface. It is this fact that seems to explain increased wear of the bronze bushing in pair with caprolon, compared with the caprolon–coating pair.

Variations in friction coefficients of the pairs tested are shown in Figure 2. Their highest values correspond to the beginning of run-in and moment of starting up of the friction machine, while the lowest values correspond to the moments of steady-state friction and friction at the end of each test.

Electrochemical measurements (plotting of polarisation curves, measurement of steady-state potentials and potentials of contacting pairs) and tests to general, contact and crevice corrosion were carried out to evaluate corrosion resistance of the Al_2O_3 coatings.

Results of corrosion tests of different Al_2O_3 coatings

Detonation coating	*Substrate*	*Test time, h*	φ_{st}, *V*	*Character of corrosion damages in contact*			
				without contact	*with alloy 3M*	*with graphite*	*with carbon steel*
Al_2O_3	Alloy 3M	3700	+0.07	No visible damages	No visible damages	No visible damages	–
	Steel 08Kh18N10T	1500	+0.05	Same	–	Same	–
	Steel 45	2000	–0.32	Brown spots, crack in coating — corrosion of substrate under coating	–	Crack in coating, heavy corrosion of substrate. Corrosion rate 0.04 g / ($m^2 \cdot h$)	Deposit of steel 45 corrosion products
Al_2O_3 impregnated by «Anatherm-1» sealant	Steel 45	1500	–0.10	No visible damages	–	No visible damages	–

Polarisation curves were taken under dynamic conditions at a rate of 200 mV / min in normal (0.5 n) solution of NaCl.

Being electrically insulating, the Al_2O_3 coating does not take part in the electrode process, although the presence of pores in it leads to formation of a compromise potential that measures electrochemical characteristics.

Measurement of steady-state corrosion potential φ_{st} of the samples was carried out using the VK7-9 voltmeter. The measurements were made every day during a period of 32 days up to establishment of the steady-state corrosion potential values (total test time is given in the Table).

Samples with the coatings in a combination with graphite, alloy 3M and steel 45 were tested to contact corrosion in synthetic sea water of a medium salinity amounting to 35 %. φ_{st} of the contacting pairs was measured every day during a period of 32 days.

Graphite does not cause corrosion of samples of alloy 3M and steel 08Kh18N10T with the Al_2O_3 coating, potential of the short-circuited pairs coincides with that of individual samples. In case of the steel 45 sample with the sprayed Al_2O_3 coating in contact with graphite, the potential difference amounts to a critical value, i.e. $\Delta\varphi = 0.22$ V. Electrolyte penetrates via pores to the substrate and causes its intensive corrosion. In contact of these samples with steel 45, the latter plays a protecting role.

Contact of alloy 3M with the 3M samples did not affect their corrosion resistance.

General corrosion tests were conducted under laboratory conditions in synthetic sea water. The time of the tests and results of periodic microscopy examinations are given in the Table.

Crevice corrosion tests were conducted on samples of the bushing–shaft type in synthetic sea water for 4000 h. The bushing was made from organic glass, the gap being about 0.1 mm.

Because of a negative effect of porosity on performance of the Al_2O_3 coating on the steel 45 sample, the coating was impregnated with the anaerobic sealant «Anatherm-1». After polarisation at room temperature, the sealant closes pores in the coating, thus preventing penetration of an aggressive environment into the substrate material (see the Table).

The coated samples of stainless steel 08Kh18N10T and alloy 3M exhibited no sensitivity to crevice corrosion, while the fact of general corrosion taking place under the coating layer was proved by an example of samples of steel 45.

The corrosion tests showed the following:

• because of the presence of pores, the Al_2O_3 detonation coating deposited on steel 45 does not protect it from corrosion in sea water; accumulation of the substrate corrosion products in pores leads to fracture of the sprayed layer;

• samples of steel 08Kh18N10T and alloy 3M with the Al_2O_3 coating had high corrosion resistance; contact with graphite did not affect corrosion resistance of the samples in synthetic sea water;

• results of general corrosion tests of the steel 45 samples with the Al_2O_3 coating impregnated with the anaerobic sealant «Anatherm-1» proved efficiency of the impregnation; the steel 45 substrate material was not corroded.

CONCLUSIONS

1. Anti-friction properties and corrosion resistance of the Al_2O_3 detonation coating provide its performance in water under a specific pressure of up to 5 MPa and at friction rate of 0.25 m / s in the similar friction pairs, whereas in a pair with caprolon its performance is ensured under a specific pressure of up to 0.5 MPa and at friction rate of 2 m / s.

2. In the case where the Al_2O_3 coating is deposited on carbon steel, to avoid corrosion of base metal and subsequent fracture of the coating layer, the latter should be impregnated with an anaerobic sealant or a corrosion-resistant sub-layer should be deposited.

3. Estimation of wear of the bronze bushing–Al_2O_3 pair made on the basis of the results of laboratory anti-friction tests showed that wear of bronze for two years of operation is no more than 500 μm, and that of the sprayed Al_2O_3 coating is no more than 25 μm, providing that the grease lubricant of the AMS-1 type is applied in water, which is 2–3 times better than in the case of the bronze bushing–caprolon pair.

4. Results of long-time tests of shafting bearings with the Al_2O_3 coating in pair with caprolon prove their good performance, as well as the possibility of replacing bronze coverings by carbon steel with the Al_2O_3 coating.

Acknowledgement. *The author expresses his gratitude to V.N. Goldfajn, Candidate of Technical Sciences, associate of the Central Research Institute for Structural Materials «Prometej» (Russian Federation), for his assistance in performing this study.*

1. Vinogradov, S.S. (1967) *Express repair of catcher boats*. Leningrad: Sudostroenie.
2. Zverev, A.I., Sharivker, S.Yu., Astakhov, E.A. (1979) *Detonation spraying of coatings*. Leningrad: Sudostroenie.
3. Kharlamov, Yu.A., Anisimov, M.I., Goldfajn, V.N. et al. (1990) Formation of aluminium oxide detonation coatings. In: *Heat-resistant inorganic coatings*. Leningrad: Nauka.
4. Goldfajn, V.N., Astakhov, E.A., Zverev, A.I. et al. (1979) Study of anti-friction properties of VK15 coatings deposited on VT5 alloy by the detonation method. *Poroshk. Metallurgiya*, **1**, 81–84.
5. Chechulin, B.B., Ushkov, S.S., Razuvaeva, I.N. et al. (1977) *Titanium alloys in mechanical engineering*. Leningrad: Mashinostroenie.
6. Vinogradov, S.S., Gavrish, P.I. (1980) *Wear and reliability of rudder and propeller complex of ships*. Moscow: Transport.

STATE-OF-THE-ART AND ADVANCED TECHNOLOGIES OF ELECTRON BEAM WELDING OF STRUCTURES*

B.E. PATON and **A.A. BONDAREV**
E.O. Paton Electric Welding Institute, NASU, Kiev, Ukraine

The paper describes a number of ingenious technological developments made by specialists of the E.O. Paton Electric Welding Institute during the period from 1969 to 2003. Advantages of electron beam welding process are shown by an example of specific structural materials. Recommendations on design of a welding process under industrial enterprise conditions are given. Examples of new technological developments, including welding of high-strength aluminium alloys alloyed with lithium and scandium, welding of dissimilar and composite materials, are described.

Keywords: *electron beam welding, aluminium alloys, programming, heat input, welded structures, dissimilar materials, composite materials, dispersion, fabrication technology, discrete scanning*

Process of EBW belongs to the category of high technologies and is mainly applied in fabrication of structures of which high requirements are made on quality, strength and reliability of the welded joints. Over more than 45 years since the moment of the first industrial introduction, it has become widely applied in aerospace engineering, power generation, aircraft construction, shipbuilding, instrument-making, etc. [1, 2].

E.O. Paton Electric Welding Institute (PWI) developed and introduced into industrial production the technologies of fabrication of large-sized casing structures and fuel tanks of ballistic missiles [3–6], navy missiles [7–10] and cruise missiles [11, 12]. Electron beam is used to weld foil systems of hydrofoils. As a final assembly-welding operation this process is applied in fabrication of gyroscopes of launch platforms, modern tanks, ship navigation systems [13–15]. EBW is used to make thick-walled shell structures of nuclear complexes and thin-walled elements of microwave devices. EBW of aluminium alloys is widely applied in fabrication of structures, of which higher requirements are made on strength, tightness of the joints operating under the conditions of alternating loads, deep vacuum and cryogenic temperatures. Examples of such structures are given in Figures 1–4.

Application of EBW of products is cost-effective under the conditions of their mass production, for instance, in welding of pistons with the oil cooling cavity of augmented diesel engines (Figure 5). An example of EBW application as a finishing operation is welding the cases and gyroscope «floats» (Figure 6). It provides the high quality and accuracy of product fabrication, which cannot be achieved, when using other welding processes. This process is particularly effective in fabrication of large-sized structures, having welded joints of one type. In this case the process of welding with local vacuumizing of the butt joint is implemented. Such a technology was used to make large-diameter shells, having several longitudinal butt joints [16, 17], as well as thick-walled panels of bottom blanks for railway tank cars of pure aluminium [18]. In order to make shells of sheet finned panels a technology of their welding with elastic pretension of the elements to be welded has been developed (Figure 7).

This list could be continued, but the main point remains to be the principle of taking into account the criteria and evaluations, which should be used when making the decision in favour of EBW application. At present technology engineers and designers, unfortunately, do not always have the complete information, characterizing the capabilities of this welding process. Experience accumulated at PWI in this area allows generalizing and formulating its main features and advantages as follows:

- improvement of strength properties of the joints by 15–25 %, compared to arc welding processes;
- narrow HAZ, and, as a result, lowering of weight parameters of the products;
- high stability of the geometrical shapes and dimensions of structures, particularly when EBW is a finish operation of making the products;
- high quality of welded joints;
- absence of oxide and tungsten inclusions; removal of impurities with metal vapours; fine-crystalline structure of weld metal and preservation of its structure in the HAZ metal, etc.;
- ability to weld structures in the absence of access to the reverse side of the butt; gravity welding of thin metal; welding in different spatial positions, also with simultaneous feed of filler wire into the weld pool;
- low level of overall heating of the structures and ability of simultaneous vacuumizing of the inner volume, particularly in sealing of instruments;
- independence of welded joint quality on the human factor, high purity, vacuum hygiene and ecological compatibility of the process;
- high efficiency of the welding process at up to 120 m / h and higher speeds, ability to implement the

*Materials of this paper in a shortened variant were presented in the 6th International Conference on Beam Technologies, held on April 20–28, 2004 in Halle, Germany (Vortrage der 6 Konferenz «Strahltechnik» in Halle vom 20 bis 28 April 2004. — DVS SLV, GDL. — S. 75–79).

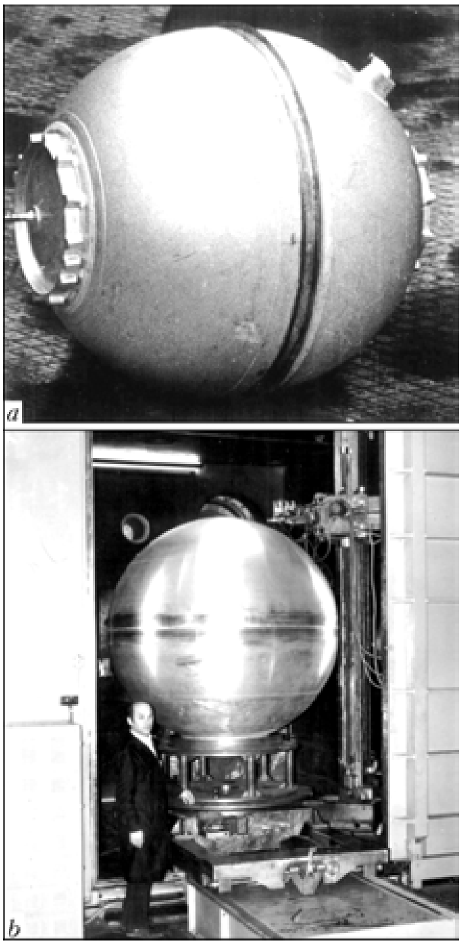

Figure 1. EBW of spherical tanks of aluminium alloys of 600 (*a*) and 2000 (*b*) mm diameter

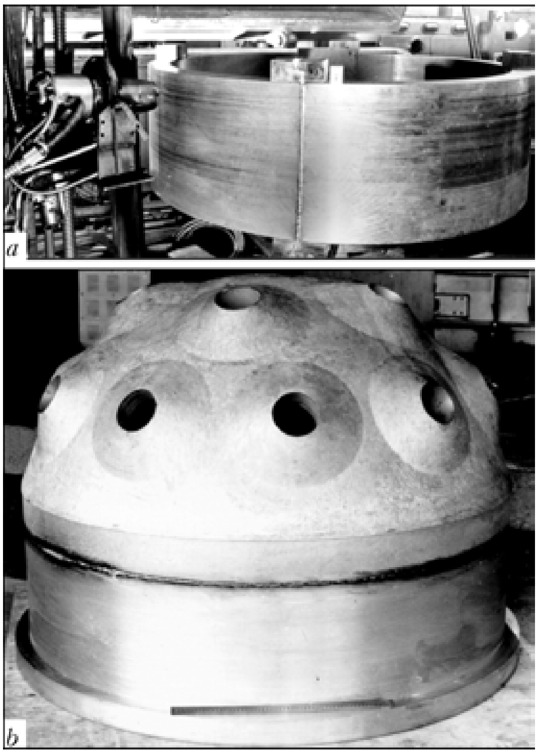

Figure 2. EB welded shell (*a*) and half-sphere (*b*) of 1201 alloy with 90 and 100 mm thickness of the edges being welded

Figure 3. Appearance of a fragment of a large-sized AMg6 alloy shell of 1145 mm diameter and with 90 mm thickness of edges being welded

group technology at simultaneous loading of a batch of parts into the chamber;

• complete automation of all the operations on control of the power source, vacuum units, manipulators, hardware for control of the beam and quality diagnostics;

• cost-effectiveness compared to argon-arc (AAW) or plasma welding (no need for shielding gases, tungsten electrodes, edge preparation in welding thick metal);

• ability to weld some types of joints which cannot be made by other welding processes.

Mastering EBW process on the shop floor requires taking a number of measures, the main list of which is given in Figure 8. The main attention should be given to fitting the EBW machine and power unit with the modern controls based on computers systems with the appropriate software. Only with such a so-

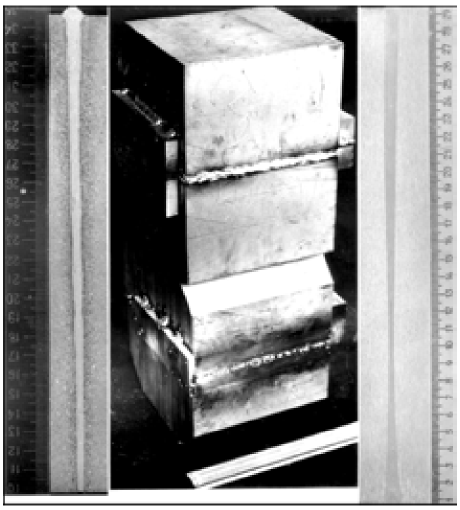

Figure 4. Appearance of mock-ups of a thick butt joint from the side of the weld, as well as transverse macrosections of 1201 alloy joints 250 mm thick (*left*) and AMg6 alloy 300 mm thick (*right*). Uphill welding was performed in one pass with a horizontal beam

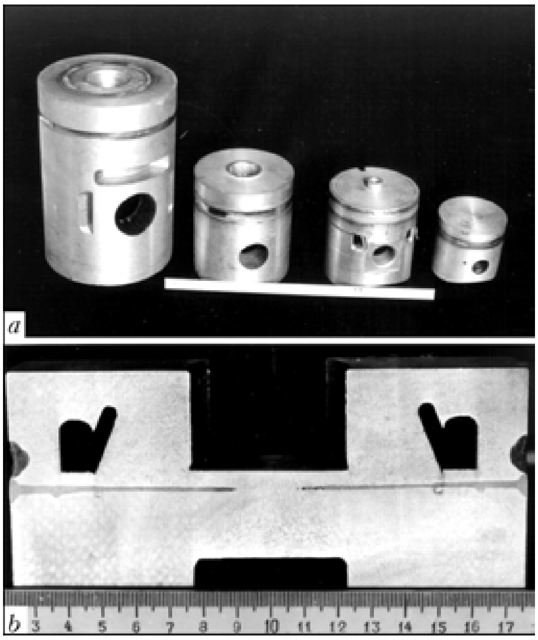

Figure 5. Range of welded pistons (*a*) and macrosection of a piston head with oil cooling cavity and hardfacing of the zone of upper compression groove made by EBW (*b*) [19]

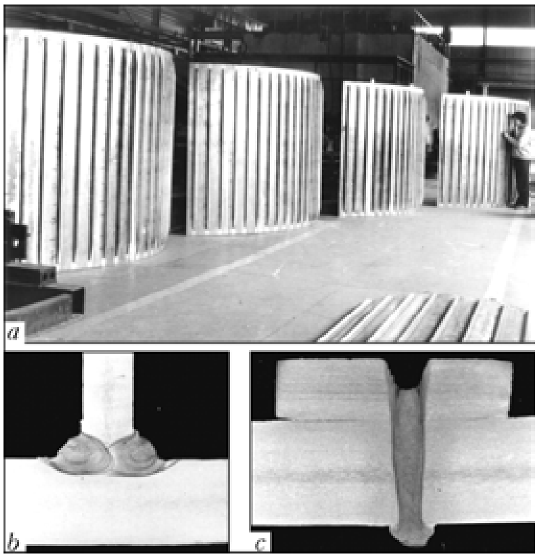

Figure 7. Appearance of a test batch of stringer panels of AMg6N alloy made with elastic pre-tension (*a*), and macrosections of a two-sided tee joint of stiffeners (*b*) and panel butt joint, when enlarging the panels (*c*), respectively

lution the impact of the human factor and external conditions on product quality will be minimal [21].

New structural materials with unique properties are now becoming available. Among such materials primarily are Al–Li alloys, Al-matrix composites, foam aluminium and nanomaterials, etc., which now are already widely used in aircraft, aerospace and defense industry. At the same time, EBW technologies, as well as equipment and controls for EBW units are continuously improved. This is due to the fact that similar to the use of the already known technologies, in welding of new structural materials it is necessary to ensure the maximum possible strength and operating properties of the joints and structures as a whole. With this purpose, PWI developed a fundamentally new EBW technology, which features the ability of controlled heat mass transfer under the conditions of a formed volume of weld pool liquid metal.

With any of the known fusion welding processes, control of liquid melt flows in the weld pool allows effectively improving the quality and tightness of the formed joints. In EBW of aluminium alloys, where the surface is covered by moisture-saturated oxide film, and the base metal in addition to dissolved hydrogen, also contains such alloying elements as zinc, magnesium, lithium, having a high vapour pressure under the conditions of the vacuum chamber, control

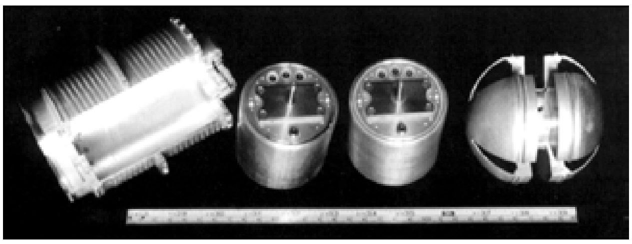

Figure 6. Cases of vacuum tubes of aluminium alloys made with EBW application [20]

of microcapillary processes and temperature conditions within the weld pool gains a special importance.

The basis of the developed technology is an instrument controlling the electron beam — a programmer, allowing discrete scanning of the electron beam by any assigned trajectory with its periodical stopping on the trajectory and with controlled dwell time in the discrete points by a pre-set program. Process control is performed using modern computer systems, and the programmer proper is adapted to operation with any power source, irrespective of the manufacturer of the power unit. Use of the developed hardware and software enabled solving at a higher level many design and technology problems [22]. Control of beam power distribution in the heated spot enables, for instance:

- controlling the fine structure of weld metal and on this basis improving the mechanical properties of joints;
- avoiding the anisotropy of strength characteristics in the joints in welding butt joints with very thick edges;
- producing joints of uniform weld width across edge thickness and thus reducing residual angular deformations;
- performing welding of joints with a large gap in the butt without electron beam penetration into the gap;
- performing welding of dissimilar materials having different thermophysical characteristics due to provision of different heat input along the butt edges;
- producing joints at difference in edge thickness of 1:50 and more;
- performing butt welding with simultaneous feed of filler wire from any side of the weld pool relative to the direction of beam displacement;
- welding joints with incomplete penetration without formation of root defects, and in circumferential welding avoiding formation of defects in the section of crater fading out and weld overlapping;

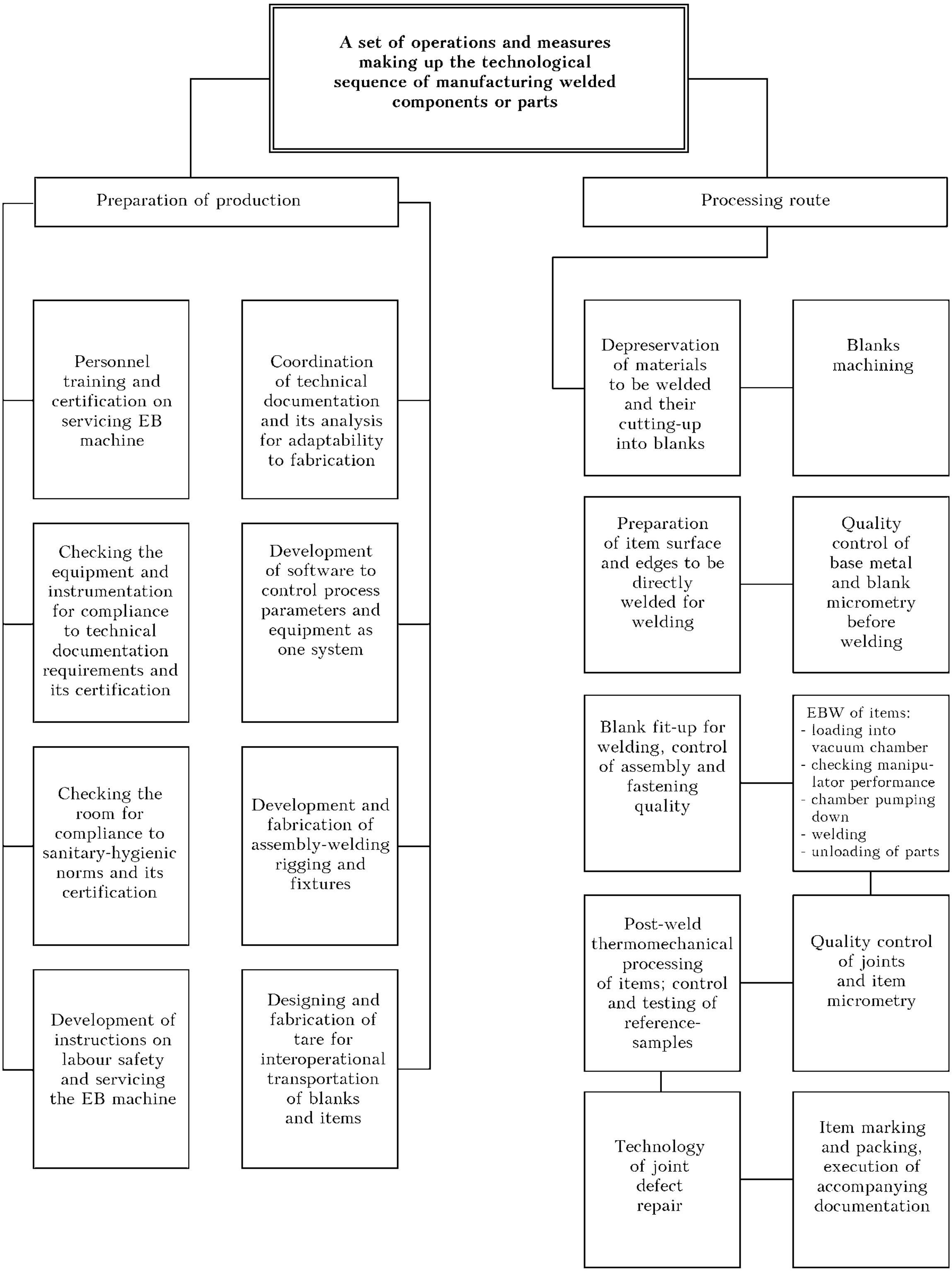

Figure 8. Schematic of measures for preparation of a shop section and technological process of structure fabrication with EBW application

• performing modification of surface layers of parts with alloying of the surface layer without dilution of matrix material.

Technological sequences of discrete scanning of the beam and diagram of spatial distribution of power density shown in Figure 9, are plotted using the computer and developed software [23–26]. Welding operator develops the program for making a specific joint (while meeting the requirements made to the quality of weld formation and weld tightness) in keeping with the developed algorithm, independently establishing all the necessary parameters of discrete scanning (path shape, its number of points, sequence of beam displacement from point to point, scanning amplitude, beam dwell time in each of the discrete points, etc.), and controls the result of implementation of the selected program on the monitor in the visual design mode (Figure 10). After establishing the main parameters of the welding process, the operator starts automatic running of the designed pro-

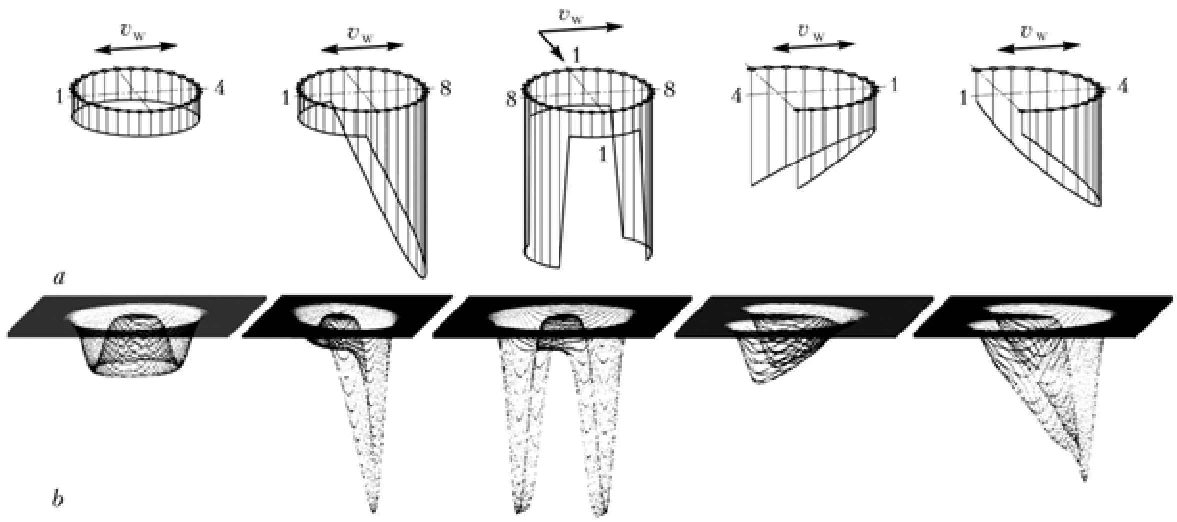

Figure 9. Technological sequences of discrete scanning of the electron beam (*a*), and diagrams of spatial distribution of power density (*b*) (numbers show relative time of beam dwelling in the discrete points on the scanning contour)

gram in the mode of real welding of products without operator involvement. Technique of EBW with programming of power density distribution in the heated spot enables at unchanged values of beam power and heat input parameters, producing joints of such a shape and structure, which cannot be reproduced with other fusion welding processes.

Figure 11 shows examples of asymmetric penetration of a weld of alloy AMg6 at a circular scanning of a 5 mm diameter beam and remelting of a powder-like filler on the surface of a blade of ChS70 alloy at up to 40 mm width of simultaneously processed zone in the cross-section and partial melting of the matrix base material of the blade to a not more than 150 μm depth. Variant of controlling the weld metal structure formation, depending on the scanning frequency and position of the beam focal spot relative to the weld surface is given in Figure 12.

Let us consider specific examples of implementation of new technology solutions in manufacture or welding of structures using advanced materials, which are difficult to weld or are believed to be unweldable.

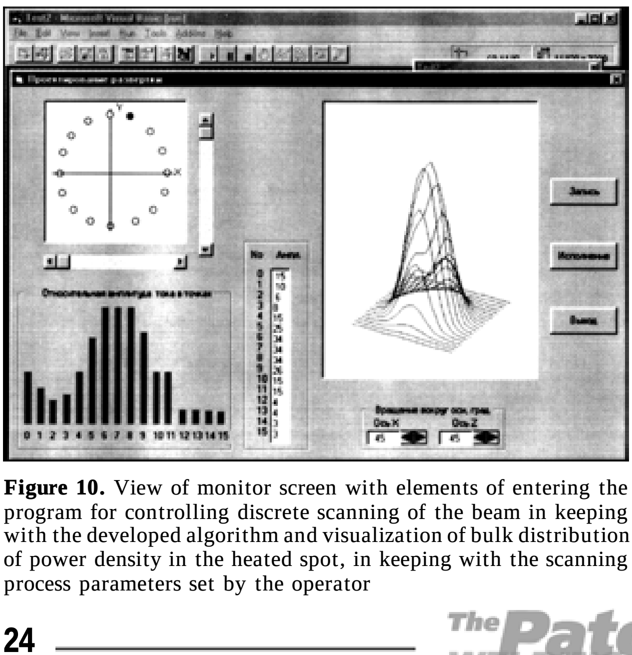

Figure 10. View of monitor screen with elements of entering the program for controlling discrete scanning of the beam in keeping with the developed algorithm and visualization of bulk distribution of power density in the heated spot, in keeping with the scanning process parameters set by the operator

We developed a technology of welding advanced high-strength Al–Li alloys with a guaranteed provision of high mechanical properties of welded joints (Table) and weld metal tightness.

Al–Li alloys have higher strength properties compared to the widely used AMg6 and 1201 alloys, and promote reduction of welded structure weight by 15–20 % due to a lower specific weight.

The problem of welding tubular transition pieces of dissimilar materials, namely stainless steel to aluminium alloys for cryogenic engineering has been solved in a fundamentally new manner. Nowadays, welding processes without edges melting, namely explosion welding, metallurgical rolling of the bimetal or diffusion welding are often used to make such transition pieces. All the above processes have one condition in common — a mandatory contact of pure aluminium with steel. In such a form the joint will have the strength properties on the level of pure aluminium, but its performance under thermal cycles will be limited due to the presence of an intermetallic interlayer in the transition zone.

PWI developed a method of welding materials, which excludes direct contact of aluminium to steel. With this purpose first a thin 3–7 μm layer of modi-

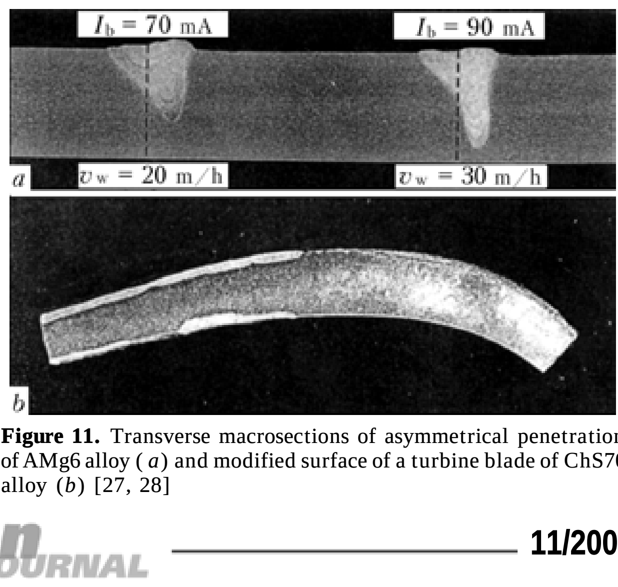

Figure 11. Transverse macrosections of asymmetrical penetration of AMg6 alloy (*a*) and modified surface of a turbine blade of ChS70 alloy (*b*) [27, 28]

Strength properties of Al–Li alloys and their welded joints

Alloy grade	Alloying system	Mechanical properties of base metal			Ultimate tensile strength of the joints, MPa	
		σ_t, MPa	$\sigma_{0.2}$, MPa	δ, %	AAW	EBW
1420	Al–Mg–Li	470	292	11.8	352	402
1421	Al–Mg–Li--Sc	490	358	9.8	385	407
1430	Al–Mg–Li--Cu	460	350	10.0	330	355
1440	Al–Mg–Li--Cu	505	440	5.0	295	317
1460	Al–Cu--Li	580	425	11.0	290	305

fiers such as nickel, zirconium, niobium etc. is applied from the vapour phase in vacuum onto the surface of the stainless pipe to be welded (Figure 13). A certain temperature mode ensures a reliable adhesion bonding of the deposited layer to the steel material. Then, after assembling the stainless steel pipe with that of any aluminium alloy, butt welding is performed so as to penetrate the aluminium pipe to the entire thickness, while the edge from the steel side is just preheated and wetted with liquid aluminium.

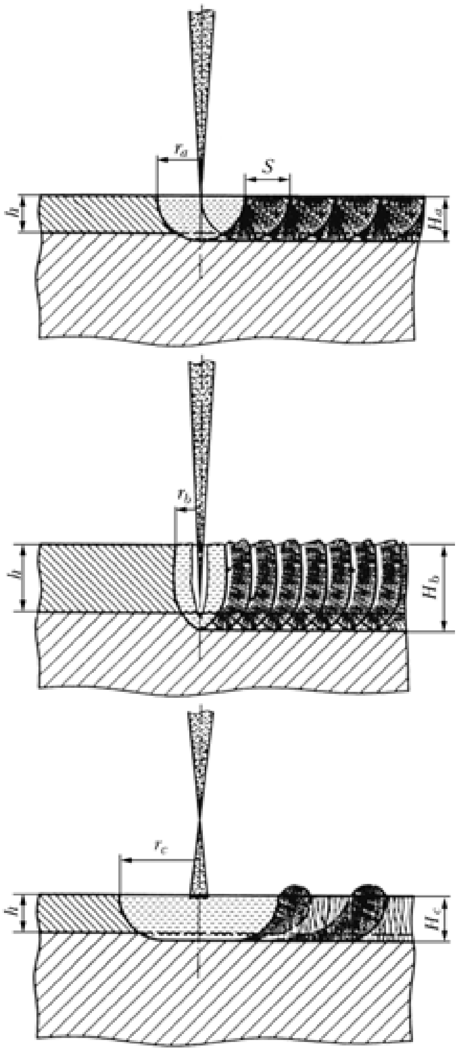

Figure 12. Schematic of surface layer structure formation at surface melting of a pre-deposited filler, depending on variation of parameters of a discretely scanning beam [29]

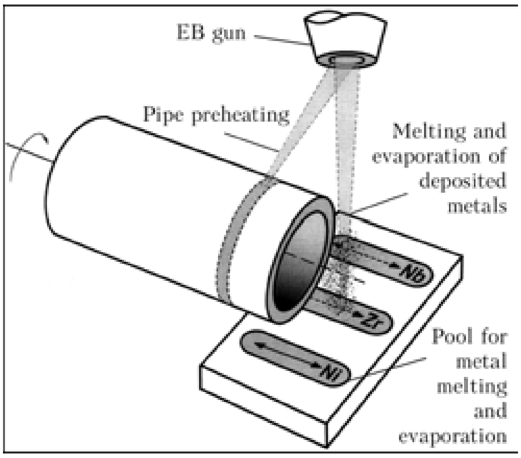

Figure 13. Technological sequence of vacuum deposition of a barrier coating of modifiers from the vapour phase on a stainless pipe surface before its welding to an aluminium alloy pipe

Implementation of this process became possible only when using the principle of programming the heat input in the required volume into each of the billets. Modifiers on the steel pipe surface provide additional alloying of the aluminium pool melt, and the joint acquires completely new properties. At rupture testing the ultimate strength was 320–350 MPa, which is 4--5 times higher than in testing the joints having an interlayer of intermetallics and pure aluminium (Figure 14).

Also developed was the technology of EBW of Al-matrix composites strengthened by SiC and Al_2O_3 particles, without melting the edges. Such joints are welded by applying onto the edges to be joined a dispersed flow of fine drops of filler material. Both the composite matrix material and another aluminium alloy can be used as the filler material. The consumable electrode of filler material is here surface melted by the electron beam, and due to its high-velocity rotation the finest drops, while falling on the edges, form a joint without any defects or interfaces (Figure 15). The same process could also be used to produce metal powders of superpure composition without surface layer oxidation, as well as superfine flakes. For this purpose a cooled target is placed in the dispersed

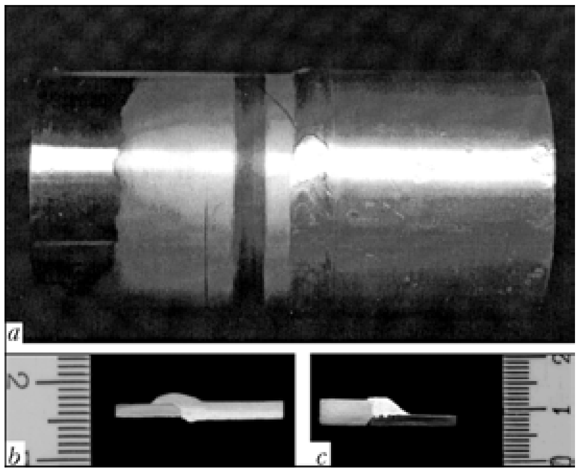

Figure 14. Appearance of a tubular transition piece of stainless steel--aluminium alloy (*a*), and macrosections of joints made by EBW with pre-deposition of modifiers from the vapour phase on stainless steel edge (*b*, *c*) [30]

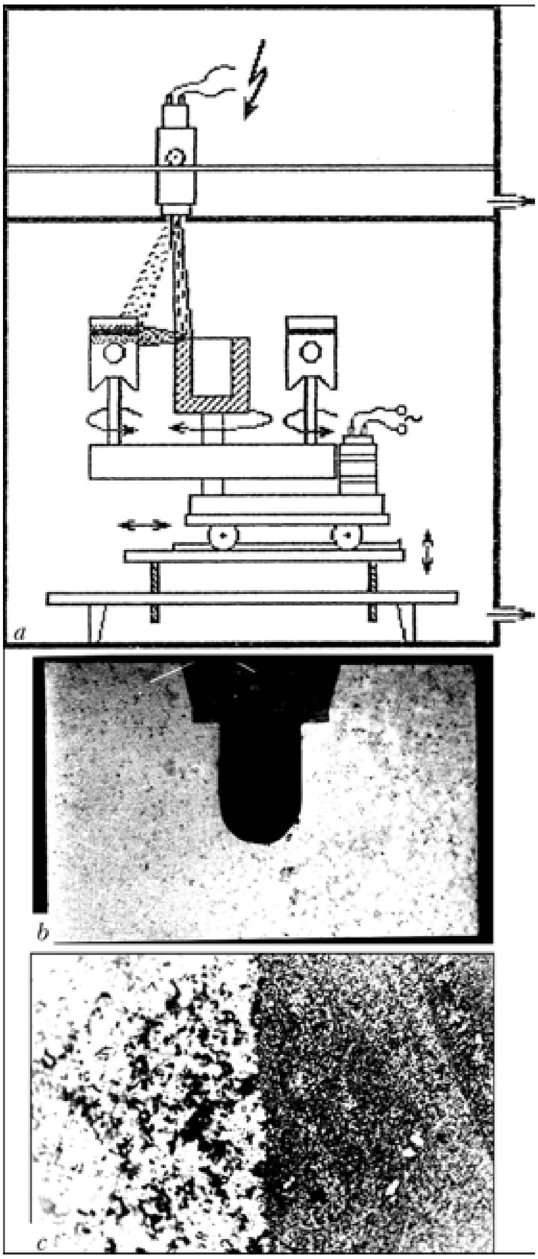

Figure 15. Process sequence of making joints by deposition of consumable electrode by EB vacuum dispersion (*a*); macrosection of sealing the oil cooling cavity in the piston head made of composite material of aluminium alloy + 18 % SiC (*b*); microstructure of composite–dispersed filler transition boundary (*c*) [31]

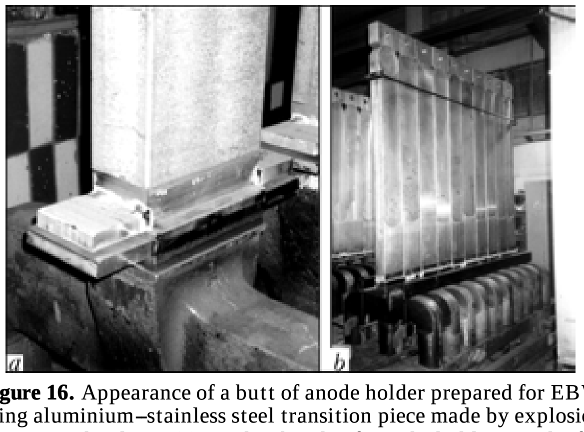

Figure 16. Appearance of a butt of anode holder prepared for EBW using aluminium–stainless steel transition piece made by explosion joining technology (*a*), and a batch of anode holders ready for shipment to metallurgical works (*b*)

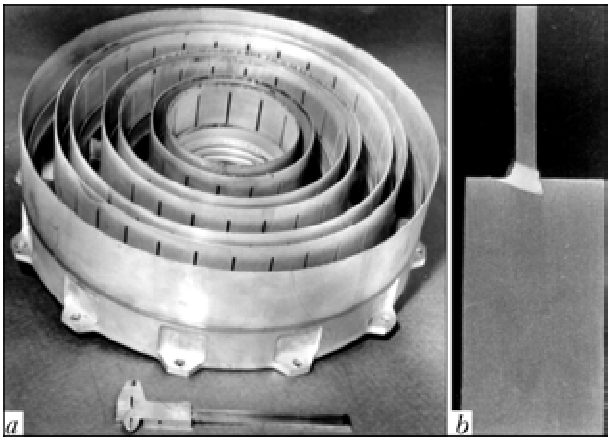

Figure 17. Fragment of a microwave radiation system made of aluminium alloy and EB welded (*a*), and transverse macrosection of a one-sided weld joining a thin-walled shell to a thick flange (*b*)

flow path, which is where drop flattening and solidification proceed. Such flakes have a nanocrystalline structure and can be used in manufacturing for extrusion of parts with special properties and structure.

A combined technology of making anode chutes for electrolyzers in aluminium production and apparatus clamps for power engineering has been introduced over the recent years. In the first case, explosion technology is used to make flat aluminium–stainless steel flat transition pieces, in the second case the same technology is applied to perform one- or two-sided cladding of pure aluminium to steel. Then the first transition pieces are used for EBW of the aluminium layer to aluminium buses, and the stainless layer is welded to the steel bracket. Steel-aluminium joint in this case is not subjected to any significant heating, and no growth of the intermetallic interlayer proceeds

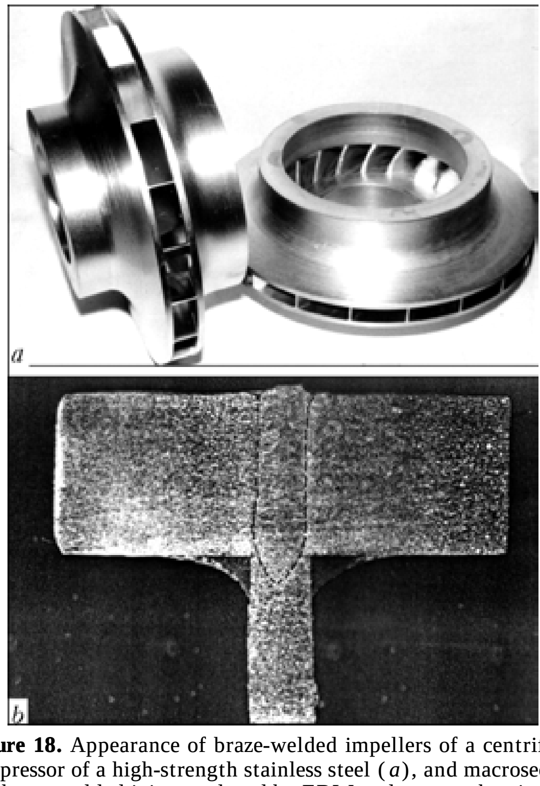

Figure 18. Appearance of braze-welded impellers of a centrifugal compressor of a high-strength stainless steel (*a*), and macrosection of a braze-welded joint produced by EBW and vacuum brazing (*b*) [32, 33]

on the interface. The structure can stand very high static loads (Figure 16). The same advantages are achieved also in fabrication of terminal clamps. Electric resistance does not rise after EBW.

Welding with a programmed heat input has been successfully introduced, when making elements generating microwave radiation. In this structure, thin-walled shells of 150–500 mm diameter with 0.8 mm wall thickness are welded to a 20 mm or thicker flange. A one-sided tee joint was produced with a high tightness of weld metal, while deformation of thin-walled shells did not exceed 0.03 mm per diameter (Figure 17).

In EBW of structures with thick edges or with their variable cross-section a technology was successfully implemented, which provides microalloying of weld metal with such modifiers as scandium, zirconium etc. across the entire depth of the pool. With this purpose, a filler in the form of thin foil of 100–200 μm was placed into the joint before welding. The foil was produced by super fast solidification in vacuum (up to 10^7 K / s) and included modifiers in the amount, which was much higher than their mutual solubility in aluminium. For instance, scandium content was 2–4, that of zirconium 1.4–1.5 vol.%. This allows increasing the tightness, and, which was more important, improving the strength properties of joints of any grades of aluminium alloys, and also improves hot cracking resistance.

In manufacturing high-strength stainless steel impellers of centrifugal compressors for gas-distributing stations by EBW, the cover disc was EB welded by a slot weld to the integral blades of the main disc. Then sections with lack-of-penetration were filled with high-temperature braze alloy with a filler and vacuum brazing of the impeller was performed. The thus produced joints were equivalent to base metal at fatigue and long-term strength testing of the samples. Impellers of 450–800 mm diameter made by the combined technology are shown in Figure 18.

In conclusion it should be noted that the above technologies belong to the category of high technologies, which are being continuously developed and improved. PWI specialists are ready to cooperate in this area with representatives of industrial and scientific organizations of any profile, irrespective of their form of ownership.

1. Paton, B.E., Nazarenko, O.K., Bondarev, A.A. et al. (1983) Electron beam welding and post-weld thermomechanical treatment of large diameter shells of 1201 alloy. *Avtomatich. Svarka*, **9**, 1–5.
2. Bondarev, A.A. (1999) Electron beam welding of high-strength aluminium alloys. *The Paton Welding J.*, Pilot Issue, 50–53.
3. Bondarev, A.A., Lozovskaya, A.V., Ishchenko, A.Ya. et al. (1974) Peculiarities of electron beam welding of 1201 alloy. *Avtomatich. Svarka*, **5**, 44–47.
4. Bondarev, A.A., Tretyak, N.G. (1980) Properties of sheet and plate EB welded joints of 1201 aluminium alloy. *Ibid.*, **7**, 49–51.
5. Bondarev, A.A., Tretyak, N.G. (1981) Peculiarities of EB welded 1201 aluminium alloy forgings of up to 250 mm thickness and mechanical properties of joints. *Ibid.*, **4**, 1–5.
6. Bondarev, A.A. (1981) Fatigue strength of AMg6, AMg6N, 1201 aluminium alloys and their joints made by electron beam welding. *Ibid.*, **6**, 40–42.
7. Bondarev, A.A., Lobanov, L.M., Pivtorak, V.A. et al. (1975) Investigation of mechanical properties, structure and strains of 01420 alloy joints made by electron beam welding. *Ibid.*, **3**, 14–17.
8. Bondarev, A.A., Rabkin, D.M., Kuzmenko, O.S. (1976) Weldability of AMg6 alloy by the electron beam in different spatial positions. *Ibid.*, **12**, 34–37.
9. Bondarev, A.A., Skryabinsky, V.V. (1987) Influence of parameters of electron beam scanning on characteristics of aluminium alloy welded joints. *Ibid.*, **12**, 57–62.
10. Bondarev, A.A., Baranov, V.V. (1988) Automation of interpretation of X-ray patterns of welds. *Ibid.*, **6**, 73–74.
11. Bondarev, A.A., Lozovskaya, A.V., Bondarev, Andr.A. (2002) Influence of the processes of fusion welding of high-strength aluminium alloys on mechanical properties and structure of welded joints. In: *Proc. of 7th Int. Conf. on Problems of Metallurgy, Metals Science and Welding*. Tbilisi: IMET.
12. Ternovoj, E.G., Bondarev, A.A., Peshcherina, S.V. et al. (1991) Electron beam welding of thick plates of AMg6 alloy. *Avtomatich. Svarka*, **6**, 49–52.
13. Bondarev, A.A., Kulaeva, A.F., Mikhajlichenko, M.D. (1965) Advanced methods of processing instrument components. *Avtomatika i Priborostroenie*, **2**, 63–66.
14. Bondarev, A.A., Voropaj, N.M., Ivanov, N.P. (1972) Development of electron beam welding technology for item casings of AMg6 alloy. *Svarochn. Proizvodstvo*, **3**, 18–20.
15. Bondarev, A.A., Shevelev, A.D., Zadery, B.A. (1991) Development of electron beam welding technology of non-ferrous and refractory metals and alloys. *Avtomatich. Svarka*, **6**, 46–48.
16. Bondarev, A.A., Nekrasov, A.A., Morejnis, M.I. et al. (1984) Electron beam welding of shells in local vacuum. *Ibid.*, **2**, 75.
17. Zubrienko, G.L., Tenenbaum, F.Z., Petrovanov, V.M. et al. (1980) Electron beam welding of large-sized assemblies of aluminium alloys in local vacuum chambers. In: *Proc. of 1st All-Union Conf. on Current Problems of Welding of Non-Ferrous Metals*. Kiev: Naukova Dumka.
18. Bondarev, A.A., Tretyak, N.G., Zarechensky, A.V. (1986) Electron beam welding of ADO aluminium as applied to manufacturing of boilers of rail tank cars. In: *Abstr. of 3rd All-Union Conf. on Welding of Non-Ferrous Metals*. Toliatti: TPI.
19. Bondarev, A.A., Ternovoj, E.G., Shalaj, A.N. (1988) Improvement of structural welded-cast diesel pistons made by EBW method. *Avtomatich. Svarka*, **8**, 74–75.
20. Paton, B.E., Lobanov, L.M., Pavlovsky, V.I. et al. (1989) Manufacturing of large-sized thin-walled welded panels of high-strength aluminium alloys. *Ibid.*, **10**, 37–45.
21. Paton, B.E., Nazarenko, O.K., Nesterenkov, V.M. et al. (2004) Computer control of electron beam welding with multi-coordinate displacements of the gun and workpiece. *The Paton Welding J.*, **5**, 2–5.
22. Bondarev, A.A., Bondarev, Andr.A., Lankin, Yu.N. (2003) Electron beam welding with a controllable heat and mass transfer. In: *Proc. of Int. Conf. on Current Problems in Welding and Life of Structures*. Kiev, Nov. 24–27, 2003.
23. Lankin, Yu.N., Bondarev, A.A., Bajshtruk, E.N. (1985) Control of power density distribution of the electron beam across its section. *Avtomatich. Svarka*, **6**, 12–15.
24. Bondarev, A.A., Skryabinsky, V.V. (1987) Influence of parameters of electron beam scanning on characteristics of aluminium alloy welded joints. *Ibid.*, **12**, 57–62.
25. Bondarev, A.A., Skryabinsky, V.V. (1987) Welding of aluminium alloys with programmed power density distribution according the heated spot. In: *Automatic control of electron beam welding technological process*. Kiev: PWI.
26. Bondarev, A.A., Bondarev, Andr.A., Lankin, Yu.N. (2003) Electron beam welding with controllable heat-mass transfer. In: *Abstr. of Int. Conf. on Current Problems in Welding and Life of Structures*, Kiev, Nov. 24–27, 2003.
27. Lankin, Yu.N., Bondarev, A.A., Bondarev, Andr.A (2001) Computer control of processes in the weld pool during electron beam welding. In: *Proc. of Int. Conf. on Surface Engineering and Part Reconditioning*, Feodosiya. Kiev: ATM Ukraina.
28. Zhadkevich, M.L., Bondarev, A.A., Zelenin, V.I. et al. (2001) Production of protective-restoration coatings of heat-resistant high-nickel alloys. *Ibid.*
29. Dudko, D.A., Bondarev, A.A., Zelenin, V.I. et al. *Method of coating formation on surface of parts*. Pat. 46073 Ukraine. Publ. 15.05.02.
30. Bondarev, A.A., Bondarev, Andr.A. (2003) Electron beam welding of tubular transition pieces of stainless steel-aluminium alloy dissimilar materials. In: *Abstr. of Int. Conf. on Current Problems in Welding and Life of Structures*, Kiev, Nov. 24–27, 2003.
31. Bondarev, A.A., Bondarev, Andr.A. (1996) Some principles of centrifugal vacuum spraying and mathematical model of the process in electron beam surface melting of a quickly rotating billet. In: *Proc. of Int. Conf. on Problems of Welding, Metallurgy and Related Technologies*. Tbilisi: IMET.
32. Yushchenko, K.A., Bondarev, A.A., Starushchenko, T.M. et al. (2000) Technology of manufacturing of braze-welded highly-loaded wheels of centrifugal compressors. In: *Abstr. of Int. Conf. on Welded Structures*. Kiev: PWI.
33. Radzievsky, V.N., Gartsunov, Yu.F., Tkachenko, G.G. et al. (2001) Peculiarities of formation of a thin-walled T-joint using brazing and fusion welding. *Svarochn. Proizvodstvo*, **4**, 42–46.

EFFECT OF HALIDE FLUXES ON POROSITY OF EB WELDS IN TITANIUM ALLOY VT6

V.N. ZAMKOV, E.L. VRZHIZHEVSKY, V.F. TOPOLSKY and **I.K. PETRICHENKO**
E.O. Paton Electric Welding Institute, NASU, Kiev, Ukraine

Application of halide flux in EBW of titanium alloy allows reducing porosity of the weld metal by an order of magnitude.

Keywords: *electron beam welding, titanium alloy, halide flux, metallography methods, porosity*

Porosity is a characteristic defect of welds in titanium alloys made by fusion welding. A large number of studies is dedicated to investigation of causes of porosity. However, results of the investigations are contradictory.

It was established [1] that gas bubbles are initiated in the weld pool primarily at ends of the weld edges, while density of the welds depends mainly upon conditions of their movement in molten titanium. This suggests that pores are bubbles of gases insoluble in titanium, which had no time to evolve from the weld pool before it becomes solidified. Other conditions being equal, the electron beam welds are most sensitive to formation of pores [2]. As a rule, these are pores from 0.01 to 0.20 mm in size [3], which can be revealed only by metallography. It was found that the quantity and mean size of these pores decrease with decrease of the hydrogen content of the base metal. However, they are present in the EB welds even at a minimal concentration of hydrogen in metal (0.001 wt.%), thorough edge preparation and optimal welding conditions. Therefore, it can be suggested that increased sensitivity of the EB welds to porosity is caused by a short time of existence of metal in the molten state and a high solidification rate. Instability of the keyhole and peculiarities of local interaction of the electron beam with metal, as is the case of laser welding [4], may also play a certain role in formation of porosity during EBW.

Application of halide fluxes is the most effective method for prevention of porosity of the welds in arc welding of titanium [5, 6]. Their positive effect on density of the welds is explained by the fact [6] that a molten flux cleans the edges to dissociate moisture adsorbed on their ends and surface, and intensifies removal of bubbles from the weld pool. At the same time, flux reduces the probability of formation of gas bubbles in molten metal [5]. In this connection, it makes sense to determine the possibility and efficiency of application of halide fluxes in EBW to reduce porosity of titanium welds.

Studies were conducted on plates of alloy VT6 (Ti–6Al–4V) 300 × 100 × 12.5 mm in size, made by rolling a forging of the ingot produced by vacuum-arc remelting (VAR) and ingot produced by electron beam cold hearth melting (EBCHM). After rolling, the plates were subjected to annealing at a temperature of 700 °C for 1 h to relieve stresses. Chemical composition and mechanical properties of the base metal are given in Table 1. Differences in mechanical properties of the VAR and EBCHM metals in this case are caused by a different content of aluminium and oxygen in them, as well as by a different degree of deformation in rolling.

Welding of the plates was performed by the electron beam method using the UL-144 machine equipped with the ELA 60 / 60 power unit. The SU 220 device was used to align the electron beam with the joining line. Simulation of fading out was performed by discretely decreasing the welding current (from a nominal value to zero) at certain points located along the specified weld length, which was provided by the programmed control of the power unit. Porosity of the welds was estimated from the results of X-ray transmission analysis of welded joints and data of metallography of longitudinal microsections in three characteristic regions of the weld, i.e. along the fusion line, along the weld axis and in the

Table 1. Chemical composition and mechanical properties of titanium alloy VT6

Melting method	*Content of alloying elements and gases, wt.%*					*Mechanical properties of alloy*[*]				
	Al	*V*	*[N]*	*[O]*	*[H]*	σ_t, *Ì Pà*	$\sigma_{0.2}$, *MPa*	δ, %	ψ, %	*KCV*, *J/cm*^{2}
VAR	5.5	4.0	0.020	0.08	0.0024	950	830	12	27	43
EBCHM	6.0	3.9	0.010	0.15	0.0018	1004	970	13	30	36

[*]Average values over the results of testing five specimens.

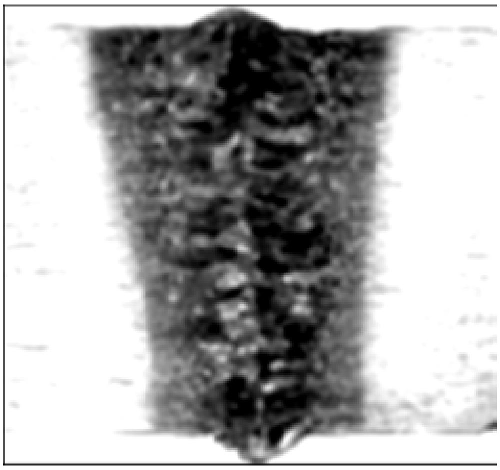

Figure 1. Macrostructure of welded joint in alloy VT6 made by EBW under optimal conditions (×3)

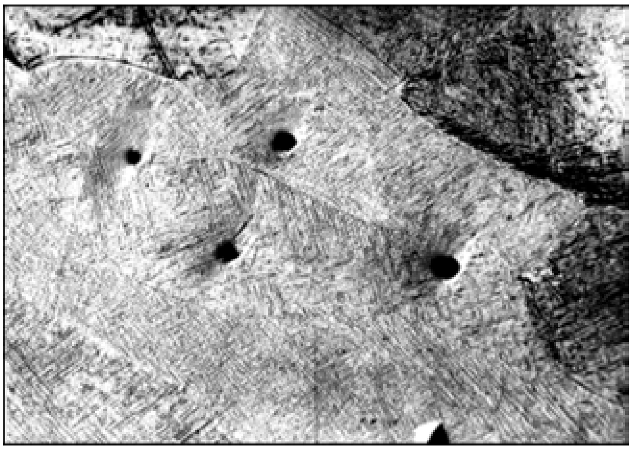

Figure 3. Group of micropores in EB weld metal (EBCHM base metal) (×200)

middle between them. The method suggested in [3] was used for comparative quantitative estimation of porosity of the welds. Flux of the ANT-23A grade (TUU 05416923.002–95) was applied for welding.

The choice of welding conditions (U_{ac} = 60 kV, I_w = 90 μA, scanning frequency — 170 Hz, scan diameter — 4 mm, v_w = 25 m / h) was based on the necessity to ensure the satisfactory formation of the weld face and root, as well as the absence of defects in the weld according to the X-ray transmission analysis (Figure 1). The optimal weld formation in the fading out region was provided by decreasing the welding current in a stepwise manner (20 steps) from 90 μA to zero during 10 s, i.e. in a region 70 mm long.

Initial experiments with EBW using flux were conducted by the same technology as that used for arc welding, i.e. the flux was applied in the form of an alcoholic suspension to the surface of the joint prepared for welding in an amount of 13 mg / cm^2. Visual examination of the welded joints thus made showed unsatisfactory weld formation, and X-ray transmission analysis fixed a large quantity of internal defects of different sizes. According to the metallogra-

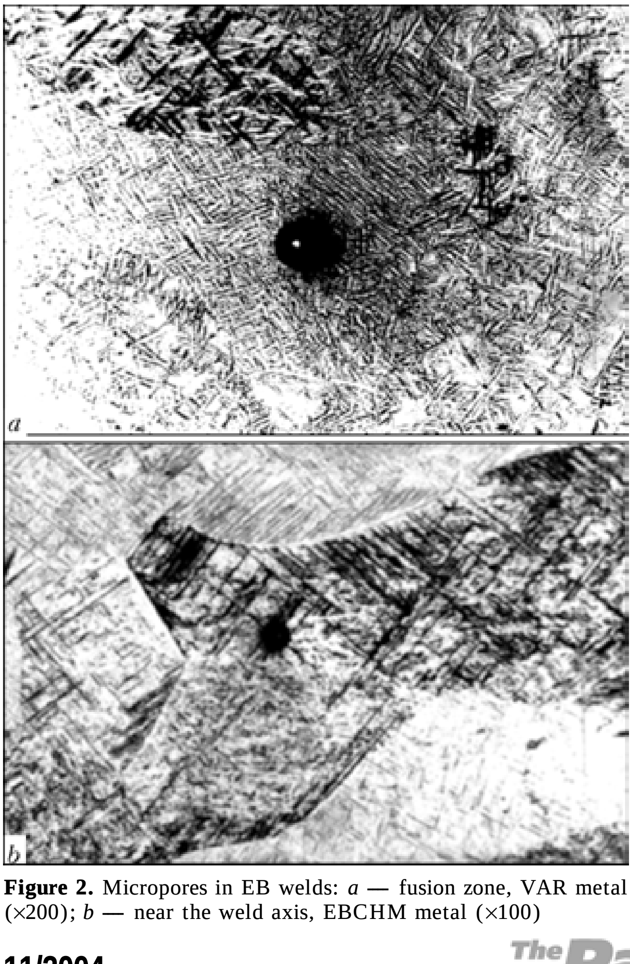

Figure 2. Micropores in EB welds: *a* — fusion zone, VAR metal (×200); *b* — near the weld axis, EBCHM metal (×100)

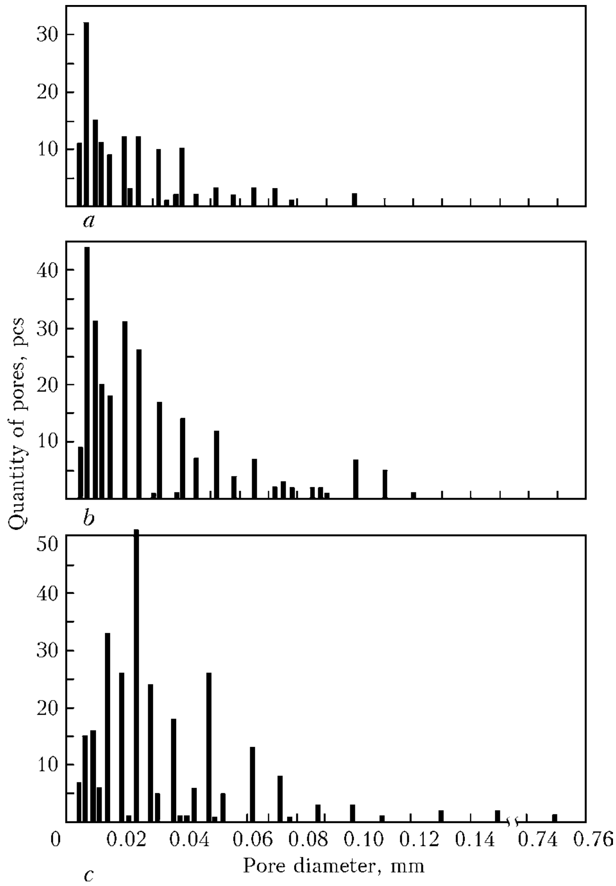

Figure 4. Histograms of distribution of pores in EB welds (weld length is 250 mm) on EBCHM metal: *a* — fusion zone; *b* — between fusion zone and weld axis; *c* — along weld axis

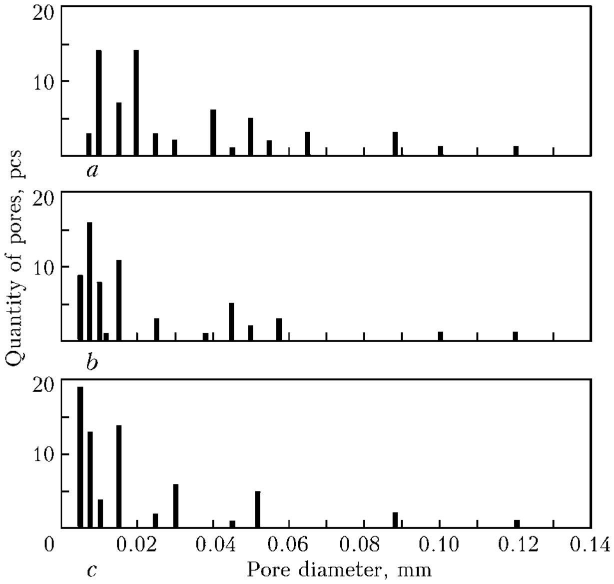

Figure 5. Histograms of distribution of pores in welds made by EBW using flux ANT-23A (weld length is 270 mm): *a*--*c* — same as in Figure 4

phy results, they were cavities with slag particles detected inside some of them. In the experiments, where the flux was applied prior to welding only to the edge ends, the quantity of defects dramatically decreased. In these cases, if the amount of the flux was about 3 mg / cm^2, the X-ray transmission analysis revealed no defects in the welds. As shown by the experiments, independently of the alloy melting method, application of an optimal amount of flux (about 3 mg / cm^2) had no effect on the weld formation and welding process stability. This proved results of the preliminary studies, according to which flux in EBW can affect only the metallurgical processes occurring in the weld pool, and has no influence on the space-energy characteristics of the electron beam.

Welded samples, including the fading out regions, were made (without and with flux) under the chosen welding conditions for further studies. X-ray inspection detected no defects in them. However, metallography revealed fine pores in the weld metal. Sometimes these were individual micropores (Figure 2), and sometimes — groups of pores (Figure 3).

Table 2. Effect of welding method on the content of impurities in the weld metal

Melting method	*Welding method*	*Content of impurities in weld, wt.%*		
		C	*[O]*	*[H]*
VAR	EBW	0.018	0.076	0.0021
	EBW with flux	0.019	0.079	0.0020
EBCHM	EBW	0.011	0.160	0.0017
	EBW with flux	0.011	0.160	0.0016

Histograms of distribution of pores in size (Figure 4) were plotted to generalise results of metallography of longitudinal sections of the welds. As shown by analysis of the histograms, pores no more than 0.06 mm in size are dominant in all the examined sections. Increase in the diameter of micropores is accompanied by decrease in their quantity. In welded joints of the EBCHM metal, pores were seen mostly in the central part of the welds, where they were larger in quantity and size (see Figure 4, *a*–*c*). Maximal porosity in the VAR metal welds was detected in the fusion zone, the total porosity level being identical. At the same time, the data obtained do not allow an unambiguous conclusion of any effect on the character of distribution of pores in the welds by the metal melting method.

The following expression [3] was used for comparative quantitative estimation of porosity:

$$\alpha = \frac{\pi(R_1^2 n_1 + R_2^2 n_2 + \ldots + R_i^2 n_i)100}{S},$$

where R_1, R_2, ... , R_i are the pore radii; n_1, n_2, ... , n_i are the quantities of pores of a given radius; and S is the surface area of a sample studied.

First the porosity of the weld metal along the entire weld length, i.e. percentage ratio of the area occupied by pores to the surface area of a sample studied (α_{av1}, α_{av2}, α_{av3}), and then the average po-

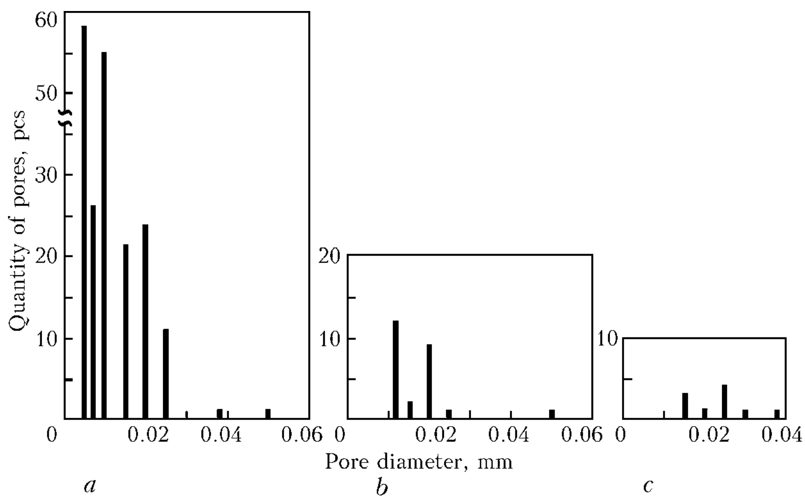

Figure 6. Histograms of distribution of pores in metal of the 60 mm long weld (in fading out region) made by EBW using flux: *a*--*c* --- same as in Figure 4

rosity of the weld or the fading out region were determined. It was found that the averaged porosity across the one-pass EB weld in alloy VT6 was 0.012 %, and that in the fading out region was from 0.025 to 0.055 %, i.e. defectiveness of this region being much higher.

As noted above, application of flux of the ANT-23A grade in EBW had no effect on stability of the welding process and weld formation. However, the presence of flux in the welding zone led to a substantial decrease, actually by an order of magnitude, in the quantity of pores in the welds (Figure 5), including in the fading out region (Figure 6). The pores considerably decreased in size as well. The averaged porosity across the one-pass weld and in the fading out region in welding using the flux was 0.0017 %.

The content of such impurities as carbon, oxygen and hydrogen (which can cause porosity) [3, 7] is almost identical in the welds made by EBW and EBW with flux (Table 2). And although the hydrogen content of the welds is somewhat lower than that of the base metal (Tables 1 and 2), this is typical for the titanium welds made by fusion welding [5]. Therefore, the effect of flux on porosity of the welds is not related to the predominant removal of, e.g., hydrogen from the weld pool. Comparing the concentration of oxygen and carbon in the base and weld metals (see Tables 1 and 2) allows a conclusion that formation of the CO bubbles in EBW as a result of interaction of carbon and oxygen in the weld pool [6] does not take place at all. Most probably that a substantial decrease in porosity of the welds made by using a halide flux is a result of a more intensive removal of bubbles from molten titanium.

CONCLUSIONS

1. Electron beam welds in titanium alloy VT6 are characterised by a large amount of fine pores with a diameter of no more than 0.2 mm. Porosity is not related to the alloy melting method.

2. It is recommended to use a halide flux to reduce porosity of the welds in EBW of titanium. Application of flux of the ANT-23A grade was proved to have no effect on the weld formation and stability of the welding process. In this case the quantity of pores is reduced by an order of magnitude.

1. Muraviov, I.I., Kholoshin, A.L. (1979) Influence of welding conditions on porosity of the weld metal in some titanium alloys. *Svarochn. Proizvodstvo*, **6**, 18--19.
2. Golub, T.V., Kashevskaya, O.N., Zamkov, V.N. et al. (1990) Density of weld metal in commercial titanium VT1-0 made by different welding methods. *Avtomatich. Svarka*, **11**, 31–33.
3. Zamkov, V.N., Shevelev, A.D. (1979) Formation of pores in EB welded joints in titanium alloy VT6. *Ibid.*, **12**, 50--54, 57.
4. Katayama, S., Mizutani, M. (2003) Elucidation of laser welding phenomena and porosity formation mechanism. *Transact. JWRI*, 32(**1**) 67--69.
5. Zamkov, V.N., Tsejger, E.N. (1983) Influence of fluoride fluxes on weld porosity in TIG welding of titanium in argon atmosphere. *Avtomatich. Svarka*, **4**, 34–38.
6. Redchits, V.V., Nikiforov, G.D., Vaks, M.A. (1974) Prevention of porosity of welds in thin-sheet titanium and its alloys. *Svarochn. Proizvodstvo*, **4**, 7--10.
7. Petrov, G.L., Khatuntsev, A.N. (1975) Role of chemical reactions in pore formation during welding of titanium alloys. *Ibid.*, **8**, 57--58.

INFLUENCE OF HYDROCARBON ADDITIVES ON THE STRUCTURE OF HYDROGEN-OXYGEN FLAME AND TEMPERATURE DISTRIBUTION ALONG THE PLUME LENGTH

V.N. KORZH and **Yu.S. POPIL**
National Technical University of Ukraine «Kiev Polytechnic Institute», Kiev, Ukraine

Boundaries are determined for transition from the laminar to turbulent mode of combustion product flow in a mixture produced by water electrolyses generators, depending on additives of vapours of hydrocarbon compounds to a mixture. Considered is temperature distribution along the plume length for different modes of the flow of a jet of combustion products and additives of hydrocarbon compound vapours to the mixture. Conditions of the possible use of the hydrogen-oxygen flame are described.

K e y w o r d s : *flame spraying, hydrogen-oxygen flame, water-electrolysis generator, laminar and turbulent flow, flame temperature, outflow velocity*

Flame coating processes, in particular flame spraying, are promising methods for controlling the corrosion and wear. Flame spraying consists in forming on the item surface a layer of spraying material particles which have the required store of thermal and kinetic energy to produce a coating due to interaction with a jet of gas flame combustion products.

One of the goals of energy saving is application of acetylene substitutes instead of the deficit acetylene. Ability to use ecologically compatible hydrogen for flame processing of materials is particularly attractive [1, 2].

The purpose of the work conducted in the Chair of Machinery Part Reconditioning of NTUU «KPI» consisted in studying the thermal characteristics of hydrogen-oxygen flame (HOF) at combustion of a gas mixture produced by water-electrolysis generators for use in flame spraying.

In thermal coating processes the coating quality is chiefly determined by such factors as temperature and velocity of spraying particles. In the above study attention is focused on such HOF characteristics as its composition and burning mode, temperature distribution along the flame plume length.

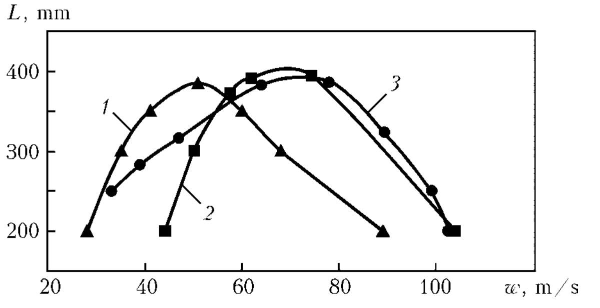

Figure 1. Dependence of plume length on average velocity of outflow of combustion products: *1* ---- HOM + benzene; *2* — HOM + alcohol; *3* ---- HOM

Mode of flow of the combustion product jet of a hydrogen-oxygen mixture (HOM) is determined by Reynolds number, which provides an estimate of the laminar or turbulent mode of the flow of flame combustion products at different flow rates, gas mixture compositions and outlet diameters in torch nozzles [3]. Transition of the combustion mode of a diffusion flame in a stationary gas environment from the laminar to the turbulent mode was recorded for different gases at different Re values. Reynolds number was determined [4] from average velocity U_m of the gas flow at outlet diameter exit of the spraying torch nozzle:

$$\mathrm{Re} = \frac{U_m d}{\nu},$$

where ν is the kinematic viscosity of the gas or gas mixture, m^2/s ($\nu = 36.93 \cdot 10^{-6}$ m^2/s for HOM consisting of O_2 + 70 % H_2); d is the torch nozzle outlet diameter, m.

Average outflow velocity of the combustible mixture from the torch nozzle can be determined from the following formula [5]:

$$U_m = 354 \frac{V_{\mathrm{g.m}}}{d^2},$$

where $V_{\mathrm{g.m}}$ is the gas mixture flow rate, m^3/h; 354 is the empirical coefficient.

For the maximum length of the plume (about 400 mm) the average velocity of the gas flow at the nozzle exit at HOM combustion is from 50 to 80 m / s, depending on the torch nozzle number and gas flow rate (Figure 1). The region of transition of the outflow of a gas jet of combustion products from the laminar to the turbulent mode starts from about 80 m / s outflow velocity of the jet from the nozzle for a torch with the nozzle outlet diameter of 1.6 mm, for a torch with 2.0 mm diameter of the nozzle outlet it begins approximately at 60 m / s, and for that of 2.2 mm diameter approximately at 50 m / s. Complete turbulization of the flame plume occurs at about 125 m / s velocities of outflow from the nozzle, when using nozzles with 1.6 mm outlet diameter, about 70 m / s at outlet diameter of 2.0 mm and 80 m / s at 2.2 mm diameter.

Analysis of the obtained results showed that for a pure HOM, transition from the laminar flow of the combustion products to the turbulent flow proceeds at outflow velocity of the combustible mixture jet from the torch nozzle, corresponding to Re ≈ 3500, this being rather close to that given in [6] $Re = 3 \cdot 10^3$ for the transition region of the gas flow.

As follows from [7], regulation of the reduction-oxidation potential of the flame, generated at combustion of a mixture which is produced by water-electrolysis generators, proceeds due to addition to HOM of hydrocarbon compound vapours by barbotage of the combustible mixture through alcohol, benzene or other hydrocarbon compounds.

Addition of 3.5 vol.% of benzene vapours to HOM promotes increase of heat content of the flame combustion products at combustion of 1 m^3 of the combustible mixture from 6.75 to 17.15 MJ / m^3. At addition of 16 vol.% of ethyl alcohol, the heat content of the combustion products is equal to 14.7 MJ / m^3.

At addition to HOM of approximately 5.5 vol.% of benzene vapours or about 16 vol.% of ethyl alcohol the regularity of formation of the laminar and turbulent modes of the flame combustion product flow in the region of a stable flame is preserved.

Analysis of average outflow velocity of a mixture of HOM + benzene vapours at the nozzle exit showed that transition of the burning mode from the laminar to the turbulent mode for all the torch tips with outlet diameters from 1.6 to 2.2 mm is within 50 to 55 m / s (Figure 1).

For a jet of combustion products of HOM with addition of 5.5 vol.% of benzene vapours transition from the laminar to the turbulent mode of the flow proceeds at the outflow velocity of the combustible mixture jet from the torch nozzle corresponding to Re ≈ 3000.

Transition to the turbulent mode of the combustion product flow of a combustible mixture of HOM + benzene vapours proceeds at lower outflow velocities from the torch, compared to HOM flow, and corresponds to lower value of the Reynolds number. This is attributable to increase of kinematic viscosity of the gas mixture due to addition of benzene vapour to the mixture.

At transition from the laminar to turbulent mode of the combustion product flow, the outflow velocity of the gas flow of a combustible mixture of HOM + 16 vol.% of alcohol vapours is equal to approximately 80 m / s for a torch with 1.6 mm diameter of nozzle outlet (Figure 1). At large diameters of nozzle outlet (2.0–2.2 mm) change of the mode of combustion product flow proceeds at practically the same velocity of outflow from the torch nozzle (≈ 65 m / s). These velocities are higher, compared to similar velocities produced when adding benzene vapours to HOM.

Analysis of gas-dynamic condition of a combustion product jet of HOM + 16 vol.% of ethyl alcohol vapours showed that the start of transition to the turbulent mode of combustion product flow proceeds at outflow velocities of the combustible mixture jet from the tip, corresponding to Re ≈ 4250.

At gas flow turbulization the plume length becomes smaller, opening angle of combustion product flow and plume core become larger. Changes in geometric dimensions of flame elements, depending on composition and flow rate of combustible mixtures, are given in Table 1.

Analysis of the influence of average outflow velocities of the combustible gas mixture flows from the torch nozzle showed that the limits of stable burning of pure HOF are in the range of 30–125 m / s, and the boundary of transition from the laminar mode of the combustion product flow to the start of the turbulent flow of combustion products is recorded at average velocity of the jet outflow higher than 60 m / s, this corresponding to outflow velocity of the combustible mixture jet from torch nozzle of Re ≈ 3500.

Stable burning of HOM with additives of 5.5 vol.% of benzene vapours was recorded at 25 to 100 m / s velocities of outflow of the combustible mixture from the torch nozzle. The boundary of transition from the laminar mode of combustion product flow to the turbulent mode is determined at more than 55 m / s average outflow velocity of combustible mixture jet from the torch nozzle, corresponding to Re ≈ 3000.

A stable burning of HOM with additives of 16 vol.% of ethyl alcohol proceeds at velocities of combustible mixture outflow from the torch nozzle in the range of 35–125 m / s, while the boundary of transition from the laminar burning mode to the start of turbulization of the combustion product flow was registered at more than 65 m / s velocity of outflow from the torch nozzle, which corresponds to outflow velocity of the combustible mixture jet from the torch of Re ≈ 4200.

Coating quality at thermal spraying of materials is greatly influenced by the temperature of spraying material particles. In thermal spraying the particle temperature depends on the length of the effective region of the flame plume, in which the particles can be heated up to melting temperature. Heating of material particles up to melting temperature through convective heat exchange between the flame combustion products and spraying particles is possible at more than 300 °C temperature of the combustion products in the plume [8].

In view of the above, the length of effective region of the flame plume for metals melting at the temperature of up to 950 °C (for instance, copper, brass, bronze), will be determined by temperature isotherm

Table 1. Characteristics of flame plume elements

Composition of combustible mixture; mode of combustion product flow	*Torch nozzle outlet diameter, mm*	*Gas mixture flow rate, dm^3/h*	*Outflow velocity of combustible mixture, m/s*	*Plume length, mm*	*Core length, mm**	*Plume width, mm**
HOM; laminar	1.6	300--600	40–80	200--400	5.0	7
	2.0	400--620	30–60	200--415	6.0	8
	2.2	400--700	30–50	200--400	7.0	9
HOM; turbulent	1.6	600--760	80--125	400--200	7.0	9
	2.0	620--820	60–70	415--200	8.0	10
	2.2	700–1100	50–80	400--200	9.0	12
HOM + benzene; laminar	1.6	200--400	25–55	200--390	6.5	11
	2.0	300--520	35–50	200--400	7.0	12
	2.2	310--720	35–50	200--400	11.0	13
HOM + benzene; turbulent	1.6	400--780	55--100	390--200	11.0	14
	2.0	520--900	50–90	400--200	11.5	14
	2.2	720–1220	50–90	400--200	12.0	15
HOM + alcohol; laminar	1.6	400--600	55–80	200--400	5.0	12
	2.0	420--780	35–65	200--400	7.0	12
	2.2	520--900	40–65	200--400	11.0	13
HOM + alcohol; turbulent	1.6	600--920	80--125	400--200	11.0	13
	2.0	780–1180	65--105	400--200	11.5	14
	2.2	900–1250	65--195	400--200	11.5	15

*Core length and plume width are specified for maximum gas mixture flow rate.

of 1250 °C. For metals with up to 1200 °C melting temperature, the length of the effective region is determined by temperature isotherm of about 1500 °C. For powder materials based on iron and other metals with up to 1500 °C melting temperature, the length of the effective temperature region is determined by temperature isotherm of about 1750 °C.

Temperature distribution along the plume length, depending on the mode of flame burning and combustible mixture composition, was studied to establish the length of the effective region of the flame plume. Two regions can be singled out here: high-temperature region determined by flame core length and zone of flame normal distribution (middle zone), where flame temperature reaches its maximum value, and afterburning zone located after the zone of flame normal propagation, where flame temperature becomes essentially lower.

Maximum temperature in HOF high-temperature zone, calculated experimentally, is equal to about 3110 °C [1].

At addition of hydrocarbon compound vapours to HOM a tendency is observed to lowering of the maximum temperature in the high-temperature zone (approximately to 3100 °C at combustion of a HOM with 5.5 vol.% of benzene vapours and to 3080 °C at combustion of HOM with 16 vol.% of ethyl alcohol vapours) [1].

Analyzing temperature distribution along the flame plume length, we find the length of effective regions, where the temperature is higher than that of melting of the spraying material by 300 °C. For this purpose we single out three temperature ranges along the flame plume length: from maximum temperature of the flame to 1750 °C, from maximum temperature to 1500 °C, from maximum temperature to 1250 °C.

Temperature distribution along the flame plume (Figure 2, *a*) showed that the first two temperature regions are longer in turbulent mode of the combustion product flow, the third region being longer in laminar mode of the flow.

Addition of 5.5 vol.% of benzene vapours to the combustible mixture changes temperature distribution along the plume length (Figure 2, *b*). In addition, in this case a tendency can be seen to a greater length of temperature regions, compared to the flame in combustion of pure HOM. This is attributable to the fact that afterburning of excess fuel proceeds in the plume behind the high-temperature region. If at addition of 5.5 vol .% of benzene vapours to HOM, the maximum design temperature in the core and near-core zone of the flame is lower than that at combustion of pure HOM, in the afterburning region the temperature rises. Relative lowering of oxygen in the combustible mixture composition lowers the maximum temperature in the high-temperature zone, and in the after-

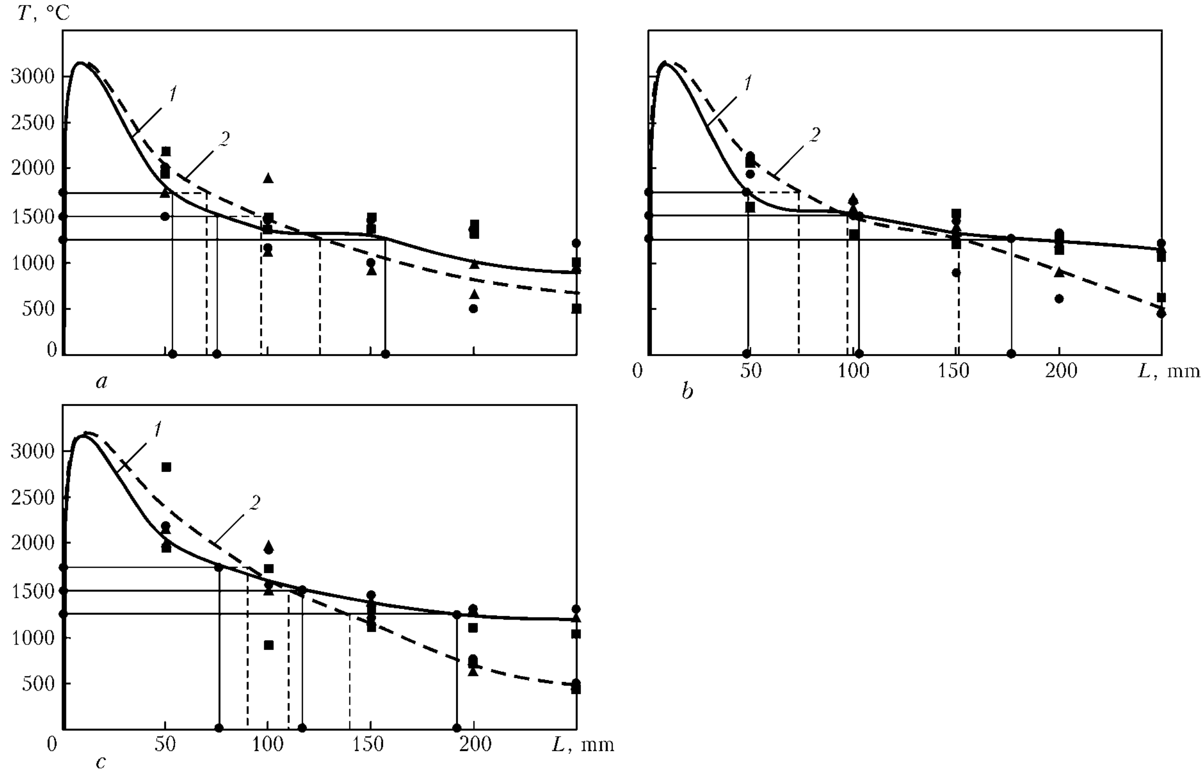

Figure 2. Temperature distribution along the flame plume length at laminar (*1*) and turbulent (*2*) mode of combustion product flow of HOM (*a*), HOM + 5.5 vol.% of benzene vapours (*b*), HOM + 16 vol.% of alcohol vapours (*c*) and different diameters of nozzle outlets: 1.6 (▲), 2.0 (■) and 2.2 (●) mm

burning region (due to additional oxidation of the fuel by air oxygen) the temperature of this zone rises, and the third region becomes longer.

At turbulent mode of the flow of combustion products of a combustible mixture of HOM + 5.5 vol.% of benzene vapours, the length of effective temperature regions has a noticeable tendency to increase, compared to the laminar flow mode, only for the first region, and the tendency to extension of the third region of effective temperatures is preserved for the laminar flow mode.

Analysis of the length of effective temperature regions at addition of up to 16 vol.% of ethyl alcohol vapours to HOM (Figure 2,*c*) demonstrates extension of all the above effective regions of the flame plume both for the laminar, and for the turbulent mode of the combustion product flow, compared to the flame plume obtained at combustion of pure HOM. A tendency is preserved to extension of the first effective region of the flame at turbulent flow mode compared to laminar mode; shortening of the third effective region of the flame at turbulent mode of the flow, compared to the laminar mode.

Results of studying temperature distribution along the flame plume, depending on mixture composition and combustion mode of HOF (Table 2) showed that the length of the plume region with temperatures above 1500 °C is greater at turbulent mode, and that of a region below 1500 °C is greater at laminar mode of the flow.

At addition of vapours of hydrocarbon compounds to the combustible mixture, a tendency is observed

Table 2. Length of effective temperature regions along the flame plume

Combustible mixture composition	*Flow mode of combustion products*	*Temperature range, °C*	*Length of effective temperature region, mm*	*Temperature range, °C*	*Length of effective temperature region, mm*	*Temperature range, °C*	*Length of effective temperature region, mm*
HOM	Laminar	3110–1750	55	3110–1500	75	3110–1250	150
	Turbulent		70		95		125
HOM + 5.5 vol.% of benzene vapours	Laminar	3100–1750	50	3100–1500	100	3100–1250	175
	Turbulent		75		100		150
HOM + 16 vol.% of alcohol vapours	Laminar	3080–1750	75	3080–1500	110	3080–1250	190
	Turbulent		90		110		140

to extension of the considered effective temperature regions. It is manifested even stronger with addition of alcohol vapours to HOM.

CONCLUSIONS

1. At addition of hydrocarbon compounds to HOM, the boundaries of transition from the laminar to the turbulent mode of the combustion product flow shift towards lower flow velocities. The length of temperature regions, where the spraying material particles can reach the melting temperature, becomes greater.

2. For flame spraying of powder materials with up to 1000 °C melting temperature, there is a high probability of producing a sound coating when using a flame generated at combustion of a mixture produced by water-electrolysis generators with addition of 5.5 vol.% of benzene vapours or 16 vol.% of ethyl alcohol vapours to HOM, and at laminar mode of the combustion product flow jet. For spraying powder materials with melting temperature above 1000 °C, the probability of obtaining a satisfactory quality of the deposited layer is higher, when using a flame produced in combustion of a mixture of HOM + 16 vol.% of alcohol vapours or HOM + 5.5 vol.% of benzene vapours at a turbulent nature of the combustion product flow.

1. Korzh, V.M., Popil, Yu.S. (2002) Control of parameters of hydrogen-oxygen flame burning in flame treatment of materials. *Nauk. Visti NTUU «KPI»*, **4**, 81–-91.
2. Korzh, V.M., Popil, Yu.S., Glukhovsky, V.Yu. (2002) Study of thermal and kinetic characteristics of hydrogen-oxygen flame in coating deposition. *Problemy Tekhniky*, **2**, 61–66.
3. Dyban, E.N., Mazur, A.K. (1982) *Convective heat transfer in spray flow of bodies*. Kiev: Naukova Dumka.
4. Abramovich, G.N. (1976) *Applied gas dynamics*. Moscow.
5. Evseev, G.B., Glizmanenko, D.L. (1974) *Equipment and technology of flame treatment of metals and nonmetallic materials*. Moscow: Mashinostroenie.
6. Bryukhanov, O.N. (1983) *Microflame burning of gases*. Leningrad: Nedra.
7. Korzh, V.N. (1983) Control of the mode of combustible gas mixture burning by addition of liquid hydrocarbon compounds. *Avtomatich. Svarka*, **11**, 65–66, 69.
8. (1964) *Application of gases-substitutes of acetylene in flame treatment of metals*. Ed. by I.A. Antonov. Moscow: Mashinostroenie.

INCREASE IN SENSITIVITY OF DEPOSITED STEEL 110G13L TO STRAIN HARDENING

K.A. VALITS and **S.Yu. PASECHNIK**
Donetsk National Technical University, Donetsk, Ukraine

It is shown that electroslag cladding of high-manganese steel 110G13L provides substantial increase in steel sensitivity to strain hardening, in addition to restoration of geometry and improvement of performance of parts, which leads to increase in wear resistance of metal and extension of service life of parts.

Keywords: *electroslag cladding, steel 110G13L, excavating machine bucket teeth, shock-dynamic effect, deformation, hardening, wear, microhardness, slip lines, dislocations, wear resistance*

As proved more than once, electroslag cladding (ESC) of worn-out bucket teeth of quarry excavating machines EKG-8I and EKG-12.5 provides improvement of performance of the reconditioned teeth, compared with performance of those mass-produced by casting [1–3]. Part of an extremely worn-out tooth is used as a consumable electrode in ESC (deposited and base metals are high-manganese steel 110G13L), which is very important for operation of teeth under conditions of high-hardness rock faces under increased shock-dynamic loads. The above steel is known to have high impact toughness and sensitivity to strain hardening (ratio of microhardness before deformation to that after deformation).

Comparative studies were conducted to investigate characteristics of strain hardening of steel 110G13L in the as-cast condition and as metal deposited by ESC using standard flux ANF-6 and a new flux [4]. All samples were subjected to standard heat treatment recommended for steel 110G13L.

Sensitivity of the steel to strain hardening was studied under dynamic compression by the method described in [5]. Test specimen were trihedral prisms 5 mm high, made by diagonally cutting a square. Dynamic load was applied to the prism edges. Values of the impact energy were selected from a range of 25–75 J, as hardening of steel 110G13L becomes pronounced at an impact energy of 25 J, and a maximal hardening is achieved after the very first shock at an impact energy of 75 J.

The test specimens were cut from a working surface of worn-out mass-produced and reconditioned bucket teeth of the excavating machines. Metallography of worn-out surfaces of the teeth was performed using the MIM-8M microscope and PMT-3 hardness meter, and magnetometry was carried out using the alpha-phase meter.

Results of the studies are shown in Figure 1. It can be seen from the Figure that the degree of hardening of steel 110G13L grows from 2.30 in the as-cast condition to 2.70 and 3.09 in the condition after ESC using flux ANF-6 and the new flux, respectively.

The cast steel 110G13L has a maximal degree of hardening at an impact energy of 50 J and after the three-fold shock, whereas the steel deposited by ESC (independently of flux) has a maximal degree of hardening at an impact energy of 50 J and after the five-fold shock.

As proved by examinations of microstructure of the hardened surface layer of worn-out mass-produced cast teeth and teeth reconditioned by ESC, the degree of hardening of the deposited metal is higher than that of the cast metal. Figure 2 shows the slip lines evidencing hardening of the steel during operation of the bucket teeth in a rock face. Increase in the quantity of the slip lines and decrease in the distance between them after ESC using the new flux confirm a higher sensitivity of the steel to hardening, compared with the cast steel and steel deposited by ESC using flux ANF-6.

Metallography and magnetometry of worn-out surfaces of the teeth revealed no magnetic phases in the hardened layer. Therefore, according to the data of studies [6, 7], the high degree of hardening of the deposited steel 110G13L is related to formation of crystalline structure defects (dislocations, stacking

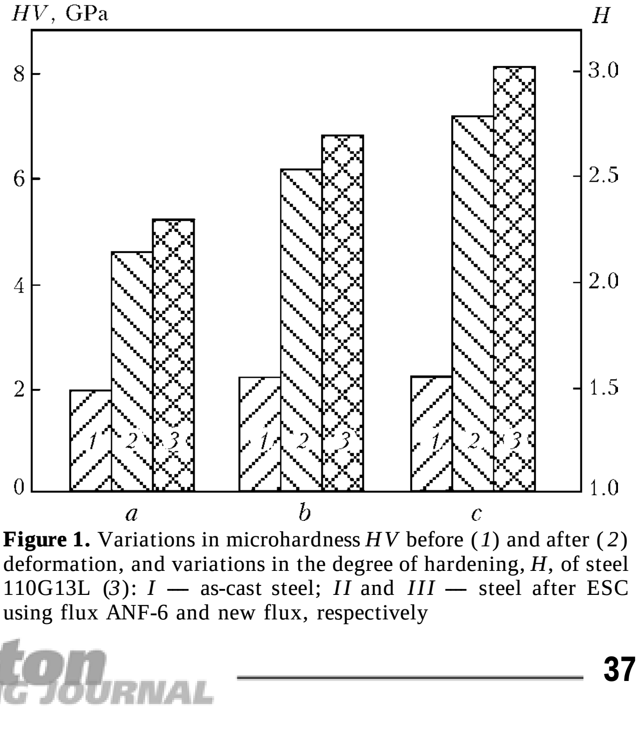

Figure 1. Variations in microhardness HV before (*1*) and after (*2*) deformation, and variations in the degree of hardening, H, of steel 110G13L (*3*): *I* — as-cast steel; *II* and *III* — steel after ESC using flux ANF-6 and new flux, respectively

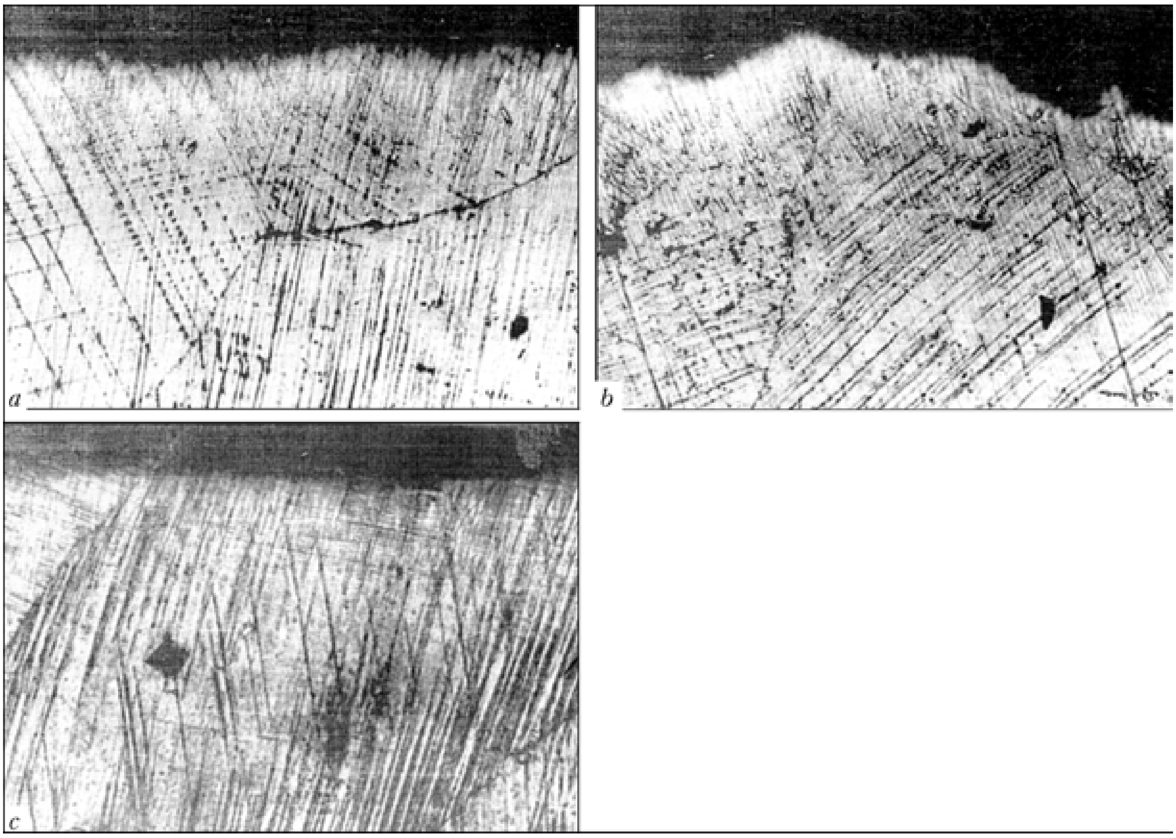

Figure 2. Microstructure of the hardened layer of steel 110G13L: *a* — worn-out cast tooth; *b*, *c* — reconditioned tooth after ESC using flux ANF-6 and new flux, respectively (×300)

faults, deformation twins), as well as to substantial refining of the mosaic blocks. In addition, substantial decrease in contamination of steel with carbides and non-metallic inclusions in ESC leads to a more intensive and deep deformation of metal.

Results of investigations of strain hardening of actual teeth are in sufficiently good correlation with the data of the above laboratory studies.

As the degree of wear of steel 110G13L is in inverse proportion to its hardness due to work hardening under the shock-dynamic effect, it can be considered that the degree of strain hardening is a direct characteristic of wear resistance, which explains a marked improvement of performance of the ESC reconditioned parts of mining equipment operating under intensive shock-dynamic loading conditions.

1. Valits, K.A., Stojko, V.P., Shvartser, A.Ya. et al. (1981) Reconditioning of bucket teeth of excavating machines EKG-8I by electroslag cladding. *Gorn. Zhurnal*, **1**, 16--17.
2. Valits, K.A., Stojko, V.P. (1986) Extension of service life of quarry excavating machine bucket teeth. In: *Abstr. of Conf. on New Structural Steels and Alloys, and their Treatment Methods for Improvement of Reliability and Extension of Service Life of Parts*, Zaporozhie, Nov. 26–28, 1986. Zaporozhie: Kommunar.
3. Valits, K.A., Shvartser, A.Ya., Koritsky, G.G. (1988) Reconditioning of parts of high-manganese steel 110G13L by electroslag cladding. *Avtomatich. Svarka*, **5**, 64–65.
4. Valits, K.A., Shvartser, A.Ya., Stojko, V.P. (1985) Flux for electroslag cladding of high-manganese steel. *Problemy Spets. Elektrometallurgii*, **4**, 26--28.
5. Ponomarenko, V.P., Shvartser, A.Ya., Stojko, V.P. (1982) High-manganese steel for electroslag cladding. *Metallovedenie i Term. Obrab. Metallov*, **10**, 57–60.
6. Bogachyov, I.N., Egolaev, V.F. (1973) *Structure and properties of iron-manganese alloys*. Moscow: Metallurgiya.
7. Grigorkin, V.I., Korotushenko, G.V. (1966) Properties of austenitic high-manganese steel alloyed with carbide-forming elements. *Metallovedenie i Term. Obrab. Metallov*, **10**, 27–29.

HISTORY OF ORIGINATION, TECHNOLOGICAL FEATURES AND TECHNICAL CAPABILITIES OF THE FIRST METHODS OF SOLDERING AND BRAZING

A.M. ZHADKEVICH
E.O. Paton Electric Welding Institute, NASU, Kiev, Ukraine

Retrospective review of development of brazing technique in manufacturing bronze, gold and silver items by the ancient and medieval craftsmen is given. Technology of brazing the intricate tin items is described. It is noted that the heat source was hearth furnaces with an air blowing through a tube, and the composition of fluxes included metallic powders of metals, carbonates and nitrides. Composition of brazing alloys was selected from the condition of a minimum temperature of eutectic transformation and similar color and glitter as that of the metal brazed.

Keywords: *history of technology, technology of brazing, heat sources, fluxes, brazing alloys, brazed items*

At the present time the brazing is a highly-developed technology of manufacture of different-purpose products made from various metals and alloys. It finds an application in different branches for joining both of the smallest parts, for example, of electron instruments, and also assemblies of the large-sized objects of rocket construction, power engineering and others.

Over the recent decades the fundamentals of brazing were developed intensively and arsenal of heat sources was widened greatly. Compositions of brazing alloys are developed taking into account the multicomponent diagrams of state of alloys. The present achievements and capabilities of brazing are shown in numerous publications and periodic editions, and also in manuscripts and handbooks [1].

However, to describe more completely and comprehensively the importance of the technology in the history of the society, it is necessary to analyze the origin of the technology and its historical progress [2].

In most publications on history of metal working the technology of manufacture of brazed items is described coming from known archeological materials. Moreover, some authors, for example, V.A. Kolchin, B.A. Rybakov, S.P. Nedopaka, G.A. Voznesenskaya and others [3–5] are based on the results of metallographic examinations. Nevertheless, the technique of heating, capabilities of manufacture of brazing alloys and some other peculiar features of brazing of intricate metallic items have not been yet sufficiently studied until now.

The aim of the present work was to analyze the technological possibilities of brazing in the ancient world with allowance for its present status.

Brazing represents a process of joining of metallic pieces, being in a solid state, using a molten brazing alloy [6]. Coming from this definition, the obligatory conditions of the brazing are as follows: 1) heat source of up to temperature of brazing alloy melting; 2) brazing alloy from metal alloy, whose liquidus and solidus temperatures should be lower than the temperature of melting of metals of the pieces brazed.

Brazing as one of technologies of joining in manufacture of items from metals is referred to one of the most ancient technologies [3]. It originated simultaneously with beginning of manufacture of items from artificial metallic materials, i.e. bronze, and then iron and steel implements of labor, weapon and household goods. The most important premises of the brazing appearance were the mastering of heating technique, creation of furnaces, hearths and other devices for combustion of organic fuel using natural or artificial blowing. The progress in the field of technology and technique of brazing is defined mainly over the centuries and up to the present time by the method of heat supply to the joint zone.

Most archeologists consider that the first brazing alloys were tin and bronze because of a low temperature of melting that allowed their melting in an open flame of campfire with use of methods of blowing known at those times [3]. Really, the archeological materials confirm that brazing appeared at the transition of copper and bronze ages, i.e. at III–II centuries B.C. At that period the technology of bronze melting was developed in places where, alongside with deposits of native copper, the most ancient metallurgists mastered the technology of artificial melting of copper and the deposits of tin-containing minerals were simultaneously mined. The bronzes were often produced in mixing of different ores, and the ores contained usually the impurity metals, except the compounds of copper and tin. Thus, it was observed that the foundry quality of the alloy depends on the type of ore (the best castings are produced from arsenic and antimonial-arsenic bronzes).

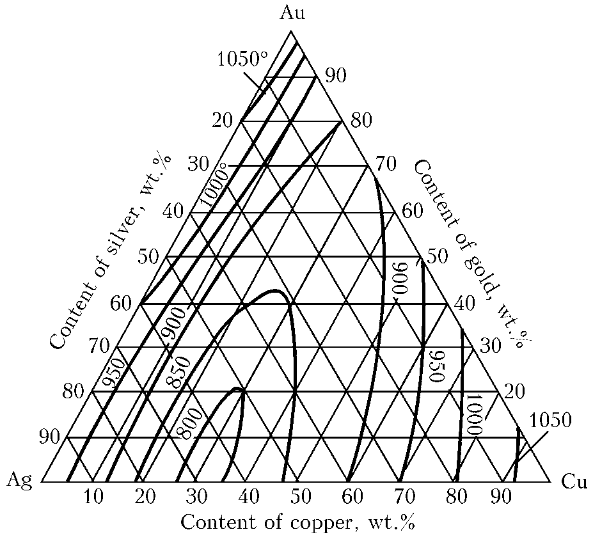

Figure 1. State diagram of gold–silver–copper [9]

The most ancient origins of bronze melting were in Sumeria, Babylon, regions of China and Thailand. It should be noted that such states as Egypt and Greece, where there were no deposits of tin ores, had to bring these ores or the metal itself and bronze from the Central Africa and Sumeria (Egypt), countries of Middle East (Greece). Phoenicians had got the British Isles where they discovered the deposits of tin ore, i.e. cassiterite. Thus, the search for components of bronze was a cause of conquest of territories, stimulus of cruises, trade. Demand for bronze ornaments, weapon, household goods stimulated the development of mining, metallurgy, different technologies of metal working [7].

Studies of items of the IV–III centuries B.C., discovered at the territory of states of the Middle East (present Iran, Syria, Iraq, Turkey) prove the high level of metal working. Most of items from copper and bronze were cast into alumina vertical molds (blades, spikes, etc.). Sometimes the peening was used for hardening, often with intermediate annealing [8]. At the transition of the IV–III centuries B.C. there was a particular specialization in Sumeria in the manufacture of items from metal that contributed to the improvement of the technologies. Thus, the metallographic examinations of ornaments prove the high quality of not only small castings, but also the mastering of art in filigree, granulation, engraving, and also the application of brazing [8].

In casting, especially in brazing with bronze consisting of a number of alloying elements, it was necessary to pay a special attention to the temperature of heating. It is seen from the state diagram, for example of the three-component alloy Au–Cu–Ag, that the solidus–liquidus boundary can vary in the ranges from 800 to 1050 °C (Figure 1). The process of brazing (with a control of composition) is shown on frescos in tomb of the Egyptian Pharaoh Mererub (2315–2190 B.C.), where the flame in a melting hearth was kept by blowing through tubes by several persons (Figure 2). This technique of heating, unlike the campfire, allowed very quick adjustment of the temperature.

It should be noted that M. Bekkert, the historian of technology, assumes the application of a silver wire for copper brazing in Egypt, except the brazing alloys of tin, tin-lead and bronze [10], and this cannot but agree with him.

Sarmat tribes of the Volga and South Ural regions had in their disposal the quite developed technology of manufacture of items from bronze as far back as the VI century B.C. In particular, they used bronze for manufacture of mirrors, consisting of a number of alloying elements, such as copper, lead, tin, nickel, whose proper ratio provided good casting properties and high reflectivity [11].

If before the beginning of mastering the iron production the bronze remained to be the main metal for manufacture of weapon and labor tools, then such noble metals as gold and silver were used mainly for ornaments. The man acquainted with a native gold as far back as the late Stone Age and since that time he began to gain the experience which was used later in working of other metals. Various items of the IV–III centuries B.C. made by Sumerians and Egyptians prove a sufficiently high technique of gold working.

Among the Greek cities-states of the North bank of the Black Sea in the VII–V centuries B.C., the Pantikapey, the large handicraft center, is distinguished, where the working of non-ferrous metals was

Figure 2. Representation of brazing process on frescos in the tomb of Pharaoh Mererub

greatly developed. Antique samples of items of household purpose and art, found during diggings, prove that Greek torevates (artists of skilled working of metal) possessed various techniques of casting, stamping, forging, riveting and brazing. Thus, in the Museum of Historical Jewelry of Ukraine there is a Scythian sword-akinac in golden sheath, discovered in a burial mound near khutor (hamlet) Shumejko of Sumy region. Ornaments of the upper part of the sheath and the sheath tip are made in the form of deepened triangles, filled with graining, i.e. small golden balls brazed to a golden base.

In the valley of the Supoj river near the village Peschanoe of Cherkassy region 15 bronze Greek vases of the VI–IV centuries B.C. were discovered. Welds of walls of all the vases are forged, while the cast handles, alto-rilievos and appliques are joined by brazing and riveting, moreover, some of pieces are gold-plated (Figure 3, *a*, *b*) [12].

In the museums of Ukraine there are hundreds of objects of household goods, jewelry and samples of weapon, decorated in ancient Greek and Scythian style using brazing, and also those decorated with fine granulation. Golden pectoral, the breast decoration, found in 1971 in the Scythian burial mound near Ordzhonikidze city of Dnepropetrovsk region is of a special interest (Figure 3, *c*, *d*). This unique item consists of three tiers: between the tracery upper and lower tiers the cast figures of people, real and mythical animals are brazed on [12, 13].

By their appearance the brazed joints do not differ from all-cast items of gold or its alloys. Technique of

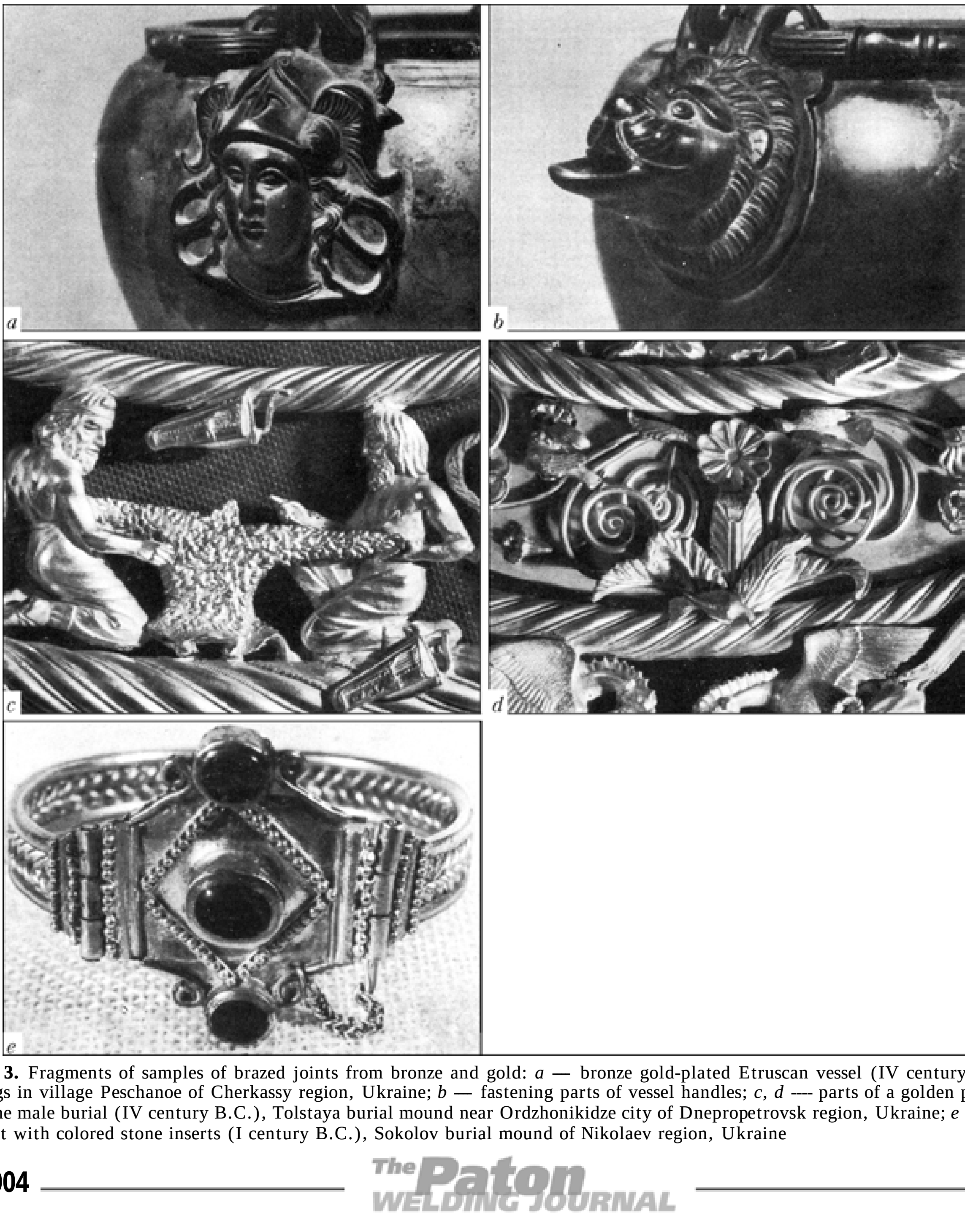

Figure 3. Fragments of samples of brazed joints from bronze and gold: *a* — bronze gold-plated Etruscan vessel (IV century B.C.), diggings in village Peschanoe of Cherkassy region, Ukraine; *b* — fastening parts of vessel handles; *c*, *d* — parts of a golden pectoral from the male burial (IV century B.C.), Tolstaya burial mound near Ordzhonikidze city of Dnepropetrovsk region, Ukraine; *e* — gold bracelet with colored stone inserts (I century B.C.), Sokolov burial mound of Nikolaev region, Ukraine

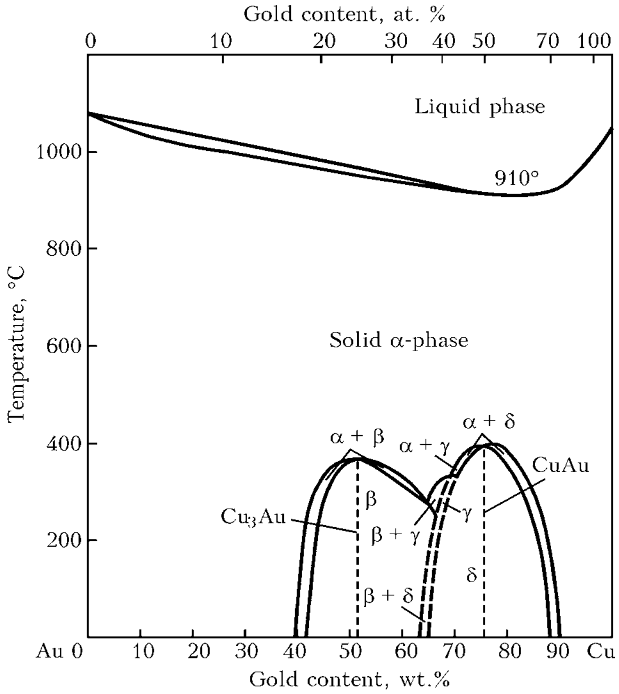

Figure 4. State diagram of gold–copper alloy

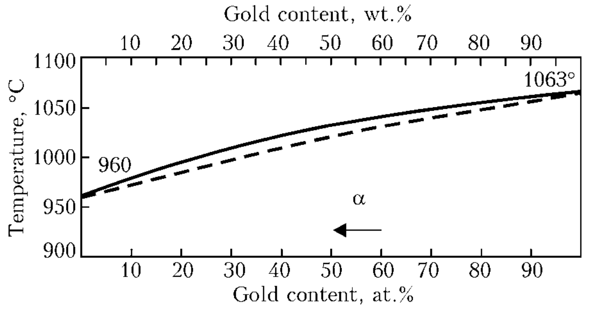

Figure 5. Dependence of melting temperature of gold–silver alloy on ratio of components

brazing grains is especially difficult. At the surface whose area reaches on some items several square centimeters, the brazed balls of 0.1–1.0 mm diameter were arranged (Figure 3, *e*). Here, the difference in temperatures of melting of gold and brazing alloys (gold–copper and gold–silver) is negligible (Figures 4, 5), therefore, the jeweler had to maintain the precise condition of heating within the ranges of one-two tens of degrees. The similar technique of brazing of gold was described in the sixties of A.D. in the «History of nature» (37 books), the works of Guy Pliny the Elder, the Roman scientist, writer and government figure, who noted the great difficulties in joining of parts of decorations and other intricate items [14].

One of the main methods of producing the monolithic joints of items, made from iron, was a forge welding and cast welding [15]. In brazing, the brazing alloys from bronze and brass were used and, as the difference in temperature was sufficiently high, then it was much easier to maintain the heating condition than in brazing of gold, silver and bronze.

One of the most ancient origins of metallurgy of iron was considered to be Transcaucasus. Archeologists refer the appearance of iron items at the territory of present Dagestan, Azerbaijan, Armenia and Georgia to the II–I centuries B.C. In that period the local specialists made a contribution into the development of metal extractive and metal working technologies. Here, the process of replacement of bronze weapon and labor tools, starting as far back as the VII century B.C., was accelerated remarkably [16].

Findings from burial mounds of the South Dnieper region prove the high technique of iron and bronze working by Cimmerian tribes of the VIII–VII centuries B.C. For example, daggers, consisting of a steel blade and bronze handle, represent a great interest [17].

Technique of manufacture of items from iron and bronze was mastered excellently by skilled masters of Kiev and Novgorod. When diggings were made in layers of the X –XIV centuries, hundreds of household goods, jewelry and weapon were discovered [14]. Rings, bells, bracelets, crosses, parts of loin-clothes and belts were manufactured from non-ferrous metals. During microstructural analysis of these parts the use of brazing was revealed (Figure 6). Thus, the catalogue of findings at the site of ancient settlements at the south suburbs of Novgorod land under No.150 stated: «Bronze bells of two brazed semi-spheres with a linear slot and a transverse linear weld which is projected approximately in the middle of their height. They were used as pendants, parts of suit and even as buttons» [18].

Somewhat different technology was used in brazing of tin items. Over the many centuries the tin was one of main materials for manufacture of cast buttons, dishes, sculptures, parts of instruments and toys. As the pure tin fills poorly the mold, then the lead was added to it (for dishes of not more than 3–4 %) for

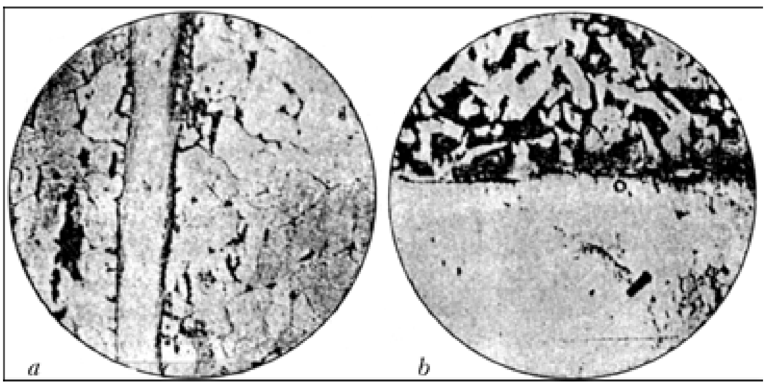

Figure 6. Microstructure of jewelry brazed items [3]: *a* — ×100; *b* — ×50

Figure 7. Warming pan (?) in the form of a book with an engraved decoration. Master is Rudolf Mice, Slavkov, 3rd quarter of XVII century [19]

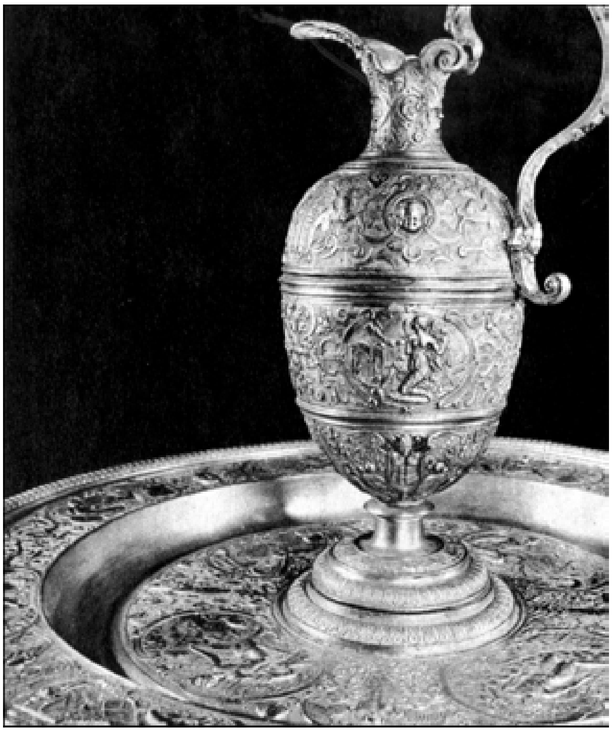

Figure 8. Dish for hand washing «Temperantia» with a jug. Master Francois Brio, Montbeliard, Lorraine, about 1585–1590 [9]

the better fluidity and the casting is performed into hot brass, sand and other molds.

Shapes of sculptures, household goods, dishes, stored at the Hermitage and other museums of the world surprise by their complexity. Many of them are manufactured from several brazed parts (Figures 7–9) [19]. At the end of the XIX century the following technology of brazing the tin items was used: «Joining by brazing is performed not by the more fusible alloy, but the same alloy, from which the item itself was manufactured, otherwise the weld will become soon darker and seen. For brazing, the ordinary copper soldering iron and a pork fat instead of a brazing water are used, but in operation the edges brazed are also melted; therefore, after aligning of parts the tinsmith put accurately a thick felt under the place being brazed, which withstands the temperature of tin melting to prevent the molten metal flowing out, and to provide its solidification in the previous shape» [20].

If the specifics of technology of heating at the first methods of brazing can be studied on the basis of metallographic examination of archeological samples and evaluated from the positions of modern metals science, then the technique of removal of oxide films, more precisely the flux application, can be judged only from rare remained descriptions [14].

One of the most full treatises of middle ages about the technologies of metals is the work «Diversarum atrium scheduta» (date of writing is approximately the IX–XI centuries) by Pheophile, the monk of Svyato-Gallensky monastery. The manuscript copy, preserved in the library of Cambridge University, is referred to the XIII century, it was reedited in Paris in 1843 under the title «Théophile prêtrepretre at meine, Essaisur divers art». The part of the treatise was devoted to casting and brazing of metals. Saint Pheophile recommends to prepare flux in the form of a paste (like soap) from alkali lye and fresh fat of a good pork, then to add salt and metallic copper. Check out of technology at the modern level, developed within the walls of Gallensky monastery, showed that the quality of the joints can be in conformity to the present requirements of the jewelry industry. Paste

Figure 9. Bell decorated with a forged ornament made from flowers and branches, Bohemia, XVII century [19]

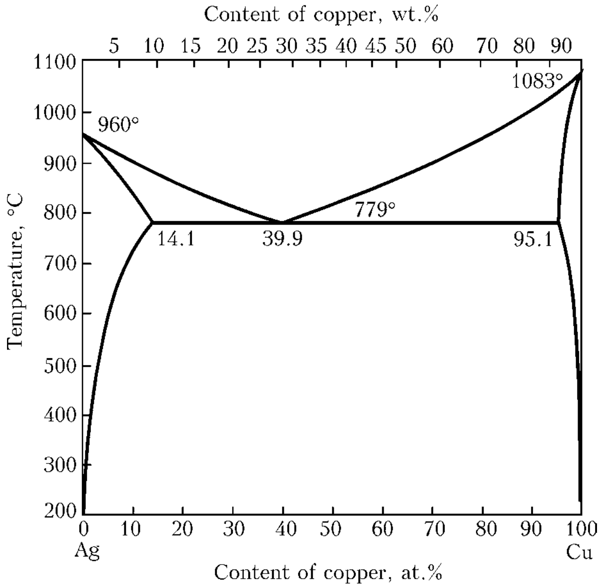

Figure 10. State diagram of silver–copper alloy

from pork fat and alkali lye is a good flux which decomposes the films at the copper surface at high temperatures. The purified copper is easily fused with gold, and the impurities formed are removed into a slag.

In the Pheophile's works the other methods and compositions of preparation of fluxes are given. For gold brazing the «chrysolite of a green tint, which is more preferable that other salts of copper is necessary. Chrysolite is mixed with Cyprian verdigris and urine of a beardless boy. Then the nitrate is added and all this is crushed in a mortar into powder. The produced mixture is called Santerno (borax). In brazing of gold by the brazing alloy with an addition of one seventeenth part of silver this mixture (flux) provides a glittering weld. From the other hand, it is difficult to braze gold, which contains copper, and the weld is produced dark». P. Roberts analyzed the flux which was used by gold smiths in Ancient Rome and decoded the composition: chrysolite hydrade of copper silicate ($CuSiO_3 \cdot 2H_2O$); verdigris, the main carbonate of copper ($CuCo_3 \cdot CuO$); urine, the ammonia salts; soda (Ca_2CO_3) [21].

It should be noted that the use of pork fat, soda, wood ashes is also mentioned in other, later treatises. In addition, Pheophile suggests for silver brazing to take two parts of pure silver and one (third) part of copper, to grind in a mortar, then to add «the cream of tartar, taking it from the vessel wall, where a good red wine was stored for a long time». To add salt into this mixture (sodium chloride) and to heat in the fire until evaporation and, then, to grind the ash again. The water solution of this mixture is used for brazing.

It is interesting to note when studying this technology that at this ratio of silver and copper the alloy with a minimum point of melting of 779–800 °C is formed (Figure 10), while a quite active flux on the base of caustic potassium is formed from the tartar and common salt. As a whole, powders containing brazing alloy and flux in an optimum ratio were used in brazing.

Over the later centuries the brazing remained to be the most widely spread technology of producing the permanent joints of items made from non-ferrous metals. Materials and technique of brazing were updating with the progress in chemistry and improvement of heat sources. However, the fluxes were based, as before, on potassium and substance on the base of carbonates.

The intensity of heating was increased due to blowing using bellows and pumps. Only in the XIX century the efficiency of brazing was increased owing to the application of highly-caloric combustion gases and electric heating.

CONCLUSIONS

1. The first methods of brazing were developed in the period of manufacture of cast items from native metals, and then from bronze and iron. Heating was realized in hearth furnaces in combustion of a solid organic fuel and air blowing-in.

2. Minerals and organic materials, which form compounds in heating, clean the surface from contaminations and oxide films.

3. In the ancient world the compositions of brazing alloys, whose ratio of components corresponded to low-fusible eutectics, were defined. Components of the brazing alloys were added to the composition of fluxes in the powder state.

1. (1975) *Handbook on brazing*. Ed. by S.N. Lotsmanov, I.E. Petrunin, V.P. Frolov. Moscow: Mashinostroenie.
2. (1979) *Technology in its historical development*. Ed. by S.V. Shukhardin, N.K. Laman, A.S. Fyodorov. Moscow: Nauka.
3. Kolchin, B.A. (1975) Problems of study of technology of most ancient manufacturing. In: *Essays of technology of the ancient manufacturing*. Moscow: Nauka.
4. Rybakov, B.A. (1948) *Handicraft of Ancient Russia*. Moscow-Leningrad: AN SSSR.
5. (1967) *Archeology and natural sciences*. Transact. Moscow: Nauka.
6. Khrenov, K.K. (1970) *Cutting and brazing of metals*. Moscow: Mashinostroenie.
7. (1989) *History of ancient world*. Ed. by I.M. Diakov, V.D. Nerovnaya, I.S. Sventsitsky. Book 2: Onset of ancient societies. Ed. by I.S. Sventsitsky. Moscow: Nauka.
8. Maryon, H. (1949) Metal working in the ancient world. *Amer. J. Archeol.*, **2**, 93–125.
9. Dochvar, A.A. (1945) *Metals science*. Moscow-Leningrad: Metallurgizdat.
10. Beckert, M. (1980) *World of metal*. Moscow: Mir.
11. Moshkova, M.G., Ryndina, N.V. (1975) Sarmat mirrors of the Volga and Ural regions (chemical-technological examination). In: *Outlines of technology of most ancient productions*. Moscow: Nauka.
12. (1984) *Museum of historical jewellery of Ukr. SSR*. Kiev: Mystetstvo.
13. Tysyachna, N. (2004) Gold evolution of Ukraine. *Den*, **94**, 8.
14. Maryon, H. (1938) The technical methods of the Irish smith in the bronze and early iron ages. *Proc. of Royal Irish Acad.*, **3**, 181–225.
15. Kornienko, A.N. (1996) Origin of first methods of welding. *Avtomatich. Svarka*, **1**, 53–57.
16. Suprunenko, O.B., Kulakova, I.M., Mironenko, K.M. et al. (2004) *Ancient sites of Kremenchuk. Archeological momuments at the territory of the city and its outskirts*. Poltava: VTs Arkheologiya.
17. Gzelishvili, I.A. (1964) *Iron smelting in Ancient Georgia*. Tbilisi: Sakartvelo.
18. Avdusin, D.A. (1967) *Archeology of the USSR*. Moscow: Nauka.
19. Gejdova, D., Dudik, Ya., Kibalova, L. et al. (1982) *Big illustrated encyclopedia of antiquities*. Praga: Artia.
20. Lermontov, V.V. (1898) *Tinner (Encyclopedic vocabulary)*. Ed. by K.K. Arseniev, F.F. Petrushevsky. St-Petersburg: M.A. Efron Tipo-Litografiya.
21. Roberts, P.M. (1974) Early evolution of brazing. Part 2. *Welding and Metal Fabr.*, **12**, 412–416.

PROSPECTS OF APPLICATION OF NEW METHODS OF DISTANCE EDUCATION OF ENGINEERING PERSONNEL IN WELDING INDUSTRY

S.N. POPOV and **D.A. ANTONYUK**
Zaporozhie National Technical University, Zaporozhie, Ukraine

Main methods of organizing the technology of distance education of engineering personnel in welding industry are presented. The statistic data are given and prospects of implementation of these technologies at the Chair of Equipment and Technology of Welding of the Zaporozhie National Technical University (ZNTU) are shown.

Keywords: *distance education, bachelor, specialist, master, information-educational resource, cyber communicative space, training of personnel, engineering personnel, method of a case-technology, TV-technology, network technology*

Wide application of information and communication technologies is a characteristic feature of the world progress over the recent decades. The today's scientific-technical progress, informatization of industry, sphere of business and society as a whole put forward the requirements for education of a radically new personnel with a high level of comprehensive knowledge, being fully in possession of the newest achievements of the computer engineering.

Already today there is a growing need in highly-qualified specialists in welding industry, knowing the applied programs (MS Office, Photoshop, Corel Draw, MathCAD, MathLab, Mathematica, AutoCAD, PLAXIS, ANSYS and others) and capable to apply them. This is, first of all, connected with change in management of technological manufacture of welded structures, their new feasibilities in the field of engineering, in particular in 3D graphical design of welded modular elements, that is important at dynamic analysis and restructuring of marketing schemes of satisfying the demands of purchasers (customers).

The solution of this problem is possible at a radical revision of education system, guarantee of identity of tools, technologies, information medium of engineer, manager and marketing expert, who provide the process of welding manufacturing and realization of ready products. For this, it is necessary to use the information technologies in teaching the courses of both general professional and also special disciplines.

The use of information systems in education of specialists in the field of welding and wear-resistant technologies requires the creation of information-educational resources (IER), combining the best teacher's potential, the newest educational-methodical developments, electron libraries, new methods of education on the basis of a distance education [1].

IER represents a systematic-organized combination of means of creation, actualization and transfer of data, intellectual and information resources, protocols of interaction, hardware-software and organization-methodical support, purposefully oriented to the satisfaction of actual educational needs of people of different regions.

The application of informational technologies makes it possible to open up the new opportunities for the systems of education of engineers, bachelors, specialists in the fields dealing with welding, namely visual, dynamic representation of welding and surfacing processes using the video and sound means; freedom in selection of methodology, style and means of education, that will facilitate the self-conscious opening of potential prospects of knowledge gained; creation of scientifically-methodologically grounded system of basic education (mathematics, physics, chemistry, thermodynamics, resistance of materials) using the new synergetic principles of development of information technologies. The use of these technologies gives an opportunity to provide the continuity and sequence of computer education at all the levels of education with the creation of computer software of all disciplines of the educational process.

The offered system of educational technologies enables us to open up the opportunities for renewal of scope of education and methods of teaching; to widen the access to general and professional education; to modify the procedure of acquisition and systematizing of knowledge bases; to change the role of teachers in the educational process [2, 3].

Analysis of total number of students of the ZNTU (Figure 1) shows that if to preserve the dynamics of growth of total number of students of day form of education and by correspondence, their number can amount to about 10,000 in the nearest future. In addition, the number of students which use the technologies of a distance education is growing continuously.

Over the recent years the works on implementation of principles and technologies of distance and open educations are carried out in education systems of different countries [2–5]. In our opinion, to train the engineering-technical personnel in the field of welding and related technologies it is necessary to create an integrated method of education which is based on updating the known procedures in a single cyber communicative medium of information network resource [1].

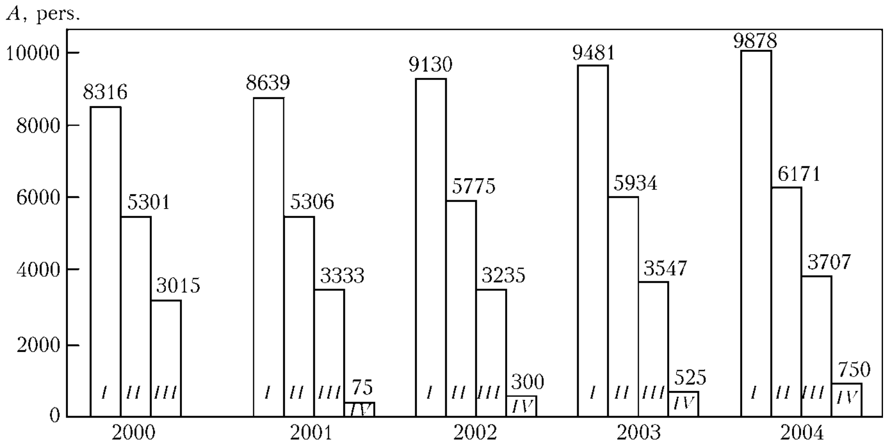

Figure 1. Dynamics of growth in total number of students of ZNTU: *I* — in total; *II* — day form of education; *III* — by correspondence; *IV* — distance

Thus, for simple general knowledge-information courses, necessary for receiving the higher education, such as history of Ukraine, culture, bases of religion, fundamentals of treatment of materials, physical-chemical and metallurgical fundamentals of production of metals, bases of labor protection, ecology, introduction into specialty, a method of a case-technology can be used (Figure 2), which consists in compiling and completing of a special system of educational-methodological materials [6] with a subsequent transfer it (by mail, E-mail) to the student for a self-study and next periodic contact with a consultant for explanation [3].

The use of this method allows teacher to understand how competent is the student in the given problem. At the same time the one-sided use of only these forms prevents the real contact with the teacher. The absence of a dialog in a real time reduces the effectiveness and term of material digestion. This is connected with a loss of individual personal effect of the teacher as a mature personality, as an «alive carrier of knowledge».

The presence of mutual dialog in education can be provided to a certain degree by use of so-called TV-technology or video-seminars (Figure 3) which are based on application of TV lectures with consultations of teachers-consultants by network of cyber communicative resource using telephone, radio and other channels of communication.

These technologies should be used at the higher courses (third–fifth), in the course and diploma designing for such disciplines as theoretical mechanics, machine parts and bases of designing, applied mechanics, theory of welding processes, welding power sources, triboengineering and reliability of machines, fusion welding, pressure welding, design and fabrication of welded structures, quality control of welding, technological fixture and other subjects. The rapid development of TV-communication allowed abrupt reduction of expenses for use of the necessary equipment. Thus, today the cost of a delivery set of equipment for conductance of video-seminars is approximately 100 US dollars per a camera, and a special software can be obtained in network of Internet in the form of a bonus [6].

There are also other new technologies in image transfer which are actively used for a distance education. For example, the digital TV, the standard ATCS [7], has been already certified by the American Federal Commission on TV communications. At the end of 1998 the TV broadcasting in this format started in Seattle, USA.

However, the present burst in a distance education can be provided by the new cyber communicative web-

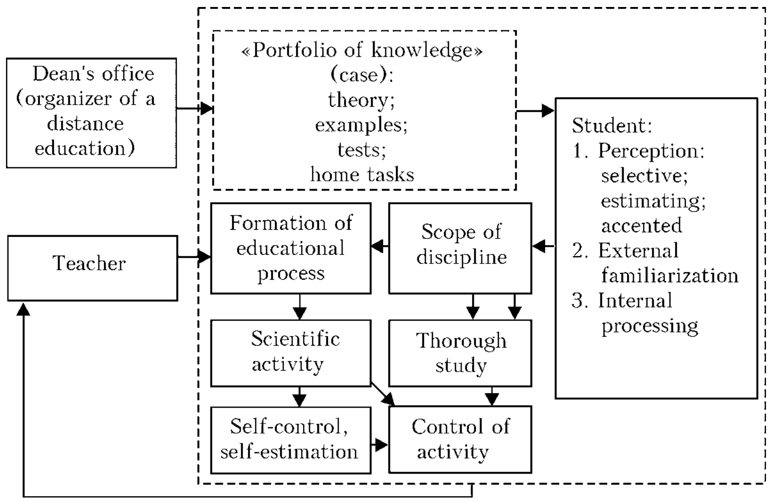

Figure 2. General scheme of the method of a case-technology

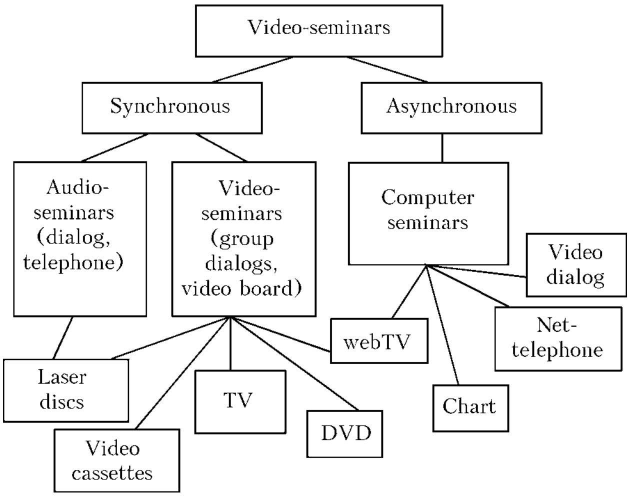

Figure 3. Classification of video-seminars

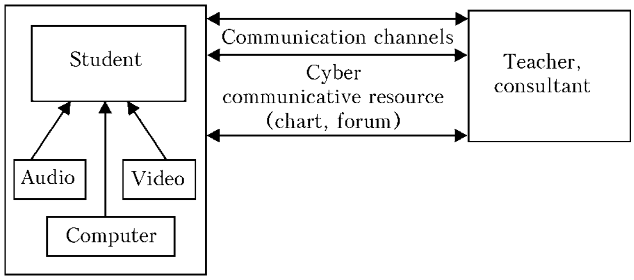

Figure 4. Scheme of organizing the TV-technology

TV technology (Figure 4) allowing your home TV set to receive educational programs through Internet using a decorder [4]. The use of this method of education is most actual and progressive, in particular in study of engineering specialties in the field of welding, surfacing, tribotechnologies of deposition of special coatings, creation of bimetal structures, as it can evaluate visually the processes proceeding in action of heat radiation source or contact of abrasive particles with a surface layer.

Cyber communicative network technology is based on use of Internet network for organizing the educational process on the basis of a virtual methodical web-support and interactive continuum between the teacher and student (Figure 5).

Network web-method of a distance education stimulates intensively the progress of systems of information support of the educational process, namely the network electron libraries, web-courses [6] and other information resources. This is associated with the fact that today the web-information is the main problem in the sphere of welding, wear resistance and related trends.

Analysis of network resources in Internet showed that the number of sites, devoted to the solution of problems of tribotechnology, wear of steels and alloys, weldability and materials science, is less than 3 % of all the number of web-proposals.

Thus, the newest methods of organization of educational process by specialties connected with welding, tribomaterials science and others, open up the widest opportunities for improvement of the level of educational-methodological equipping of the university, widening of laboratory and production facility of the educational process, inviting of new groups of people for receiving the higher technical education (bachelor, specialist, master), updating of traditional

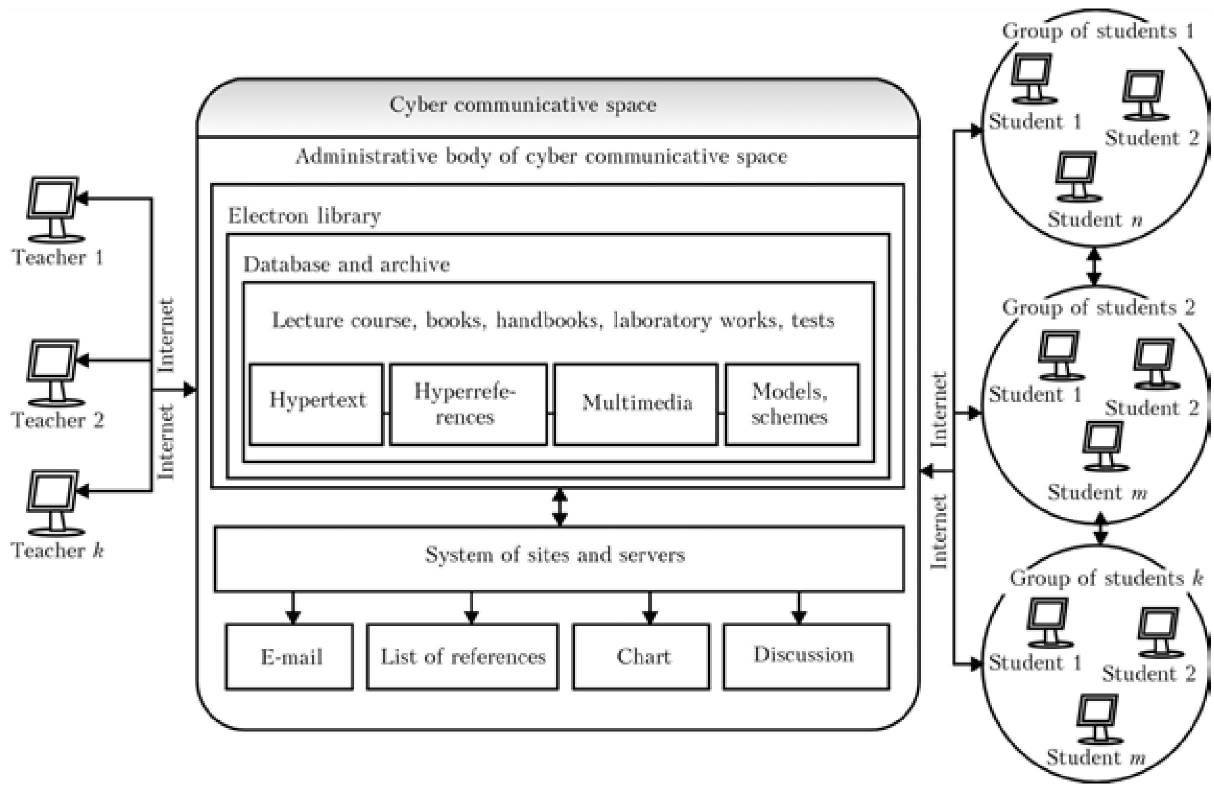

Figure 5. Principle of organizing of network technology of education

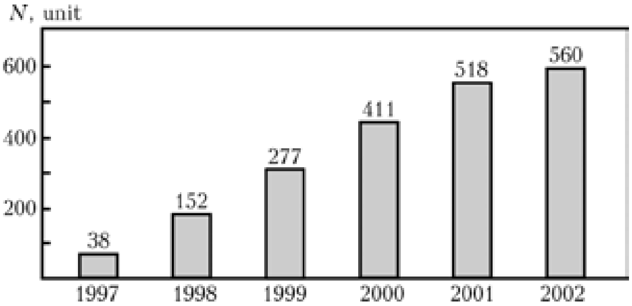

Figure 6. Dynamics of total number of personal computers *N* in ZNTU

and creation of new forms of receiving the engineering education.

However, it should be taken into account that the development and implementation of offered technologies is possible only at large material and intellectual expenses. In connection with a sufficient provision of ZNTU students with computers (Figure 6) and display sites (Figure 7) the implementation of these technologies in the educational process will be already real in the nearest time.

Authors have studied statistically the number of computers in ZNTU which have the program of mathematical analysis. The prediction shows that if to preserve the achieved rates of growth of number of educational sites equipped with computers, the park of computers will amount to about 1900 units by 2013. This states that almost each student will have a feasibility to use the technologies and methodologies of a distance education in the educational process.

At the Chair of Equipment and Technology of Welding of ZNTU the works are carried out on the creation of principles and methodological approaches of open distance education with allowance for the world tendencies of organizing the education [3–5], that will make it possible with time to widen the level and to upgrade the quality of education of personnel in the field of welding and wear-resistant technologies.

Implementation of new cyber communicative technologies is necessary to realize, in our opinion, in two stages.

The first stage will include the formation and realizing of educational courses (educational packages), which contain textbooks, manuals, interactive course on discs, subject literature of the course; development of methodical support and software of acceptance of exams and test programs; training of teachers for organizing the educational process.

At the second stage the on-line Internet technologies, multimedia programs for training of specialists in the field of welding and wear resistance will be used.

The creation of a distance course is connected with the fulfillment of a complex, long methodological and organizational work. At the world market the cost of development of one such course is more than 1,000 USD. Implementation of a distance education envisages the use of an appropriate hardware. TV communication networks should maintain a sufficiently high rate of data transfer.

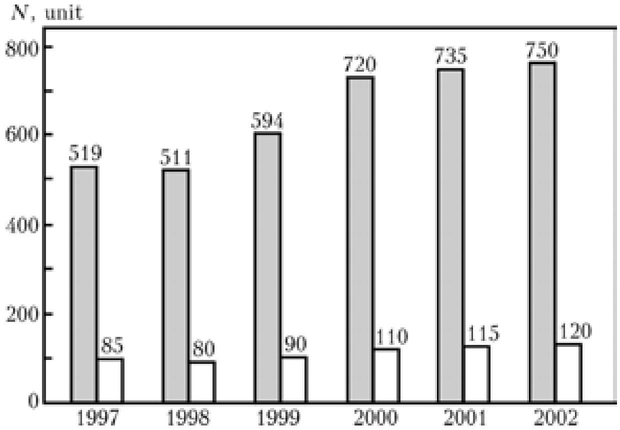

Figure 7. Computerization of educational process in ZNTU: ■ — number of display sites; □ — number of hours for one student per year; *N* — number of computers

Calculations show that the cost of education of one specialist, excluding the expenses for travel and boarding, and also reduction in a total cost of courses, is almost 5 times decreased.

Thus, the application of offered technologies in an integrated system makes it possible to increase significantly the quality and level of engineering personnel dealing with welding and related technologies. In our opinion, the use of system-integrated case-technologies, technologies of video-seminars and network technologies in a single cyber communicative space with specially-trained and educated personnel (management and service of the Chair, technical services, teachers) is most rational and effective.

It can be concluded that the distance form of education is not an alternative, it supplements the traditional forms. It takes into consideration the individual manner of education, as each student receives differential knowledge which were selected by him taking into account the motivations and terms of education. This form of education has a special motivation base, not always associated with knowledge acquisition for the further realization in a professional career, but, for example, for satisfying the personal needs. The distance form of education has a high dynamics in knowledge updating.

1. Popov, S.N., Antonyuk, D.A. (2003) Principal aspects of development of information-educational systems of welding and related technologies based on cyber communicative resourse. In: *Pap. of All-Russian Sci.-Techn. Conf.* Moscow: MATI-RGTU.
2. Hara, N., Kling, R. (2000) WP 00-01-31. Student's distress with a web-based distance education course. In: *CSI Working paper*, March 30.
3. *Conception of Russian portal of open education*. http: / / www.opennet.ru
4. Farrel, Gl. (1999) *The development of virtual education: a global perspective*. http: / / www.col.org / virtualed / index.htm: The Commonwealth of learning.
5. Wheeler, S. (2000) The traditional university is dead — long life the distributed university. In: *Proc. of 19th Europ. Conf. on Death and Rebirth of University Education*, Bergen, Norway, May 4–6, 2000.
6. Popov, S.N., Antonyuk, D.A. (2004) Procedure of construction of multimedia course «Triboengineering and reliability of machines» on the basis of distance computer-aided teaching of students. *Otkrytoe Obrazovanie*, **1**, 13–21.
7. *The American communication association*. http: / / www.americancomm.org

APPLICATION OF EXTERNAL ELECTROMAGNETIC ACTIONS FOR IMPROVEMENT OF MECHANICAL PROPERTIES OF WELDS IN UNDERWATER WET WELDING

R.N. RYZHOV[1], **V.A. KOZHUKHAR**[1], **S.Yu. MAKSIMOV**[2] and **E.A. PRILIPKO**[2]
[1]National Technical University of Ukraine «Kiev Polytechnic Institute», Kiev, Ukraine
[2]E.O. Paton Electric Welding Institute, NASU, Kiev, Ukraine

Optimization of conditions of external electromagnetic actions for conditions of underwater wet welding was realized on the basis of analysis of experimental dependencies of mechanical properties of welds on induction of controlling magnetic field.

Keywords: *underwater welding, external electromagnetic action, mechanical properties of weld metal*

Increased requirements are specified for the structures welded under water, in particular for strength characteristics. This is due both to the specifics of their service and also to technical difficulties and expensiveness of repair welding jobs.

Process of underwater welding is characterized by much higher rates of cooling the welded joint metal than in air [1], that leads to the increase in level of internal stresses. In combination with an increased metal saturation with hydrogen this causes the deterioration of strength characteristics of weld metal and increase in hazard of cold crack formation.

It is possible to prevent the above-mentioned negative effects by using technological procedures allowing influence the weld solidification in the process of welding. Taking into account the specifics of wet underwater welding the metallurgical measures of effect are most often used, that consist in correction of charge composition of the flux-cored wires.

As follows from work [2], to have an effective control of weld metal solidification processes in air welding, the external electromagnetic actions (EMA) are used, at which the volumetric ponderomotive forces are created in the pool volume as a result of interaction of electric field of welding current with an axial constituent of the controlling magnetic field. These forces make it possible to control the hydrodynamics of the melt. Moreover, periodical changes in temperature are occurred in the region of crystallization front, influencing positively the formation of primary structure, thus improving greatly the mechanical properties of the weld metal [3]. The earlier investigations showed that application of EMA in underwater wet welding 2.5 times decreases the amount of hydrogen dissolved in weld metal [4].

The aim of the present work was to make the quantitative assessment of effect of parameters of EMA conditions on structure and mechanical properties of the weld metal.

Experiments were carried out at depth down to 1 m. Multipass welding of steel 17G1S specimens of 20 mm thickness and V-shaped edge preparation was performed using flux-cored wire PPS-AN2 at the following condition: I_w = 180 A (reverse polarity), U_a = = 36 V, v_w = 9 m / h. Axial controlling magnetic field (CMF) in the zone of welding was generated using a cylindrical electromagnet arranged coaxially to a nozzle. Induction in CMF was adjusted using a control unit F91 [5]. Mechanical properties of the weld metal were determined by tension of specimens in test machine of MI12 type. Here, the ultimate strength σ_t, yield strength σ_y, elongation δ and reduction in area ψ of fracture region were recorded.

Under the conditions of experiment the negligible improvement of strength properties of weld metal with increase in CMF induction up to 10 mT (Figure 1) is due to the fact that the melt flows at the given EMA conditions, formed in the pool head part, have no time to move for a sufficient distance along the pool tail part. Here, the processes of crystallization are differed negligibly from initial conditions in central weld regions, adjacent to a longitudinal axis, from which the specimens were manufactured. At B = 15 mT the increase in σ_t by 8.5 % and σ_y by 10 % was observed.

The further increase in induction has led to the deterioration of characteristics examined. This was due both to excessive hydrodynamics of the pool melt and also to the deterioration of processes of electrode metal transfer, that has a negative influence on weld formation and stability of the welding process as a whole.

Application of EMA can increase greatly the weld metal ductility. With increase in induction of CMF up to 15 mT the monotonous increase in δ (by 66 %) and ψ (by 33 %) was observed. Reaching extreme values by relationships of Figure 1 at similar induc-

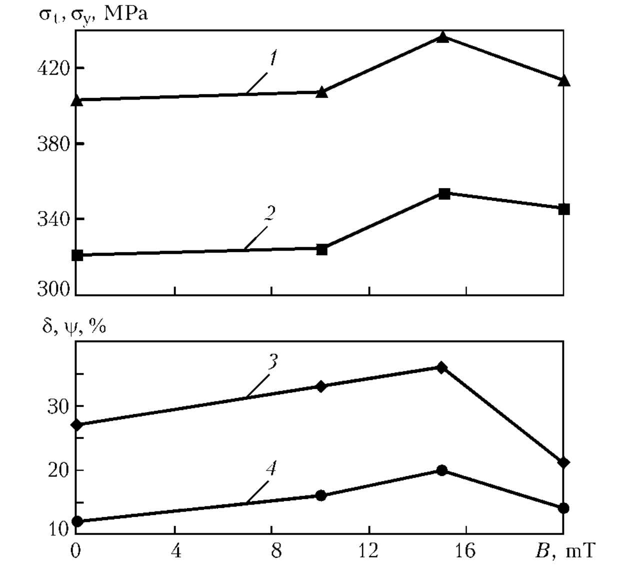

Figure 1. Effect of CMF induction on mechanical properties of welds: *1* — σ_t; *2* — σ_y; *3* — ψ; *4* — δ

tions of CMF proves that changes in strength and ductile properties have similar grounds and are associated with appropriate changes in processes of crystallization. In this case, in the range of B = 0–15 mT the uniform increase and next abrupt decrease in ductility can be explained by the interrelation of the given mechanical characteristic with saturation of welds with hydrogen and oxygen [4].

Change in metal ductility in horizontal and vertical directions from longitudinal axis of deposited beads was evaluated by the level of microhardness by Vickers HV at 0.981 N load. It was established that the use of EMA with B = 10–15 mT in the area of longitudinal axis (in Figure 2, l = 0 mm) makes it possible to decrease HV by 13 %. In all the specimens examined the negligible increase in HV is observed at the removal from longitudinal axis into the side of fusion line in horizontal plane, while the exponential decrease in HV is observed in vertical plane in the direction of weld root.

These changes in hardness of metal of a cast zone is explained by the fact that the root region of welds under experiment conditions was cooled at a lower rate, while the lateral surface regions were cooled at the higher rate. It is known here that the increase in

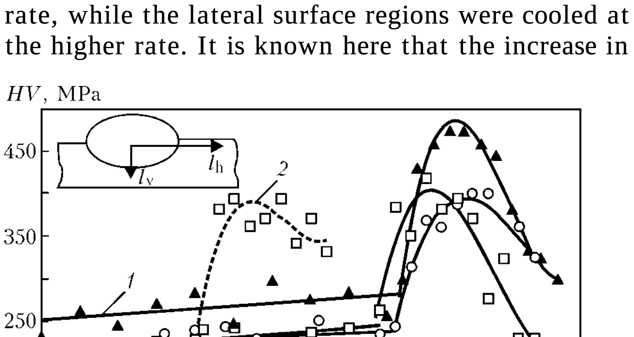

Figure 2. Distribution of hardness in transverse section of welds in horizontal l_h (*1*) and vertical l_v (*2*) direction: Δ — welding by conventional technology; ❒, ❍ — welding with EMA, respectively, at B = 10 and 15 mT

the cooling rate during crystallization promotes the formation of structures of a lower ductility.

This effect is manifested to a greater extent in metal of the HAZ, whose length was about 2 mm under the conditions of experiment (Figure 2). The hardness HV in metal of the given region is 2 times higher than that in weld metal using the conventional technology of welding. It was established that application of EMA does not almost influence the HAZ width. However, at B = 10 mT the HV decrease by 15 % was observed. The further increase in induction of CMF did not lead to change in HV. The similar level of hardness in HAZ regions adjacent both to lateral surfaces and also to a root part of welds, can show the negligible differences in rates of cooling the given regions.

The evaluation of EMA effect on the process of crystallization was realized by analysis of microstructures of sections made from specimens examined. It was established that the microstructure of weld metal made by the conventional technology consists mainly of pearlite with very fine ferrite interlayers along the boundaries of crystals (Figure 3, *a*). In specimens produced with use of EMA, the significant decrease in sizes of crystals was observed, in particular at B = = 10 mT.

In parallel with increase in thickness of ferrite interlayers the regions of a structurally-free ferrite were revealed, that can result from increase in diffusion mobility of carbon due to decrease in amount of imperfections of the crystalline lattice (Figure 3, *b*).

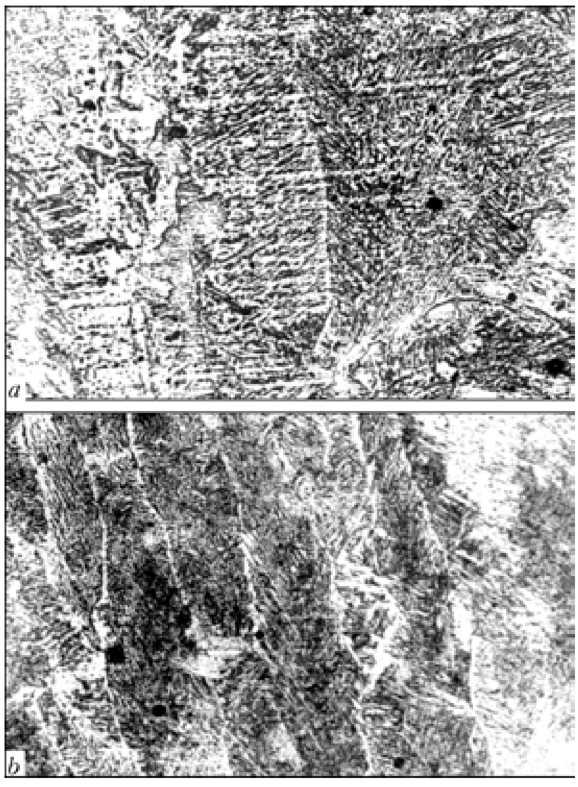

Figure 3. Microstructures of weld metal: *a* — conventional technology; *b* — with EMA at B = 10 mT (×200)

Thus, to achieve the maximum improvement of mechanical properties of weld metal in underwater wet welding with EMA the induction of CMF should be in the range of B = 10–15 mT.

Close geometric parameters and chemical compositions of metal of specimens being welded, used in conductance of the above-mentioned investigations and given in work [3], allow us to make the comparative evaluation of the results obtained. In both cases the relations σ_t and σ_y are described by the curves with extremum that allows us to optimize the EMA condition. However, in case of underwater wet welding the maximum improvement of mechanical properties is attained at lower (by 25 %) inductions of CMF, that is explained by the lower volume of the weld pool melt.

In air welding the increase in σ_t and σ_y was observed at low values of induction, that was not revealed in conductance of the given investigations. The mentioned circumstance can be explained both by differencies in procedures of mechanical tests, and also by high viscosity of the melt in underwater welding, that deteriorates greatly the hydrodynamics of the pool at low values of CMF induction.

Thus, the EMA application in underwater wet welding with optimum values of induction of CMF (10–15 mT) makes it possible to increase the strength (by 10 %) and ductility (by more than 60 %) of weld metal by control of the crystallization processes, thus proving the improvement of quality of the welded joints.

1. Melnik, Yu.P., Savich, I.M., Glukhova, E.V. (1976) Peculiarities of thermal cycle of low-carbon steel underwater welding. *Avtomatich. Svarka*, **1**, 17–21.
2. Chernysh, V.P., Kuznetsov, V.D., Briskman, A.N. et al. (1983) *Electromagnetic stirring welding*. Kiev: Tekhnika.
3. Gagen, Yu.G., Martynyuk, T.A. (1978) Influence of parameters of longitudinal magnetic field on structure and mechanical properties of welded joints of gas-oil pipelines. *Avtomatich. Svarka*, **9**, 37–38.
4. Maksimov, S.Yu., Prilipko, E.A., Ryzhov, R.N. et al. (2003) Effect of external electromagnetic action on hydrogen content in weld metal in wet underwater welding. *The Paton Welding J.*, **6**, 41–43.
5. Korab, N.G., Skachkov, I.O., Matyash, V.I. (1993) System of control of electromagnetic actions in welding. *Avtomatich. Svarka*, **11**, 52–53.

THESIS
FOR THE DOCTOR OF TECHNICAL SCIENCES DEGREE

E.O. Paton Electric Welding Institute, NASU, Kiev, Ukraine

Vladimir M. Nesterenkov (PWI) defended on September 29, 2004, thesis for the Doctor of Technical Sciences degree on the subject «Theory and Practice of Stable Weld Formation in Electron Beam Welding of Heavy Sections of Metals».

The thesis describes the studies elaborating theoretical notions of the hydrodynamic processes occurring in the weld pool metal, establishing peculiarities of natural oscillations of the melt flowing over the walls of deep keyholes, identifying conditions for stable formation of welded joints and developing, on this basis, commercial technologies for EBW of large-size critical-application parts.

The most important scientific results obtained by the candidate for the Doctor's degree include:

• results of investigation into natural oscillations of molten metal in deep keyholes, showing that the first harmonic of oscillations of the melt having minimal frequency and maximal amplitude exerts a substantial effect on formation of welded joints of a large thickness;

• results of investigation into the effect of the beam reflected from long-wave instabilities of the surface of molten metal on the front keyhole wall on formation of defects in the weld root. It is shown that frequency of formation of the penetration peaks corresponds to frequency of the first harmonic of oscillations of the melt in the keyhole. Higher harmonics of natural oscillations of the melt in the keyhole do not affect the value of the penetration peaks and formation of the root defects;

• proving of the fact that stability of formation of the welds more than 100 mm deep can be improved through inclining the plane of the welded joint and electron beam to an angle close to 10° to the horizon. This spatial orientation of the weld pool increases frequency of the lowest oscillation harmonics, decreases the amplitude of instabilities of the melt surface on the front wall of the keyhole and, as a result, improves stability of the welding process as a whole.

Results of theoretical and experimental studies of stability of the weld pool in EBW of thick metals with fading out of circumferential welds were used as the basis for the development of technological processes of EBW of some low-alloy steel parts up to 150 mm thick and aluminium alloy parts up to 300 mm thick, which found application in the CIS countries, France, Great Britain, China and USA.